MICHIGAN STATE UNIVERSITY LIBRARIES
3 1293 01020 1675

This is to certify that the

dissertation entitled

Polymer-Clay Nanocomposites

presented by

Tie Lan

has been accepted towards fulfillment
of the requirements for

Ph.D. degree in Chemistry

Thomas J. Pinnavaia
Major professor

Date Nov. 3, 1994

*MSU is an Affirmative Action/Equal Opportunity Institution*

O-12771

LIBRARY
Michigan State
University

PLACE IN RETURN BOX to remove this checkout from your record.
TO AVOID FINES return on or before date due.

| DATE DUE | DATE DUE | DATE DUE |
|---|---|---|
| FEB 0 2 1998 MAGIC 2 | | |
| MAY 2 0 1999 | APR 0 3 2003 | |
| MAY 3 0 2001 | | |
| MAY 3 0 2002 | | |
| MAR 0 8 2007 | | |
| | | |
| | | |
| | | |

MSU Is An Affirmative Action/Equal Opportunity Institution
c:\circ\datedue.pm3-p.1

# POLYMER - CLAY NANOCOMPOSITES

by

Tie Lan

A DISSERTATION

Submitted to

Michigan State University

in partial fulfillment of the requirements

for the degree of

DOCTOR OF PHILOSOPHY

Department of Chemistry

1994

# ABSTRACT

## POLYMER - CLAY NANOCOMPOSITES

by

Tie Lan

Nanocomposites represent a new family of materials that are attracting great attention by chemists and materials scientists. The properties of nanostructured materials are determined by a complex interplay between the building blocks and their interfaces. Smectite clays are promising for preparation of nanostructured polymer-clay composites by polymer intercalation or by *in situ* polymerization of monomers. Alkylammonium exchanged smectite clays were used as organoclays in this study. The present work reports novel methods to prepare polymer-clay nanocomposites and discusses the dependence of the nanocomposite properties upon the structural features.

We systematically studied the intercalation of epoxy resin, Epon-828, into different organoclay galleries and proposed a swelling model to predict their performance in the nanocomposite formation. Polyether-clay nanocomposites have been synthesized by epoxide self-polymerization in the presence of organoclays. XRD and TEM studies indicate that the finial products contain a uniform dispersion of 10 Å-thick clay plates dispersed uniformly in the polyether matrix. DSC results show that two exothermic catalytic processes occur during the reaction. The acidity of the clay exchanged cation plays a major role in catalyzing the epoxy self-polymerizations, especially the intragallery polymerization. The lower

temperature process is attributed to intragallery epoxy self-polymerization and higher temperature reaction is attributed to outergallery polymerization.

Epoxy-clay nanocomposites have been synthesized by exfoliating organoclays in a glassy epoxy matrix. The extent of silicate layer separation is governed by the chain length of gallery cations, the clay layer charge density and the acidity of the gallery cations. Mechanical measurements show that the exfoliated epoxy-clay nanocomposites have higher failure strength and tensile modulus than the non-exfoliated composites. Novel epoxy-clay nanocomposites with sub-ambient $T_g$ have been prepared by the reaction of epoxy resin and a polyetheramine in the presence of organoclays. The expansion of the clay galleries upon polymer network formation facilitates the uniform dispersion of the clay plates in the matrix. Both the tensile strength and the modulus of the nanocomposite increased with increasing clay content. The reinforcement provided by the 10 Å-thick silicate layers at 15 wt% loading was manifested by a more than ten-fold improvement in tensile properties. The rubbery state of the matrix may allow alignment of the exfoliated silicate layers upon applying strain, thereby enhancing reinforcement.

Polyimide-clay composites have been prepared by reacting organoclays with pre-formed polyamic acid in dimethylacetamide and subsequent heating. These films exhibit excellent barrier properties towards $CO_2$ at low clay loading (<5%). X-ray diffraction results reveal that the clay layers are oriented within the polyimide matrix. However, TEM images show there are two different types of aggregated clay domains within the composite matrix. It is suggested that the fractal behavior of clay in the polymer matrix may govern the barrier properties of the films.

**TO MY FAMILY**

## ACKNOWLEDGMENTS

I would like to express my deep respect and gratitude to my research advisor Dr. Thomas J. Pinnavaia for his inspiration and support during the course of this work. His research expertise and outstanding personality were the main factors to develop my contribution and accomplishment to his work. I am proud and pleased to receive my graduate study in his group. I also thank Lyn Pinnavaia for her hospitality and each group parties; summer picnics, Christmas and tailgate parties.

I would like to thank my committee members, Dr. H.A. Eick, who served as second reader, Dr. C.K. Chang, for his advice and friendship, and Drs. J. Ledford and N. Jackson for their time and discussion.

My thanks are extended to MSU physics professor Dr. Duxbury, for his advice in understanding the mechanical and barrier properties of the polymer-clay nanocomposites; to Dr. Giacin, Dr. Hernandez, who are professors in the MSU Packaging School, for their kindness and help in the permeability measurements. I would also like to thank Dr. Klomparens and Dr. Drzal for the use of their EM and mechanical measurement instruments, respectively.

I would also like to thank the TJP group members past and present. I enjoy the collaborations with Dr. "Kavie" very much. His experience and help are highly acknowledged. I have a special thank to Dr. Jialiang Wang for his instructive help. Many thanks go to Mr. Zheng Wang, who made the over-night lab work to be not unbearable and for his helpful discussion.

Financial support given by the Center for Fundamental Materials Research and the Chemistry Department Michigan State University, National Science Foundation is gratefully acknowledged and appreciated.

I deeply thank my family in China for their support, understanding and encouragement in the last five years. The letters and gifts from my parents, sister and brother are inspirational and unforgettable.

Most importantly I am appreciative to my wife Ying for all the love and understanding she has given me over the years. There is no words which I can use to express my feelings to her in this world. Should success of her research work and happiness come to her.

# TABLE OF CONTENTS

**Chapter** **Page**

**LIST OF TABLES** ..... xiv

**LIST OF FIGURES** ..... xvii

**ABBREVIATION** ..... xxvii

**CHAPTER I Introduction**

A. Composite Materials ..... 1

B. The Nanocomposite Concept ..... 3

C. Recent Advances on the Synthesis of Hybrid Organic-Inorganic Composites ..... 4

1. Inorganic Network Formation via the Sol-Gel Method ..... 5
2. Inorganic Networks from Natural or Synthetic Materials ..... 7

D. Structure and Properties of Layered Silicates ..... 15

1. Introduction to Smectite Clay Structure ..... 15
2. Introduction to Structures and Properties of Organoclays ..... 17
3. Applications of Organoclays ..... 19

E. Polymer-Clay Composites ..... 20

**Chapter** **Page**


1. Conventional Polymer-Clay Composites.....22
2. Intercalated Polymer-Clay Nanocomposites .....22
3. Exfoliated Polymer-Clay Nanocomposites .....26

F. Research Objectives .....28

1. New Approaches to Polymer-Clay Nanocomposites using Organoclays .....28
2. Relationships between Structures and Properties of various Polymer-Clay Nanocomposites .....30

G. References .....32

**CHAPTER II Epoxy Monomer Intercalation in Organoclays**

A. Introduction .....38

B. Experimental .....41

1. Materials .....41
2. Preparation of Organoclays .....42
3. Intercalation Reaction .....42
4. Physical Measurements .....43

C. Results and Discussion .....44

1. Reaction Time Effect .....46
2. Reaction Temperature Effect .....46
3. Effect of Gallery Cation Chain Length .....49

4. Effect of Gallery Cation Acidity on Nanocomposite Formation ....131
5. Mechanical Properties of the mPDA-Cured Epoxy-Clay Nanocomposites ....139

D. Conclusion ....144

E. References ....145

**CHAPTER V** **Synthesis, Characterization and Mechanical Properties of Sub-Ambient $T_g$ Epoxy-Clay Nanocomposites**

A. Introduction ....148

B. Experimental ....151

1. Materials ....151
2. Synthesis of JEFFAMINE-Epoxy-Clay Nanocomposite ....152
3. Physical Measurements ....152

C. Results and Discussion ....154

1. Preparation and Characterization of D2000-Epoxy Clay Nanocomposites ....154
2. Mechanical Properties of D2000-Epoxy Clay Nanocomposites ....169

5. Mechanism of Barrier Property Enhancement of Polyimide-Clay Nanocomposites, Fractal Structure .....207

D. Conclusion .....212

E. References .....213

# LIST OF TABLES


| Table | | Page |
|---|---|---|
| II 1. | Basal Spacings of $CH_3(CH_2)_{15}NH_3^+$-montmorillonite in Epon-828 at Different Temperatures | 48 |
| II 2. | Basal Spacings ($d_{001}$, Å) of Alkylammonium Exchanged Montmorillonite | 51 |
| II 3. | Basal Spacings ($d_{001}$, Å) of Air-Dried Organoclays and Their Epoxy-Solvated Analogues (75 °C) | 52 |
| II 4. | Basal Spacings of Air-dried Organoclays Containing $CH_3(CH_2)_{15}NH_3^+$ as Exchanged Cations in Their Dry States and Solvated State by the Epoxy Resin, Epon-828 | 54 |
| III 1. | Onset Temperatures and Enthalpy Changes Associated with the Polyether-Clay Nanocomposite Formation for Different Alkylammonium Montmorillonite Clay Systems | 75 |
| III 2. | The Enthalpy Changes Associated with the Two Exothermic Peaks ($\Delta H_1$ and $\Delta H_2$), and the Percentage of the 1st Peak's ($\Delta H_1$) in the Total $\Delta H$ *vs.* the wt% of Clay in the Epon-828 - $CH_3(CH_2)_{17}NH_3^+$-Montmorillonite Reaction Systems with Different Clay Loadings | 82 |

**III 3.** Activation Energies Associated with the Two Exothermic Peaks in the Self-Polymerization of Epon-828 in the Presence of Different Alkylammonium Montmorillonite Clays at 5 wt% Clay Loading.....86

**III 4.** Activation Energies Associated with the Two Exothermic Peaks in the Self-Polymerization of Epon-828 in the Presence of Different Loadings of $CH_3(CH_2)_7NH_3^+$-montmorillonite.....87

**III 5.** Activation Energies Associated with the Two Exothermic Peaks in the Self-Polymerization of Epon-828 in the Presence of Different Loadings of $CH_3(CH_2)_{17}NH_3^+$-montmorillonite...88

**III 6.** Activation Energies of Epon-828 Self-Polymerization Reaction in the Presence of Different Clays at 1-Step and 2-Step Reactions.....97

**IV 1.** Basal Spacings of Air-Dried Organoclays and Their Epoxy-Solvated Analogues (75 $^oC$).....133

**IV 2.** Mechanical Properties of Epoxy-Clay Nanocomposites Containing 1.0 wt% of $CH_3(CH_2)_{15}NH_3^+$-Clays.....142

**V 1.** Tensile Strengths and Moduli of D2000-Epoxy Clay Composites with $CH_3(CH_2)_{17}NH_3^+$- Exchanged Montmorillonite, Hectorite, Rectorite and Fluorohectorite at 5 and 10 wt% Clay Loading.....172

**VI 1.** Coherent Scattering Domain of $CH_3(CH_2)_{17}NH_3^+$-montmorillonite in Polyimide-Clay Films.....207

# LIST OF FIGURES


| Figure | | Page |
|---|---|---|
| I 1. | Schematic illustration of the tubular silicate-layered silicate nanocomposite formed from imogolite and $Na^{+}$-montmorillonite.[22] | 7 |
| I 2. | Schematic representation of PEO intercalation in a 2:1 layered silicate, showing the replacement of the interlayer cations, water coordination shell by the polyoxyethylene chains in a helical conformation.[33] | 11 |
| I 3. | Intrazeolite polymerization of acrylonitrile.[34] | 14 |
| I 4. | Idealized structure of a smectite clay mineral. $M^{n+}\cdot xH_2O$ represents the interlayer exchange cation and its coordination water molecules.[36] | 16 |
| I 5. | The orientation of alkylammonium ions in the different layer charge density clays.[38] | 18 |
| I 6. | Structural differences in conventional, intercalated and exfoliated polymer-clay composite/nanocomposites | 21 |
| I 7. | Powder X-ray diffraction of the poly-ε-caprolactone-fluorohectorite composite before (solid line) and after (dashed | |

line) polymerization. Insets are schematic illustrations (not drawn to scale) corresponding to the intercalated monomer (left) and intercalated polymer (right).[65] .....25

**II 1.** X-ray diffraction patterns of a typical intercalation of epoxy resin monomers into organoclays.....45

**II 2.** Time dependence of epoxy resin intercalation into $CH_3(CH_2)_{15}NH_3^+$-montmorillonite (5 wt%) at 75 °C.....47

**II 3.** Proposed model for the swelling of alkylammonium exchanged clay by Epon-828. A: low charge density clay with a lateral bilayer structure and B: high charge density clay with paraffin structure. Regardless of the initial charge density of the clay and orientation of the gallery alkylammonium cations, the final gallery height is determined by the vertical orientation of the organocations in the solvated intercalates.....56

**III 1.** X-ray diffraction patterns for (a) $CH_3(CH_2)_{15}NH_3^+$-montmorillonite air-dried at 25 °C; (b) $CH_3(CH_2)_{15}NH_3^+$-montmorillonite (5 wt%) intercalated with Epon-828; and (c) reaction product of Epon-828 with $CH_3(CH_2)_{15}NH_3^+$-montmorillonite (5 wt%) upon heating to 200 °C.....69

**III 2.** TEM image of polyether-clay nanocomposite formed by epoxy self-polymerization in the presence of 5 wt% of $CH_3(CH_2)_{15}NH_3^+$-montmorillonite.....71

**III 3.** FTIR spectra of (a) Epoxy resin (Epon-828) and (b) Reaction product between Epon-828 and $CH_3(CH_2)_{15}NH_3^+$-

montmorillonite (5 wt%) upon heating to 200 °C.....73

**III 4.** DSC curve for the polymerization of Epon-828 epoxy resin in the presence of 3 wt% $CH_3(CH_2)_{17}NH_3^+$-montmorillonite at a heating rate of 5 °C/min$^{-1}$. The inset defines the reaction onset temperature.....76

**III 5.** DSC curves for the polymerization of Epon-828 epoxy resin in the presence of $CH_3(CH_2)_{17}NH_3^+$-montmorillonite at different heating rates. The clay loadings are (A) 1 wt%, (B) 5 wt%, (C) 10 wt%, and (D) 15 wt%.....79

**III 6.** DSC curves for the polymerization of Epon-828 epoxy resin in the presence of different loadings of $CH_3(CH_2)_{17}NH_3^+$-montmorillonite at a heating rate of 2 °C/min.....81

**III 7.** Dependence of $\Delta H_1$ percentage in the total enthalpy change upon the clay loading.....83

**III 8.** Linear curve fitting of $1/T_{exo}$ *vs.* $\ln\phi$ for the second DSC peak in the epoxy polymerization reaction in the presence of 5 wt% $CH_3(CH_2)_{17}NH_3^+$-montmorillonite.....85

**III 9.** DSC curve for the Epon-828 self-polymerization in the presence of 50 wt% of $CH_3(CH_2)_{17}NH_3^+$-montmorillonite at a heating rate of 2 °C/min.....90

**III 10.** X-ray diffraction patterns of (a) Epon-828 solvated $CH_3(CH_2)_{17}NH_3^+$-montmorillonite complex with 50 wt% of clay (b) Reaction product obtained by heating the Epon-828

solvated $CH_3(CH_2)_{17}NH_3^+$-montmorillonite complex (50 wt%) at 200 °C for 1 h.....91

**III 11.** DSC curve of Epon-828 self-polymerization in the presence of $CH_3(CH_2)_{17}NH_3^+$-montmorillonite (5 wt%) at 2 °C/min.....93

**III 12.** X-ray diffraction pattern of the reaction intermediate of Epon-828 with $CH_3(CH_2)_{17}NH_3^+$-montmorillonite (5 wt%) at 135 °C for 1 h.....94

**III 13.** FTIR of (a) Epon-828 solvated $CH_3(CH_2)_{17}NH_3^+$-montmorillonite (5 wt%) (b) Reaction intermediate of $CH_3(CH_2)_{17}NH_3^+$-montmorillonite with Epon-828 at 135 °C for 1h, and (c) Polyether-$CH_3(CH_2)_{17}NH_3^+$-montmorillonite nanocomposite.....95

**III 14.** DSC curves of Epon-828 self-polymerization in the presence of $CH_3(CH_2)_{17}NH_3^+$-montmorillonite (5 wt%). (a) original mixture, (b) reaction intermediate after the reaction at 135 °C for 1 h.....96

**III 15.** Proposed reaction mechanism for the polyether-clay nanocomposite formation.....102

**IV 1.** X-ray diffraction patterns of amine-cured epoxy-clay composites containing 5 wt% $CH_3(CH_2)_{15}NH_3^+$-montmorillonite at the following curing conditions, (a) 75 °C, 4 h (b) 75 °C, 2 h and 125 °C 2 h (c) 100 °C, 4 h (d) 140 °C 4 h.....116

**IV 2.** X-ray diffraction patterns of epoxy-clay composite materials formed by the polymerization of a DGEBA resin, Epon-828, with stoichiometric amount of mPDA as a curing agent in the presence of various cation exchanged forms of montmorillonite. The exchange ions are identified for each diffraction pattern...118

**IV 3.** TEM of amine(mPDA)-cured epoxy-clay exfoliated nanocomposite with $CH_3(CH_2)_{15}NH_3^+$- montmorillonite (5wt%).....119

**IV 4.** X-ray diffraction patterns of amine-cured epoxy-clay composite materials formed by the polymerization of a DGEBA resin, Epon-828, with stoichiometric amount of mPDA as a curing agent in the presence of $CH_3(CH_2)_{17}NH_3^+$ exchanged different layer charge density clays. Layer charge density values (meq./g) are given in parentheses.....122

**IV 5.** TEM images of amine-cured epoxy-clay nanocomposite with clay content of 5 wt%. Exfoliated epoxy-clay nanocomposite structure obtained with (A) $CH_3(CH_2)_{15}NH_3^+$-hectorite. Intercalated epoxy-clay nanocomposite structure obtained with (B) $CH_3(CH_2)_{15}NH_3^+$- fluorohectorite and (C) $CH_3(CH_2)_{15}NH_3^+$- vermiculite.....124

**IV 6.** X-ray diffraction patterns of a: pristine $CH_3(CH_2)_{15}NH_3^+$-rectorite. b: $CH_3(CH_2)_{15}NH_3^+$-rectorite, (5 wt%) solvated by Epon-828 at 75 $^oC$, c: amine-cured epoxy composite with 5 wt% of $CH_3(CH_2)_{15}NH_3^+$-rectorite.....127

**IV 7.** TEM of amine-cured epoxy-clay exfoliated nanocomposite with $CH_3(CH_2)_{15}NH_3^+$- rectorite (5wt%).....129

**IV 8.** X-ray diffraction patterns of different organoclays in the amine-cured epoxy-clay (5 wt%) nanocomposite formation process. A: $CH_3(CH_2)_{17}NH_3^+$; B: $CH_3(CH_2)_{17}NH_2(CH_3)^+$; C: $CH_3(CH_2)_{17}NH(CH_3)_2^+$; D: $CH_3(CH_2)_{17}N(CH_3)_3^+$ a: 75 $^oC$, 5 min. b: 75 $^oC$, 1 h. c: 75 $^oC$, 2 h. d: 75 $^oC$, 2 h plus 125 $^oC$, 5 min. e: 75 $^oC$, 2 h plus 125 $^oC$, 1 h. f: 75 $^oC$, 2 h plus 125 $^oC$, 2 h.....137

**IV 9.** X-ray powder diffraction patterns of amine-cured epoxy-clay nanocomposites formed from montmorillonite clays (5 wt%) containing primary, secondary, tertiary and quaternary onium ions with a n-C18 chain.....138

**IV 10.** Tensile strength and modulus of amine-cured epoxy-clay nanocomposites with clay loading of 2 wt%.....141

**V 1.** X-ray diffraction patterns of (A) $CH_3(CH_2)_7NH_3^+$-montmorillonite and (B) $CH_3(CH_2)_{17}NH_3^+$-montmorillonite in stoichiometric mixtures of epoxide resin and polyetheramine curing agent after reaction under the following conditions: a: 75 $^oC$, 10 min; b: 75 $^oC$, 1h; c: 75 $^oC$, 3 h; d. 75 $^oC$, 3 h. and 125 $^oC$, 1 h; e: 75 $^oC$, 3 h. 125 $^oC$, 3 h. The clay loading in each case was 10 wt%.....155

**V 2.** TEM image of the D2000-epoxy clay nanocomposite containing 20 wt% $CH_3(CH_2)_{17}NH_3^+$-montmorillonite.....158

V 3. X-ray diffraction pattern of D2000-epoxy composite containing 10 wt% of $CH_3(CH_2)_{17}NH_3^+$-rectorite. Inset is the enlarged region from 1 to 10°.....160

V 4. X-ray diffraction pattern of D-2000-epoxy composite containing 10 wt% of $CH_3(CH_2)_{17}NH_3^+$-hectorite. Inset is the enlarged region from 1 to 10°.....161

V 5. X-ray diffraction patterns of $CH_3(CH_2)_{17}NH_3^+$-fluorohectorite in stoichiometric mixtures of epoxide resin and polyetheramine curing agent after reaction under the following conditions: A: 75 °C,10 min; B: 75 °C, 1h; C: 75 °C, 3 h; D: 75 °C, 3 h and 125 °C, 1 h; E: 75 °C, 3 h and 125 °C, 3 h. The clay loading in each case was 10 wt%.....164

V 6. TEM image of the D2000-epoxy clay nanocomposite containing 10 wt% $CH_3(CH_2)_{17}NH_3^+$-fluorohectorite.....165

V 7. X-ray diffraction patterns of D2000-epoxy solvated (A) and D2000-epoxy composite (B) with 10 wt% of $CH_3(CH_2)_{17}N(CH_3)_3^+$-montmorillonite.....167

V 8. X-ray diffraction patterns of D2000-epoxy solvated (A) and D2000-epoxy composite (B) with 10 wt% of $CH_3(CH_2)_{17}N(CH_3)_3^+$-fluorohectorite.....168

V 9. Dependence of tensile strength and modulus of epoxy-organoclay composites on the chain length of the clay-intercalated alkylammonium ions. The clay loading in each case was 10 wt%. The dashed lines indicate the tensile

strength and modulus of the polymer in absence of clay.....169

**V 10.** Dependence of tensile strength and modulus on clay loading for D2000-epoxy-$CH_3(CH_2)_{17}NH_3^+$-montmorillonite nanocomposites.....171

**V 11.** Comparison of tensile strengths and moduli of intercalated nanocomposites containing $CH_3(CH_2)_{17}N(CH_3)_3^+$-montmorillonite (curve A) and exfoliated nanocomposites containing $CH_3(CH_2)_{17}NH_3^+$-montmorillonite (curve B)...174

**V 12.** Comparison of tensile strengths and moduli of intercalated nanocomposites with different clay layer separation distances. Curve A: $CH_3(CH_2)_{17}N(CH_3)_3^+$-fluorohectorite with $d_{001}$ = 38.8Å. Curve B: $CH_3(CH_2)_{17}NH_3^+$-fluorohectorite with $d_{001}$ = 110 Å.....175

**V 13.** Proposed model for the fracture of (A) a glassy and (B) a rubbery polymer-clay exfoliated nanocomposite with increasing strain.....178

**VI 1.** X-ray diffraction patterns (Cu $K_\alpha$) of air dried polyamic acid-$CH_3(CH_2)_{n-1}NH_3^+$-montmorillonite complexes with clay loading of 10 wt%.....189

**VI 2.** X-ray diffraction patterns of $CH_3(CH_2)_{17}NH_3^+$-montmorillonites films solvated by DMAc. a. pristine organoclay. b. air-dried after solvation by DMAc. c. Vacuumed-dried at room temperature. d. Vacuumed-dried at 80 $^oC$.....190

**VI 3.** X-ray diffraction patterns of polyimide-clay films after heating the polyamic acid-$CH_3(CH_2)_{n-1}NH_3^+$-montmorillonite complexes with 10 wt% clay loading at 300 $^oC$.....192

**VI 4.** Dependence of the basal spacings of $CH_3(CH_2)_{n-1}NH_3^+$-montmorillonites on the carbon number, n : (A) clays dispersed in air-dried polyamic acid films, (B) air-dried pristine clays, and (C) clays dispersed in cured polyimide films. Curves A and C were obtained at clay loadings of 10 wt%.....193

**VI 5.** X-ray diffraction patterns of a polyamic acid $CH_3(CH_2)_{17}NH_3^+$ - montmorillonite complex film after different heating treatments. The clay loading is 15 wt%. a. original clay, b. air-dried polyamic acid clay film; The air-dried polyamic acid clay films have been heated at the following temperatures for 3 h. c. 100 $^oC$, d. 200 $^oC$, e. 300 $^oC$.....195

**VI 6.** TGA profile of $CH_3(CH_2)_{17}NH_3^+$-montmorillonite at 5 $^oC$/min; $N_2$ is the carrier gas. Insert is the derivative curve. 196

**VI 7.** X-ray diffraction patterns of $CH_3(CH_2)_{17}NH_3^+$-montmorillonite after different heating treatment. a. original clay, b. 200 $^oC$, 3 h; c. 300 $^oC$, 3 h; d. 400 $^oC$, 3 h; e. 600 $^oC$, 3 h.....197

**VI 8.** TEM images of polyimide-$CH_3(CH_2)_{17}NH_3^+$-montmorillonite composite films with clay content of 10 wt%. (A) exfoliated structure and (B) ordered intercalated structure.....200

**VI 9.** Proposed four steps of the formation of polyimide-clay intercalated nanocomposite. A. Solvation of DMAc and

polyamic acid to the organoclays. B. Deintercalation of alkylammonium cations through the formation of ion pairs between polyamic acid and onium ions. C. Elimination of DMAc solvent molecules. D. Thermal condensation of polyamic acid to polyimide.....202

**VI 10.** $CO_2$ permeability of polyimide-clay composites prepared by curing polyamic acid-$CH_3(CH_2)_{17}NH_3^+$montmorillonite films at 300 $^oC$. The measurements were performed on films of 2.5 cm diameter and 25 μm thickness. Curve B was generated by least-squares fitting of the permeability equation to the experimental data. Curves A and C are calculated for fillers with W/T aspect ratios of 20 and 2,000, respectively.....204

**VI 11.** Structural difference of clay normal stacking and staircase stacking.....209

**VI 12.** Proposed model for the clay fractal structure in the polyimide matrix. Same fill-in patterns indicate that the clay plates come from the same original clay aggregates.....209

**VI 13.** Comparison between exfoliated polyimide-clay nanocomposite and intercalated polyimide-clay nanocomposite.....210

## ABBREVIATIONS

| | |
|---|---|
| CEC: | Cation Exchange Capacity |
| D2000: | Texaco JEFFAMINE D2000 |
| DMAc: | Dimethyl acetamide |
| FTIR: | Fourier Transformed Infra Red |
| mPDA: | meta-phenylenediamine |
| TEM: | Transmission Electron Microscopy |
| TGA: | Thermal Gravimetric Analysis |
| XRD: | X-ray Diffraction |

# CHAPTER I

# Introduction

## A. Composite Materials

There is a truism which states that technological development depends upon advances in the field of Materials. Composite materials are extremely important simply because they process properties the individual components could achieve alone. Composite materials do not belong solely to modern technology, since nature is full of examples of wherein the idea of composite materials are utilized. The coconut palm leaf, for example, is a cantilever using the concept of fiber reinforcement. Wood is a fibrous composite: cellulose fiber in a lignin matrix. Bone is another example of a natural composite that supports the weight of different bodies. Besides these naturally occurring composites, there are many engineering materials that are composites in a very general way and have been in use for a long time, such as carbon black in rubber and cement mixed with sand. For a general composite material, the continuous phase is called the matrix, and the discontinuous phase is called the filler. According to the natures of the matrix and the filler, composites can be classified as metal/metal, metal/ceramic, ceramic/ceramic, ceramic/polymer, and polymer/polymer composites. For instance, glass fiber reinforced epoxy composite is an example of ceramic/polymer composites, concrete with a steel beam as reinforcement is called a metal/ceramic composite.

Since the early 1960's there has been an ever increasing demand for materials increasingly stiffer and stronger but lighter, in fields as diverse as space research, aeronautics, energy, civil construction and civil transportation. The demands made on materials for ever better overall performance are so great and diverse that no one material is able to satisfy them all. This led to the application of the naturally occurring composite concept into materials science. Combining different materials in an integral-composite material can satisfy user requirements. Such composite material systems result in a performance unattainable by the individual constituents and offer great advantages in flexible design. The design and fabrication of composite materials have benefited from the development of organic polymeric materials. Fiber reinforced composites have been more prominent than other types of composite for many years, owing to advances in the manufacture of high strength, light weight fibers, such as carbon fiber, silicon carbide fiber and boron fiber. The arrangement of fiber in two- and three-dimensions allows the fabrication of anisotropic composites. But the high cost of these novel fibers restricts their application to mainly high-tech areas. Fortunately, there are various materials that consist of structured analogs to these high strength fibers on the nanometer scale, such as molecular wire imogolite, layered silicates and zeolites which are examples of one-, two- and three-dimensional natural and synthetic micro assemblies. The recent development of nanocomposites provides a promising opportunity to apply micro assemblies as reinforcement in composite materials.

## B. The Nanocomposite Concept

Nanocomposites are composite materials consisting of building blocks in the nanometer or tens of nanometer size scales. Generally speaking, any composite material that contains grains or particles 1 to 100 nm across, or layers of similar thickness, can be considered a nanocomposite. The properties of nanocomposites are determined not only by the bulk properties of each of the components, but also by complex interactions between the building blocks and the interfaces between them. The types of nanocomposites that have been studied can be classified in several broad categories, such as ceramic/ceramic, metal/ceramic, metal/metal, and ceramic/polymer. Nanocomposites promise to be the wave of the future, having major implications for industry and technology.

Metal/metal nanocomposites have been found to possess remarkable mechanical, magnetic and electronic properties. The Copper/Nickel nanocomposite which processes a multilayered structure and is prepared by using sputtering techniques, has a measured strength 50% of the theoretical strength, compared to the normal 10% of conventional alloys.[1] The nanometer-scale structure greatly reduces the microscopic defects in conventional alloys. An iron/silica composite system, a metal/ceramic composite with nanometer-scale structure, has been investigated.[2,3] The system consists of iron nanoparticles dispersed in a silica matrix. By changing only two parameters; the size of the iron particle and the volume fraction occupied by iron, the electrical conductivity can be tuned by 14 orders of magnitude.[2] Ceramic/ceramic nanocomposites such as alumina/silicon carbide, prepared by grinding the constituent powders very

finely in a slurry using a ball mill and then sintering the powder mixture at a temperature of 1600 $^{o}$C, show two to five times greater toughness and strength at room temperature than single-phase materials.[4,5] The $\gamma$-$Fe_2O_3$/polymer nanocomposite is one example of a ceramic/polymer nanocomposite that has shown significant improvement in magnetic and optical properties over commercial hydrocarbon- or water-based $Fe_3O_4$ ferrofluids.[6]

The ceramic components in a ceramic/polymer nanocomposites can exist in either amorphous or crystalline phases. Amorphous phases such as silica, have been synthesized by hydrolysis followed by condensation of mononuclear species such as tetraethoxysilane (TEOS) and tetra-methoxysilane (TMOS). Silicas formed this way normally adopt a spherical particle morphology. Crystalline phases are generally layered materials, such as layered silicates,[7,8] $MoS_2$,[9] and $V_2O_5$,[10]. By the formation of ceramic/polymer nanocomposites, mechanical, optical, conductive, nonlinear optical and barrier properties can be significantly enhanced over the single components and conventional composites.

## C. Recent Advances in the Synthesis of Hybrid Organic-Inorganic Composites

The synthesis of hybrid organic-inorganic composites has been known for some time. An early method was to blend different components together, but high degrees of dispersion and strong binding between inorganic solid and organic matrix were not often achieved. Recently, treatment of the inorganic surfaces has increased the binding forces between the inorganic and organic phases,[11] but the degree of dispersion is still dependent upon

the original dimension of the inorganic solid which is usually on the order of micrometers. The synthesis of hybrid inorganic-organic composites on the nanometer scale has been achieved over the past 10 years. One approach is to apply the so-called sol-gel reaction, in which the inorganic components are formed *in situ* in the hybrid composites, via hydrolysis and condensation of mononuclear species. Self-assembly nature of inorganic and organic components has been applied in the synthesis of hybrid inorganic-organic nanocomposites, where definite layers of pre-formed organic polymer are sandwiched between the layers of inorganic hosts. *In situ* intercalative polymerization also provides a promising route for hybrid inorganic-organic nanocomposite formation, in which pre-absorbed or intercalated organic monomers in the inorganic layered host undergo polymerization. By controlling the reaction conditions, the nanocomposites with both definite and indefinite layers of organic polymer within the inorganic layered host have been obtained. For the latter nanocomposite, the inorganic layered host has an exfoliated structure in the organic polymer matrix, wherein single layers of the inorganic components are dispersed uniformly within the matrix.

## 1. Inorganic Network Formation *via* Sol-Gel Methods

One successful approach producing enhancement of the degree of mixing is the *in situ* polymerization of metal alkoxides in organic polymer matrices via the sol-gel process. Such approaches have been applied in several polymer systems such as polydimethysiloxane,[12] polytetramethyleneoxide,[13] polymethacrylate,[14] epoxy,[15] polyimide[16,17] polyvinylpyrrolidone[18] and cellulosic[19] systems. The domain size is on the nanometer scale which increases the mechanical properties of

polymethacrylate-silica composites while maintaining the high transparency of the polymer, thereby making the nanocomposites suitable for hard contact lens materials.[14] Polyimide-silica nanocomposites also exhibit greatly enhanced mechanical properties which also preserve the thermal and optical properties of the polymer.[16,17] Calcination of polyvinylpyrrolidone-silica nanocomposites gives highly porous metal oxides possessing nanometer scale pores.[18] However, owing to the loss of volatile by-products formed in the hydrolysis/condensation reactions, it is difficult to control sample shrinkage after molding.

In an effort to reduce large scale shrinkage associated with the drying of the precursor gel and improve the uniformity of the composite, novel systems with tetraalkoxy orthosilicates and polymerizable alkoxide moieties have recently been developed.[20,21] By employing *in situ* organic polymerization catalysts (ring-opening metathesis polymerization or ROMP or radicals), the alcohol liberated during the formation of the inorganic network is also polymerized. By using a stoichiometric quantity of water, and additional polymerizable alcohol as a co-solvent, all components are converted into either organic polymer or the inorganic network. Because no evaporation is necessary, large scale shrinkage is eliminated. The silica contents are controllable from 10 to 50 %, and such composites are transparent materials ranging from elastic rubbers to high modulus rigid composites.

These non-shrinking organic-inorganic nanocomposites are only possible for limited polymer systems thus far, therefore naturally occurring and synthetic inorganic materials with distinct building blocks on nanometer

dimensions may be good alternatives in the preparation of hybrid organic-inorganic nanocomposites.

## 2. Inorganic Networks from Natural or Synthetic Materials

Natural and synthetic inorganic materials with building blocks on the nanometer scale are divided into three categories: one-dimensional linear chain structures; two-dimensional layered structures and three-dimensional network structures with nanometer-scale channels. Indeed, all three kinds of inorganic solids have been used as building blocks in the preparation of nanocomposites.

The one-dimensional inorganic solid such as imogolite, has been applied in the tubular silicate-layered silicate nanocomposite catalyst.[22] Imogolite is a naturally occurring aluminosilicate mineral with a unique tunnel-like or tubular structure where the external and internal van der Waals diameters of the tubes are approximately 25 Å and 10 Å respectively. Imogolite has been intercalated into $Na^+$-montmorillonite and the combination of a layered silicate and tubular silicate afforded a novel nanocomposite catalyst with unique microporosity and Lewis acidity. The structure of the imogolite-montmorillonite nanocomposite is shown in **Figure I 1**. The application of this tubular inorganic component in some polymer matrices is being studied and may attract great attention in the future.

Studies on two-dimensional inorganic solids in the nanocomposite field is the most interesting area of inorganic-organic hybrid nanocomposites due to the variety of layered inorganic components available and the established understanding of intercalation chemistry. Either the polymer

phase or the inorganic layered host can be in the nano-phase and sometimes, for example, a pure intercalated compound, both polymer and inorganic host are on the nanometer size scale.

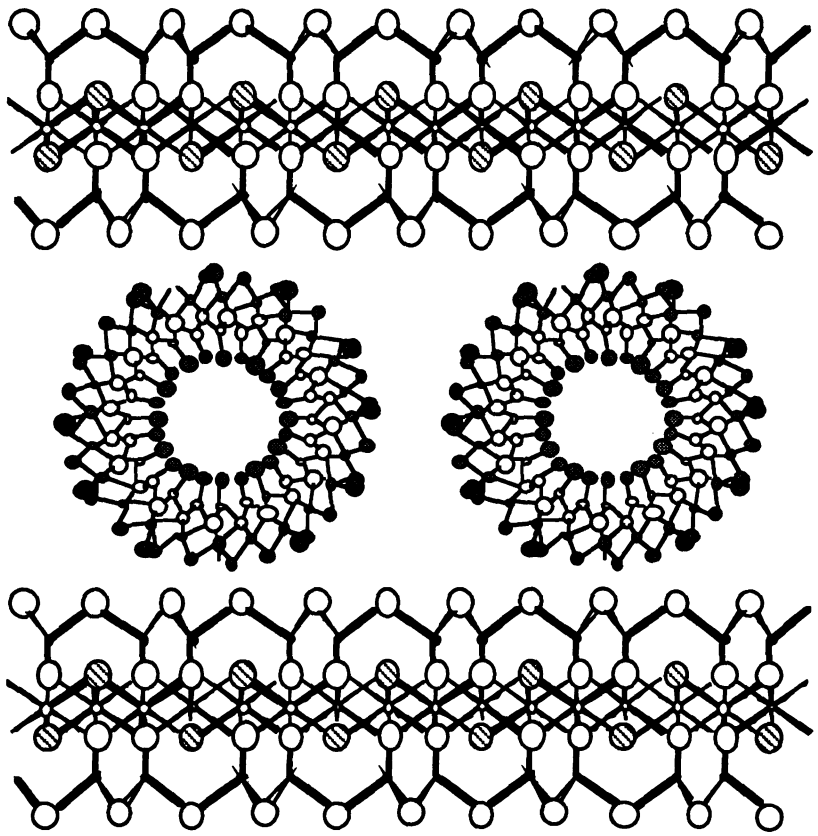


**Figure I1**. Schematic Illustration of the Tubular Silicate-Layered Silicate Nanocomposite Formed from Imogolite and $Na^{+}$-Montmorillonite.[22]

An area of intense activity involves the synthesis of electronically conducting polymers intercalated in layered solids. Pyrrole, thiophene and aniline have been intercalated and polymerized *in situ* in the interlayer space of iron oxychloride (FeOCl)[23-25] and layered vanadium oxide ($V_2O_5 \cdot nH_2O$).[26] Polyaniline intercalates have been formed by the polymerization of aniline in $Cu^{2+}$-fluorohectorite.[27-28] The spacial confinement of the polymer chains between the layered host improves the conductivity along the two-dimension directions and induces electrical anisotropy as high as $10^5$. Polymer electrolytes, such as polyethylene oxide (PEO) also have been intercalated into layered inorganic hosts including smectite clays,[29,30] $MoS_2$[31] and $V_2O_5$.[32] The helical conformational arrangement of oxythylene chains in the host galleries (**Figure I 2**), provides an environment for the mobilization of inorganic ions such as $Li^+$, thereby enhancing the efficiency of these system, which may show promise as cathodes of high-energy Li-batteries.[33]

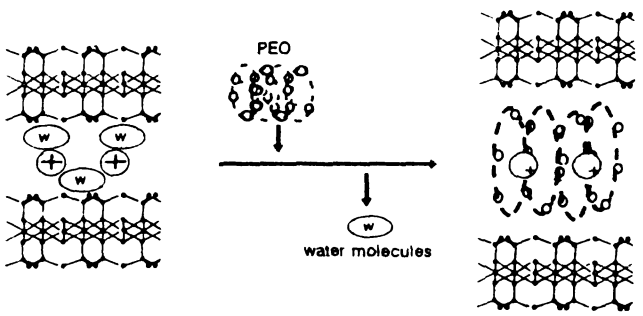



**Figure I 2.** Schematic representation of PEO intercalation in a 2:1 layered silicate, showing the replacement of the interlayer cations, water coordination shell by the polyoxyethylene chains in a helical conformation.[33]

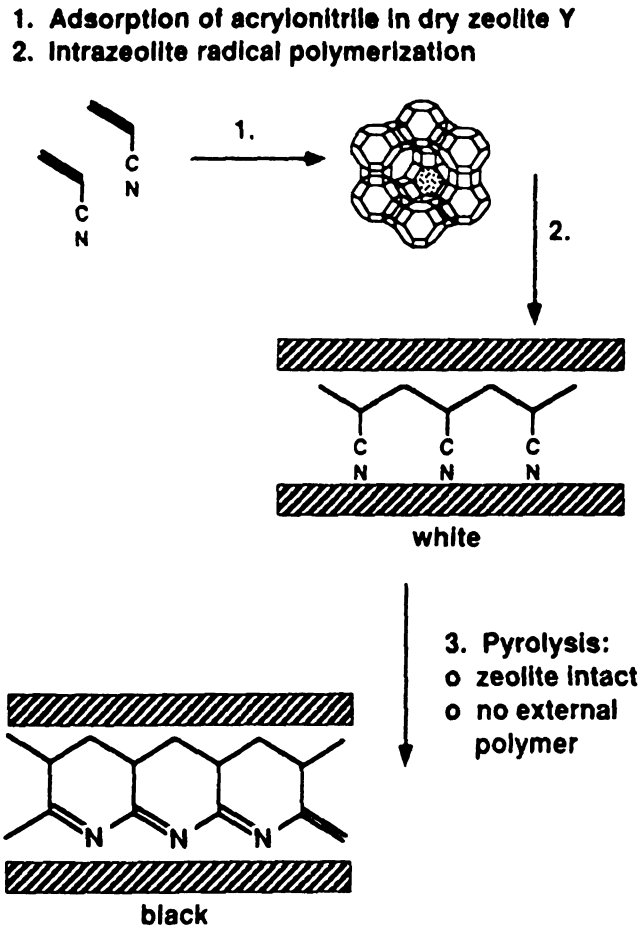
Two-dimension inorganic solids such as clay minerals have been used as reinforcement in some polymer matrices to enhance the mechanical and thermal properties, as well as barrier properties of those matrices and will be discussed in a subsequent section.

Typical three-dimension inorganic solids used in organic-inorganic hybrid nanocomposites are zeolite-type materials, in which the polymer chains are usually on the nanometer scale. The *In situ* intercalative polymerization method has been used to prepare zeolite-polymer nanocomposites.[34] For instance, acrylonitrile has been adsorbed in the inner channel systems of NaY zeolite, and polymerized to form a polyacrylonitrile-zeolite nanocomposite. This nanocomposite has been converted to a conducting material via pyrolysis, which transforms the polyacrylonitrile into a ladder polymer by cyclization through the pendant nitrile group (**Figure I 3**). With increasing pyrolysis temperature, a graphite-like structure is formed in which the delocalized electrons contribute to the electronic conductivity. The motivation of such research is to achieve charge transfer with low field as in metallic wires and to establish communication with individual electrically separated nanometer structures or molecules. Various zeolites, including the newly developed MCM-41 have been reported as hosts for such nanocomposite materials.[35] The MCM-41 has a 3-nanometer wide hexagonal channel system. Adsorption of aniline vapor into the dehydrated host, followed by reaction with peroxydisulfate, leads to encapsulated polyaniline filaments. These filaments show significant electrical conductivity while encapsulated in the channels. This demonstration of conjugated polymers with a mobile charge

carrier in nanometer channels represents a new step toward the design of nanometer size electronic devices.

Fig

**Figure I 3.** Intrazeolite polymerization of acrylonitrile.[34]



## D. Structure and Properties of Layered Silicates

The natural abundance and special structures and properties of layered alumino-silicates make clays one of the most important building blocks in the inorganic-organic hybrid nanocomposite field. Smectite clays, owing to their ion exchange, unusual intercalation and swelling properties are particularly useful in the preparation of polymer-clay nanocomposites.

### 1. Introduction to Smectite Clay Structures

Smectite clays have layer lattice structures in which two-dimensional oxyanions are separated by layers of hydrated cations.[36] The oxygen framework of a smectite layer is illustrated schematically in **Figure I 4**. The oxygen atoms define two sheets of tetrahedral sites and a central sheet of octahedral sites. The 2:1 relation between the tetrahedral and the octahedral sheets in a layer allows the smectite clays to be classified as 2:1 phyllosilicates. The type and location of cations within the oxygen frameworks determine the individual members of the smectite clay family. In a unit cell formed from 20 oxygen atoms and four hydroxyl groups, there are eight tetrahedral and six octahedral sites. When two-third of the octahedral sites are occupied by cations, the clay is termed dioctahedral. Whereas, a trioctahedral 2:1 clay has all the octahedral sites filled by cations. Montmorillonite and hectorite are typical dioctahedral and trioctahedral 2:1 clays respectively.

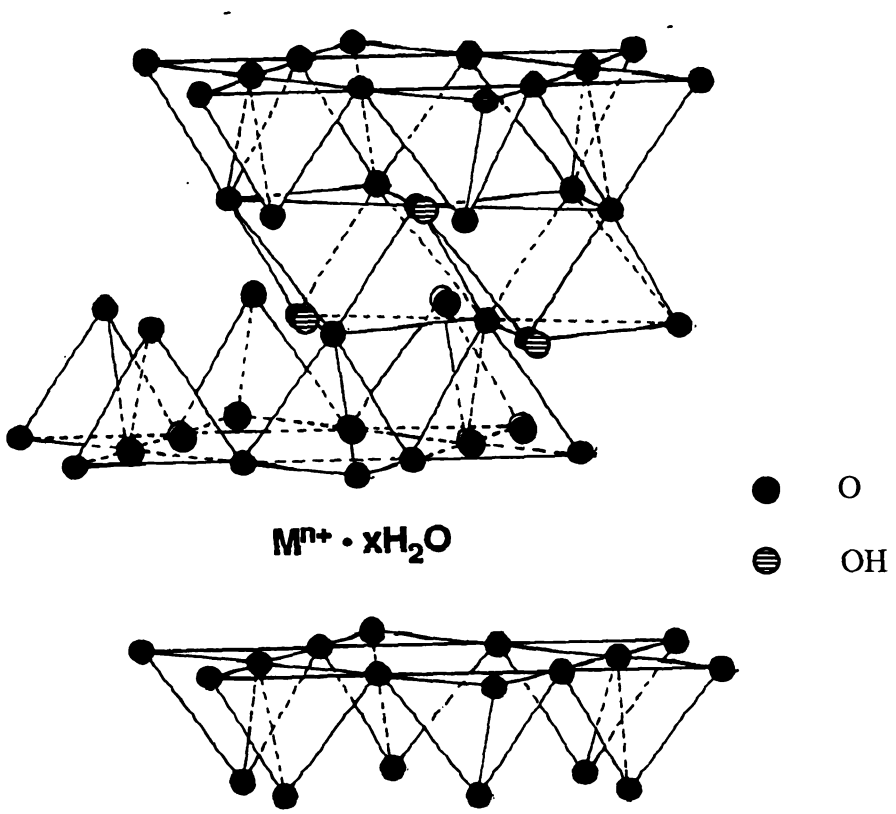



**Figure I 4.** Idealized structure of a smectite clay mineral. $M^{n+} \cdot xH_2O$ represents the interlayer exchange cation and its coordination water molecules.[36]

## 2. Introduction to Structures and Properties of Organoclays

The cation exchange capability of smectite clays is fundamental to their intercalation and swelling properties. Alkali metal and alkaline earth cations found in the pristine minerals can be replaced by almost any desired cations. Particularly novel wetting properties are obtained when the exchange ions are replaced by cationic surfactants and related long chain alkylammonium ions. Such ion exchange forms are generally referred to as organoclays.

The work of Lagaly[37-39] and co-workers has demonstrated that alkylammonium ions intercalated in smectite clay galleries form ordered assemblies in which the alkyl chains adopt specific orientations with respect to the host layers. The structures of the ordered assemblies depend in part on both the length of the alkyl chains and the charge density of the silicate host layers. Four different structural assemblies have been identified for smectite clays intercalated by long chain alkylammonium ions. These include mono- and bi-layer structures in which the long alkyl chain axes lie parallel to the silicate layers, a trimolecular structure in which the alkyl chains are kinked, and a paraffin-type structure in which the alkyl chains are inclined with respect to the silicate layers (**Figure I 5**). The mono-layer structure is favored when the clay layer charge density is low and the alkyl chain length is short. As the steric congestion within the gallery increases with increasing layer charge density, a bi-layer assemblies are formed. As the charge density increases further, tri-molecular and paraffin structures may be realized.

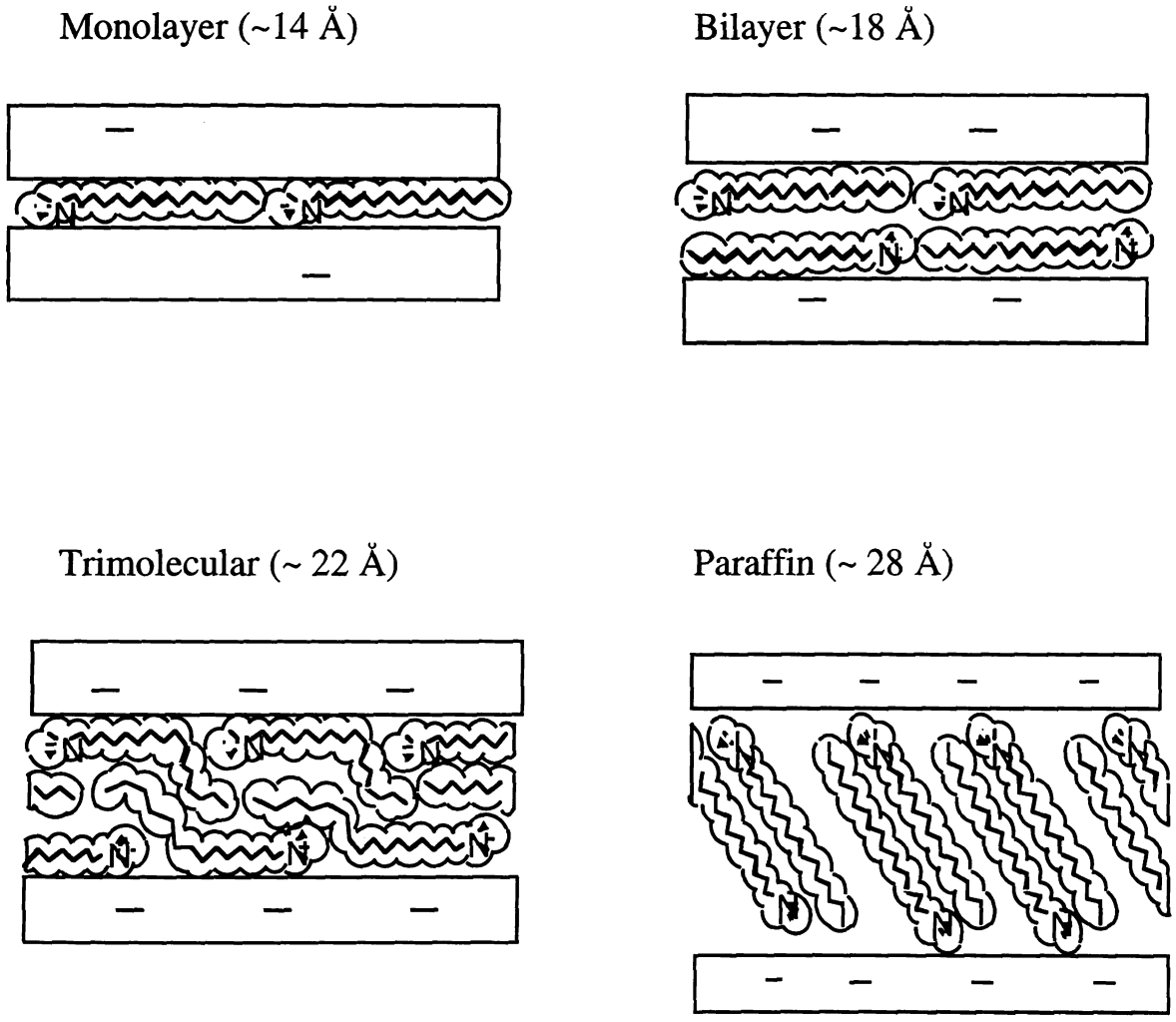



**Figure I 5**. The orientation of alkylammonium ions in the different layer charge density clays.[38]

## 3. Applications of Organoclays

Owing to the unique structures of organoclays, they have seen application as triphase catalysts,[40,41] pollutant absorbents[42,43] and additives in organic and polymer matrices. The organoclay triphase catalysts exhibit mechanistic phase transfer properties different from those of polymer supported catalysts, and have chemoselectivity and regioselectivity for different organic reactions. As absorbents for environmental pollutants, organoclays have been reported to adsorb organic contaminants, such as phenyl derivatives from aqueous solution. The sorption isotherms of benzene, toluene, ethylbenzene, propylbenzene, naphthalene and biphenyl on $C_{16}H_{33}NMe_3^+$-clays indicate that sorption occurs by intercalation with the $C_{16}H_{33}NMe_3^+$- derived phase. In general, increasing the $C_{16}H_{33}NMe_3^+$ content and basal spacings with increasing clay charge density, increased the non-ionic organic compound sorption on $C_{16}H_{33}NMe_3^+$-clays. Increased sorption of alkylbenzenes by high charge density organoclays can be attributed to the ability of the large basal spacing to accommodate these large solute molecules.

Clays have been used for decades[44-51] as fillers for a variety of plastics and rubbers. In most cases these inexpensive components simply saved on polymer costs and played no functional role in determining the performance properties of the final composites. However, researchers at Toyota have recently discovered a new family of polymer-clay composite materials that promise to revolutionize clay applications in composite formulations.[52,53]

## E. Polymer-Clay Composites

There are in general, three categories of polymer-clay composites; conventional composites, intercalated nanocomposites and exfoliated nanocomposites. As shown schematically in **Figure I 6**, conventional composites, intercalated nanocomposites and exfoliated nanocomposites exhibit important structural differences. In a conventional composite, the clay tactoids exist in their original aggregated state with no intercalation of the polymer matrix into the clay gallery regions. In an intercalated nanocomposite the insertion of polymer into the clay structure occurs in a crystallographically regular fashion, regardless of the clay to polymer ratio. An intercalated nanocomposite is normally interlayered by only a few molecular layers of polymer and the properties of the composite typically resemble those of the ceramic host.[10-13] In contrast, in an exfoliated nanocomposite, the individual 10 Å-thick clay layers are dispersed in a continuous polymer matrix by average distances that depend on loading. Usually, the clay content of an exfoliated clay composite is much lower than that of an intercalated nanocomposite. Consequently, an exfoliated nanocomposite has a monolithic structure with properties related primarily to those of the starting polymer.

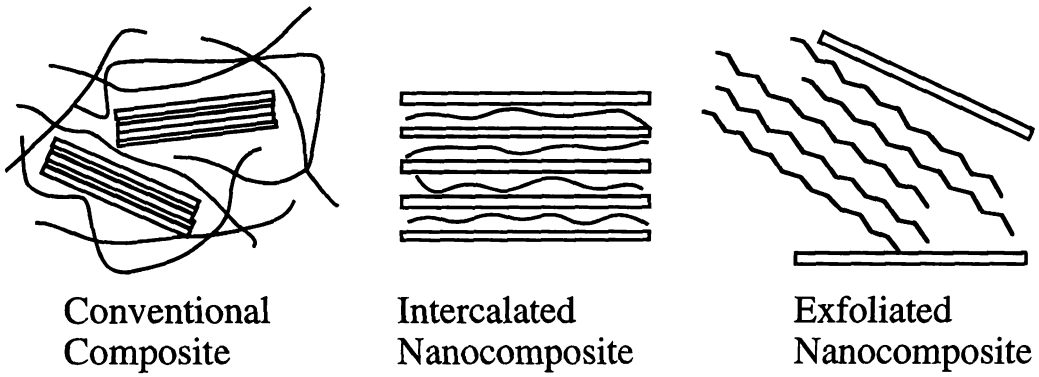



**Figure I 6.** Structural differences in conventional, intercalated and exfoliated polymer-clay composite/nanocomposites.

## 1. Conventional Polymer-Clay Composite

In conventional polymer-clay composites, mechanically crushed clay aggregates are mixed with polymer matrices, such as polyethylene,[54] polypropylene,[55] ethylene vinyl alcohol,[56] polyester,[57] and epoxy resin.[58] Some coupling agents have been applied to increase the binding between clay surfaces and polymer phase. Owing to their platy nature, clays exhibit low aspect ratios when mechanically crushed, normally 20 ~ 50. In most cases, these inexpensive clay components simply save on polymer costs and play no functional role in determining the performance properties of the final composites.

It has been reported that for conventional clay-epoxy composites, surface treatment determines processing parameters, filling limits, clay dispersions, and tensile strengths.[58] Composite strength increases in the order of surface treatment, freeze-drying < cationic surfactant alkylammonium chloride < anionic dispersant Na-polyacrylate. All the smectite clays and muscovite mica reported previously reduce the tensile strength, but enhance the tensile moduli of the composites with increasing clay loading. Therefore, the clays in a conventional polymer composite act only as fillers rather than an reinforcement.

## 2. Intercalated Polymer-Clay Nanocomposites

The intercalated polymer-clay nanocomposites are of interest because organic polymer layers and inorganic silicate layers are alternatively interstratified at the molecular level. Various polymers have been intercalated into clay galleries. Two synthetic approaches have been

rep
pre
diss
rem
poly
(EV
(PV
poly
poly
met
visc

poly
into
insi
spac
reta
beer
met
prep
poly
poly
show
inter
diffe
poly

reported to prepare intercalated polymer-clay nanocomposites. The first is preformed-polymer-intercalation. The preformed polymer and clays are dissolved and dispersed in a solvent, respectively, then mixed. Upon solvent removal, a polymer-clay intercalated nanocomposite forms. Water soluble polymers, such as polyethylene oxide (PEO),[33] polyethylene vinyl alcohol (EVOH),[59] polyvinyl alcohol (PVA),[60] and polyvinyl pyrrolidinone (PVP)[61] have been intercalated into clay galleries by this approach. Molten polymer also can be intercalated upon mixing with clays, such as polystyrene into organo-montmorillonite clays.[62] Limitations of this method are lack of convenient solvents for some polymers and the high viscosity of some molten polymers.

The second method is the so-called *in situ* intercalative polymerization method. The desired monomers are adsorbed or intercalated into the clay galleries. Then, the intercalated monomers are polymerized inside the clay galleries to form the polymer-clay nanocomposite. The basal spacing of the clay host does not change significantly and the clay particles retain the same crystallinity of the initial clay particles. This method has been utilized extensively and overcomes the disadvantages of the first method. Various polymer-clay intercalated nanocomposites have been prepared by using the second approach include polyamide (nylon-6),[63] polymethyl metharcylate,[64] polyaniline,[27] poly-ε-caprolactone,[65] polyacrylonitrile,[66] polypyrrole,[28] and polyfurfuryl alcohol.[67] **Figure I 7** shows the X-ray diffraction patterns of poly-ε-caprolactone-fluorohectorite intercalated nanocomposite. For different kinds of polymerization reactions, different polymerization initiators are required. For instance, for polyaniline-fluorohectorite nanocomposite, $Cu^{2+}$ exchanged fluorohectorite

has

poly

inter

used

oxid

has been used, because of the oxidative ability of the $Cu^{2+}$, to initiate the polymerization of aniline.[27]

Such polymer-clay intercalated nanocomposites have exhibited interesting electrical and optical properties. Furthermore, they have been used as precursors of, for example, highly-oriented graphite[68] and non-oxide ceramics[69] by heat treatment.

**Figur**
fluorc
polyn
corres
(right)

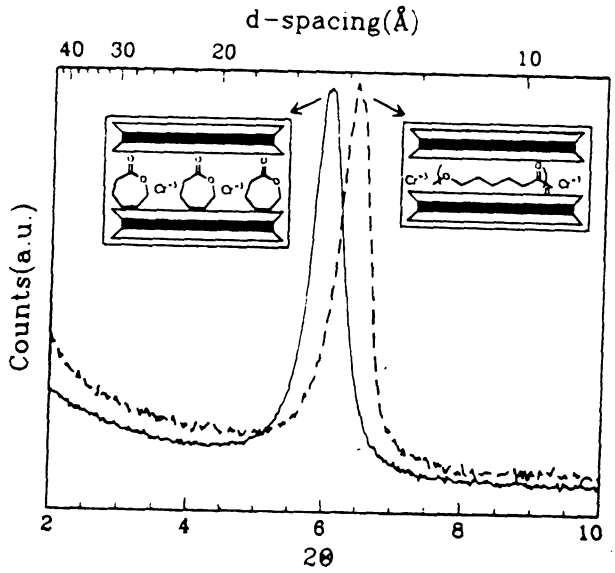



**Figure I 7.** Powder X-ray diffraction of the poly-ε-caprolactone-fluorohectorite composite before (solid line) and after (dashed line) polymerization. Insets are schematic illustrations (not drawn to scale) corresponding to the intercalated monomer (left) and intercalated polymer (right).[65]

## 3. Exfoliated Polymer-Clay Nanocomposites

Exfoliated polymer-clay nanocomposites process unique structure and properties. The exfoliated clay layers (10 Å-thick), which are dispersed inside the polymer matrix, simulate the fibers in fiber-reinforced-plastics. The successful synthesis of an exfoliated polymer clay nanocomposite requires the intercalation step plus overcoming the binding forces between the clay layers. The exfoliation process increases the aspect ratio of the embedded particles from a value of ~20 for the stacked crystallites to values of ~2000 for an exfoliated single clay sheet. The effect of the high aspect ratio platelets on the performance properties of the nylon-6 were truly spectacular.[52]

The first exfoliated polymer-clay nanocomposite was the nylon-6-montmorillonite system reported by Toyota researchers.[52,53] The montmorillonite clays are $[HOOC(CH_2)_{n-1}NH_3^+]$, n = 6 and 12, protonated amino acid exchanged clays. Intercalation of nylon-6 monomer ε-caprolactam, into the organoclay has been observed. At an elevated temperature (260 °C), the energy released from the monomer polymerization drives the exfoliation of the organoclay. The exfoliated nylon-clay nanocomposite has significant improvement of mechanical and thermal properties over the pristine polymer. For instance, the addition of ~5 wt% montmorillonite to nylon-6, increased the tensile strength and modulus, respectively, from 68.6 MPa and 1.11 GPa for the pristine polymer to 97.2 MPa and 1.87 GPa for the composite. Also, the thermal and rheological properties of the nylon were improved significantly by the nanocomposite formation. An increase in heat distortion temperature from 65 °C for nylon-

6 to 152 $^{o}$C for a nylon-clay hybrid was achieved at a 5 wt % clay loading.[70-72]

Polyimide-clay exfoliated nanocomposites have also been reported by Toyota researchers.[73,74] By simply mixing preformed polyamic acid with certain organoclays, a novel polyimide-clay composite film was obtained. From X-ray diffraction and TEM results, it was concluded that the clay was exfoliated in the polyimide matrix. The composite exhibited greatly improved barrier properties to various gases, including, $O_2$, $N_2$, Ar, and $H_2O$, due to the enhanced aspect ratio of clay plates via the exfoliation process.

Exfoliated polyether-clay nanocomposites have been prepared by the self-polymerization of an epoxy resin in the presence of acidic forms [$HOOC(CH_2)_{n-1}NH_3^+$], n= 6 and 12, of montmorillonite in our laboratory.[58,75] However, owing to their powder texture, the polyether-clay nanocomposites were not suitable for mechanical measurements.

F. R

1. N

grea
dupl
The
nano
inter
plat
poly
prim
exfo
Orga
cand

allov
their
dispe
of th
the a
galle
nano
into
clay

## F. Research Objectives

### 1. New Approaches to Polymer-Clay Nanocomposite Using Organoclays

The discovery of the nylon-6-clay exfoliated nanocomposites lead to greatly improved mechanical and thermal properties which can not be duplicated by conventional organic chemical modification of the polymer. The improvement in the performance properties is a consequence of nanoscopic composite formation, wherein the polymer structure has been interrupted on a nanometer length scale by exfoliation of 10 Å-thick clay plates. Therefore, the creation of a general synthesis of the exfoliated polymer-clay nanocomposite (rather than just the nylon-6-clay system) is the primary goal in this work. Owing to the unique structural features of the exfoliated nanocomposite, new synthetic approaches must be explored. Organoclays are hydrophobic rather than hydrophilic, and are ideal candidates for the synthesis of polymer-clay exfoliated nanocomposite.

The presence of alkylammonium ions in the organoclay galleries allows the organic molecules or polymer monomers to be intercalated into their galleries. Also the hydrophobicity of the organoclay may facilitate the dispersion of the organoclays in the monomer molecules. The chain length of the gallery ions and the layer large density determine the orientation of the alkyl chain inside the clay gallery. Organoclays with different initial gallery cation and layer charge density may perform differently in the nanocomposite synthesis. Intercalation of epoxy resin monomer, Epon-828, into different organoclays has been investigated as a model of the polymer-clay nanocomposite precursor.

The synthesis of exfoliated polyether-clay nanocomposites via self-polymerization of the epoxy resin in the presence of acidic organoclays, has been successful. However, the mechanism of the self-polymerization remains unknown. Based on our results from the intercalation of epoxy resin into organoclays and thermal differential calorimetry studies, an incisive understanding of the formation mechanism of such nanocomposites will be proposed.

The concept of the *in situ* intercalative polymerization may be applied in the preparation of exfoliated polymer-clay nanocomposites instead of the intercalated form. The fundamental difference between the synthesis of an exfoliated and an intercalated nanocomposite is the control of the separation of the clay layers in the nanocomposite formation process. The clays in an intercalated nanocomposite have a constant layer distance (basal spacing) regardless the polymer/clay ratio. In other words, the intercalated nanocomposites can be considered to be intercalation compounds. In order to achieve an exfoliated nanocomposite, expansion of the clay gallery is essential in the composite formation process. The expansion of the clay gallery polymer needs the mobile environment in the clay gallery and continuous flow of the monomer into the clay galleries. The gallery region must be sufficiently "fluid-like" under polymerization conditions to allow facile access of monomer units to the growing intragallery chains. Catalytic reaction of the polymerization inside the clay galleries may create a reactant gradient between inside and outside of the clay galleries. The epoxy-amine polymer matrix was selected based upon the commercial importance of epoxy resins and the good understanding of the epoxy-amine reaction chemistry. For the reaction between epoxy resin and curing agent (for

example, m-phenylenediamine), acidic protons act as the catalyst, therefore, alkylammonium ions with different acidities have been exchanged into the clay galleries. Together with the intercalation properties of different organoclays, an exfoliated epoxy-clay nanocomposite will be described.

The first evidence of the clay exfoliation is the absence of d$_{001}$ X-ray diffraction. The direct observation on the dispersion of the clay in the polymer matrix is possible through the TEM image of the composite materials.

**2. Relationship between Structure and Properties of Various Polymer-Clay Nanocomposites.**

The improvement of the mechanical and thermal properties achieved in the nylon-6-clay exfoliated nanocomposites is significant. The understanding of such benefits is only at the composite structure stage. Further work is required to develop a theoretical understanding of the composite morphology and polymer matrix properties, such as glass transition temperature. Nylon-6 is a semi-crystalline polymer with a glass transition temperature around 50 ~ 60 $^{o}$C. For the epoxy resin, Epon-828, by using different curing agents, the cured composites can be either rubbery ($T_g$ well below room temperature, sub-ambient) or glassy ($T_g$ well above room temperature). Epon-828 cured with m-phenylenediamine has a glass transition temperature ~ 140 $^{o}$C, and is suitable for the glassy state nanocomposite studies. Epon-828 cured with polyetheramine (MW = 2000) has a glass transition temperature ~ -50 $^{o}$C and is a good candidate for the rubbery nanocomposite studies. Tensile testing will be used to evaluate the mechanical performance of the synthetic nanocomposites, including

intercalated nanocomposites, exfoliated nanocomposites in both glassy and rubbery states.

Polyimide-clay hybrid composites reported by Toyota researchers have an exfoliated structure.[73,74] The synthetic method is the reaction between preformed polyamic acid and organoclays. For polyimide-clay hybrid composites, only the $CH_3(CH_2)_{11}NH_3^+$- rather than $CH_3(CH_2)_{11}$-$N(CH_3)_3^+$-, and $HOOC(CH_2)_{11}NH_3^+$- montmorillonite, has the exfoliated structure, while the others exhibit the interclated structure. Improvement of the gas barrier properties has been shown in the formation of the exfoliated structure without mention of the barrier properties of the intercalated products. The synthetic method is also a direct intercalation of preformed polymer into the organoclays, therefore, there is a lack of driving force for the formation of the exfoliated polymer-clay nanocomposite structure. Therefore, it is interesting to study the intercalation of polyamic acid into different organoclays, such as montmorillonite with different chain length alkylammonium ions, in order to elucidate the structure of the polyimide-clay nanocomposite and reveal the nature of the barrier property improvement. Incisive understanding of the polyimide-clay hybrid composite formation and the structure-property relationships will provide guide lines for further nanocomposite development and application.

G. R

1. T.

2. C.

3. C.
Aug.

4. A.

5. A.
448 (

6. R.
V. M

7. E.

8. T.

9. M
Kan

10. M
C.R.

11. I

12. I
War

13. I

**G. References:**

1. T.W. Barbee Jr., J. Wong, *Phys. B* (Amsterdam), **158** (1-3), 670 (1989).

2. C.L. Chien, G. Xiao, S. Hwang, US Patent 4,973,525, (1990).

3. C.M. Lukehart, J.P. Carpenter, S.B. Milne, K.J. Buranm, *CHEMTECH*, Aug. 29, (1993).

4. A. Nakahira, K. Miihara, *Fract. Mech. Ceram..*, **9**, 165 (1992).

5. A. Nakahira, C. Niihara, Nippon Seramikkusu Gakujutsu Ronbunsh, 100, 448 (1992).

6. R.F. Ziolo, E.P. Giannelis, B.A. Weinstein, M.P. O'Horo, B.N. Ganguly, V. Mehrotra, M.W. Russell, D.R. Huffman, *Sci.*, **257**, 219 (1992).

7. E.P. Giannelis, *JOM*, **44**, 28 (1992).

8. T.J. Pinnavaia, T. Lan, P.D. Kaviratna, M.S. Wang, MSR, N-4, (1994).

9. M.G. Kanatzidis, R. Bissessur, D.C. DeGroot, J.L. Schindler, C.R. Kannewurf, *Chem. Mater.*, **5**, 595 (1993).

10. M.G. Kanatzidis, C.G. Wu, H.O. Marco, D.C. Dedroot, J.L. Schindler, C.R. Kannewurf, M. Benz, E. LeGoff, *ACS Symp. Ser.*, **499**, 194 (1991).

11. B. Arkles, *CHEMTECH*, Dec., 766 (1977).

12. N.R. Langley, G.C. Mbah, H.A. Freeman, H. Huang, E.J. Siochi, T.C. Ward, G. Wilkes, *J. Colloid Interface Sci.*, **143**, 309 (1991).

13. R.H. Glaser, G.L. Wilkes, *Polym. Bull.*, **19**, 51 (1989).

14. G. Philipp, H. Schimdt, *J. Non-Crystalline Solids*, **63**, 283 (1984).

15. G. Philipp, H. Schimdt, *J. Non-Crystalline Solids*, **82**, 31 (1986).

16. S. Wang, Z. Ahmad, J.E. Mark, *Proceedings of ACS, Div. of Polymeric Materials: Science and Engineering (PMSE)*, **70**, 305 (1994).

17. M. Kakimoto, Y. Iyoku, A. Morikawa, H. Yamaguchi, Y. Imai, *Polymer Preprints*, **35-1**, 393 (1994).

18. T. Saegusa, *Proceedings of ACS, Div. of Polymeric Materials: Science and Engineering (PMSE)*, **70**, 371 (1994).

19. S.S. Shojaie, T.G. Rials, S.S. Kelley, *Proceedings of ACS, Div. of Polymeric Materials: Science and Engineering (PMSE)*, **70**, 431 (1994).

20. M.W. Ellsworth, B.M. Novak, *J. Am. Chem. Soc.*, **113**, 2756 (1991).

21. B.M. Novak, C. Davies, *Macromolecules*, **24**, 5481 (1991).

22. T.A. Werpy, L.J. Michot, T.J. Pinnavaia, *ACS Symp. Ser.* **437**, 119 (1990).

23. M.G. Kanatzidis, L.M. Targe, T.J. Marks, H.O. Marco, C.R. Kannewurf, *J. Am. Chem. Soc.*, **109**, 3797 (1987).

24. M.G. Kanatzidis, H.O. Marco, W.J. McCarthy, C.R. Kannewurf, T.J. Marks, *Solid State Ionics*, **32/33**, 594 (1989).

25. M.G. Kanatzidis, C.-G. Wu, H.O. Marco, C.R. Kannewurf, A. Kostikas, V. Papaefthymion, *Adv. Mater.*, **2**, 364 (1990).

26. M.G. Kanatzidis, C.-G. Wu, H.O. Marco, C.R. Kannewurf, *J. Am. Chem. Soc.*, **111**, 4139 (1989).

27. V. Mehrotra, E.P. Giannelis, In "Polymer Based Molecular Composites", *MRS Symp. Proc.*, D.W. Schaefer, J.E. Mark, Eds., MRS. Pittsburgh, 171, (1990).

28. V. Mehrotra, E.P. Giannelis, *Solid State Ionics*, **51**, 115 (1992).

29. E. Ruiz-Hitzky, P. Arandam, *Adv. Mater.*, **2**, 545 (1990).

30. P. Aranda, E. Ruiz-Hitzky, *Chem. Mater.*, **4**, 1395 (1992).

31. R. Bissessur, M.G. Kanatzidis, J.L. Schindler, C.R. Kannewurf, *J. Chem. Soc.*, **20**, 1583 (1993).

32. Y.-J. Liu, D.C. DeGroot, J.L. Schindler, C.R. Kannewurf, M.G. Kanatzidis, *Chem. Mater.*, **3**, 992 (1992).

33. E. Ruiz-Hitzky, *Adv. Mater.*, **5**, 334 (1993).

34. P. Enzel, T. Bein, *Chem. Mater.*, **4**, 819 (1992).

35. C.-G. Wu, T. Bein, *Sci.*, **264**, 1757 (1994).

36. T.J. Pinnavaia. *Sci.*, **220**, 365 (1983).

37. G. Lagaly, K. Beneke, A. Weiss, *American Mineralogist*, **60**, 642 (1975).

38. G. Lagaly, *Solid State Ionics*, **22**, 43 (1986).

39. A. Justo, C. Maqueda, J.L. Perez-Rodriquez, G. Lagaly, *Clay Miner.*, **22**, 319 (1987).

40. Chi-Li Lin, T. Lee, T.J. Pinnavaia, *ACS Symp. Ser.*, **499**, 145 (1992).

41. T. Lee, Ph. D. Thesis, Michigan State University, (1992)

42. S.A. Boyd, A. Jaynes, B.S. Ross, "Organic Substances and Sediments in Water", edited by R. Baker, CRC Press, Baco Raton, Florida, 181 (1991).

43. W.F. Jaynes, S.A. Boyd, *Soil Sci. Soc. Am. J.*, **55**, 43 (1991).

44. S.F. Xavier, Y.N. Sharma, *Poly. Comp.*, **7**, 42 (1986).

45. L.A. Utrack, B. Fisa, *Poly. Comp.*, **3** 193 (1982).

46. P.L. Faulkner, *Proc. 5th Intern. Conf. on Polyolefins*, Houston, TX, February 441, (1987).

47. "Plastic Additives", R. Gachter, H. Muller, Eds., Macmillan, New York, (1983).

48. "Additives for Plastics" J. Steppek, H. Daowt, Springer-Verlag, New York, (1983).

49. "Handbook of Epoxy Resins", H. Lee, K. Neville, Eds., McGraw Hill, New York, (1967).

50. "Advanced Thermoset Composites", J.M. Margolis, Ed., Reinhold, New York, (1968).

51. "Epoxy Resins Technology", J.I. Distasio, Ed., Nayes Data, New York, (1968).

52. Y. Fukushima, S. Inagaki, *J. Inclusion Phenomena*, **5**, 473 (1987).

53. Y
*Clay*
54. M
55. A
56. T
57. C
58. M
59. M
60. I
61. (
62. I
63. (
64.
65.
66.
(19
67.
**27**,
68.

53. Y. Fukushima, A. Okada, M. Kawasumi, T. Kurauchi, O. Kamigaito, *Clay Miner.*, **23**, 27 (1988).

54. M. Arina, A. Honkanen, V. Tammela, *Polym. Eng. Sci.* **19**, 30 (1979).

55. A. Rochette, L. Choplin, P.A. Tanguy, *Polym. Compo.*, **9**, 419 (1988).

56. T.C. Bissot, *ACS Symp. Ser.* **423**, 225 (1989).

57. G.M. Newaz, *Poly. Compo.*, **7**, 176 (1986).

58. M. Wang, Ph.D. Thesis, Michigan State University, (1993).

59. M. Tohoh, European Patent, 0479031A1, (1992).

60. D.J. Greenland, *J. Colloid Sci.*, **18**, 647 (1963).

61. C.W. Francis, *Soil Sci.*, **115**, 40 (1973).

62. R.A. Vaia, H. Ishii, E.P. Giannelis, *Chem. Mater.*, **5**, 1694 (1993).

63. C. Kato, K. Kuroda, M. Misawa, *Clays Clay Miner.*, **27**, 129 (1979).

64. A. Blumstein, *J. Polym. Sci.*, **Pt-A3**, 2653 (1965).

65. P.B. Messersmith, E.P. Giannelis, *Chem. Mater.*, **5**, 1064 (1993).

66. R. Blumstein, A. Blumstein, K.K. Parikh, *Apply. Polym. Symp.*, **25**, 81 (1974).

67. T.J. Bandosz, J.Jagiello, K.A.G. Amankah, J.A. Schwarz, *Clay Miner.*, **27**, 435 (1992).

68. T. Kyoyani, N. Sonobe, A. Tomita, *Nature*, **331**, 331 (1988).

69.

70.

Kar

71.

Kur

72.

Kur

73.

*Prep*

74.

*Poly*

75.

69. Y. Sugahara, K. Kuroda, C. Kato, *J. Am. Ceram. Soc.*, **67**, C247 (1984).

70. A. Usuki, M. Kawasumi, Y. Kojima, A. Okada, T. Kurauchi, O Kamigaito, *J. Mater. Res.*, **8**, 1174 (1993).

71. A. Usuki, Y. Kojima, M. Kawasumi, A. Okada, Y. Fukushima, T. Kurauchi, O. Kamigaito, *J. Mater. Res.*, **8**, 1179 (1993).

72. Y. Kojima, A. Usuki, M. Kawasumi, A. Okada, Y. Fukushima, T. Kurauchi, O. Kamigaito, *J. Mater. Res.*, **8**, 1185 (1993).

73. K. Yano, A. Usuki, A. Okada, T. Kuraychi, O. Kamigaito, *Polymer Preprints*, **32**, 65 (1991).

74. K. Yano, A. Usuki, A. Okada, T. Kuraychi, O. Kamigaito, *J. Polym Sci: Polym. Chem.*, **31**, 2493 (1993).

75. M. Wang, T.J. Pinnavaia, *Chem. Mater.*, **6**, 468 (1994).

# CHAPTER II

## Intercalation of Epoxy Monomers into Alkylammonium Cation Exchanged Clays

### A. Introduction

Nanoscopic materials have recently attracted the attention of the scientific community because of their promising novel and unique properties.[1-5] Nanoscale composite materials containing exfoliated layered silicate clays as additives in thermoplastic nylon-6 polymer matrices have been reported by the researchers at the Toyota Research Center.[6-10] Clay exfoliation in the nylon-6 matrix gives rise to greatly improved mechanical, thermal and rheological properties, making possible new materials application of this polymer matrix. However, studies of the possibility of making nanocomposite materials incorporating layered silicate clays in thermoset polymer resins are very limited.[11-14] In order to obtain nanoscopic composite materials with very good mechanical and thermal properties, it is a prerequisite that nanoscale dispersion of the inorganic layered silicate clay occurs within the organic polymer matrix. Swelling of the layered silicate clay galleries in an organic polymer matrix will facilitate uniform dispersion, especially in thermoset polymer resins prior to the thermal setting of the polymer.[15,16]

Clays are lamellar compounds, and the properties of such lamellar solids within the two-dimensional plane are very different from that in the third direction.[17] The swelling behavior of montmorillonite by water

molecules has been reported.[18-20] The inorganic cations in the clay gallery such as $Na^+$, provide an environment for water molecule coordination around the cations, and the water molecules may form monolayer or multilayer structures in the clay galleries. With increasing water content, the interlayer spacing of Na-montmorillonite increases stepwise from 10 Å to 20 Å, then jumps to 40 Å, which is followed by a linear increase in proportion to the total water content. Owing to the cation exchange properties of smectite clays, the smectite clay gallery ions can be replaced by organic cationic species, such as alkylammonium ions.[21,22] By changing the gallery cations from inorganic to organic, the surface property of the clay changes from hydrophilic to hydrophobic. The swelling of $[CH_3(CH_2)_{n-1}N(CH_3)_3]^+$ exchanged montmorillonites, where n = 1 ~ 18, by toluene was reported by Fukushima.[23,24] When n < 10, $[CH_3(CH_2)_{n-1}N(CH_3)_3]^+$-montmorillonite clays are not swollen by toluene, but when n > 12, the clays are swollen by toluene, judged by basal spacing increase from X-ray diffraction. As a result of this swelling, the alkyl chains of the gallery cations changed their initial orientations in the clay gallery to a configuration perpendicular to the silicate layers of the clays. The layer separation is limited to twice that of the alkyl chain length regardless of the excess of toluene. The swelling of $[HOOC(CH_2)_nNH_3]^+$-montmorillonite by ε-caprolactam, the monomer of nylon-6, also has been studied.[6] Upon the filling of ε-caprolactam inside the clay galleries, the protonated aminoacid molecules were arranged perpendicular to the silicate layers. From these swollen clays it is possible to obtain a nylon-6 - clay hybrid, i.e., a molecular composite of nylon-6 and montmorillonite.[6]

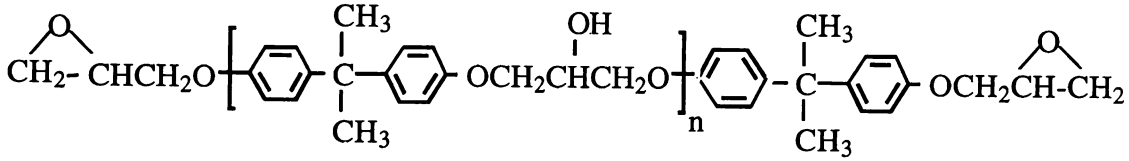
Organoclays solvated by resins function as the precursors to final composites. The intercalation of polymer resins, such as epoxy resin, could provide a better understanding of the chemistry that controls clay exfoliation in composite formation processes. We have systematically studied the solvation of an epoxy resin, Epon-828, within the alkylammonium exchanged 2:1 layered silicate clays. The effects from reaction conditions and clay nature on the resin solvation of organoclays will be discussed.

## B. Experimental

### 1. Materials

Natural hectorite and montmorillonite from California and Wyoming respectively, were obtained from the Source Clay Mineral Depository, University of Missouri, Columbia. These minerals were purified by sedimentation to exclude particles larger than 2 μm, followed by removal of carbonates by using pH5 acetate buffer solution and elimination of iron oxide by using sodium hydrosulfate. The unit cell formula of hectorite is $Na_{0.67}[Li_{0.67}Mg_{5.33}(Si_{8.00})O_{20}(OH)_4]$,[25,26] with a cation exchange capacity at 73 meq./100g.[27] The unit cell of montmorillonite is $Na_{0.86}[Mg_{0.86}Al_{5.14}(Si_{8.00})O_{20}(OH)_4]$, with a cation exchange capacity of 88 meq./100g.[28] Texas vermiculite also obtained from the Source Clay Mineral Repository was in a crystalline form, and was used after grinding to particle size less than 46 μm (325 mesh). Rectorite was obtained from Bao-Tou,[29] China and purified by the same method as stated for hectorite. The chemical composition for rectorite is $[(Na_{0.72}K_{0.02}Ca_{0.05})$-$(Ca_{0.24}Na_{0.07})](Al_{4.00}Mg_{2.00})[Si_{6.58}Al_{1.12}]O_{22}$, with a cation exchange capacity of 60 meq./100g.[29] Synthetic fluorohectorite, $Li_{1.60}[Li_{1.60}Mg_{4.40}(Si_{8.00})O_{20}F_4]$, from Corning Glass, Corning, New York, with a particle size larger than 2 μm and a cation exchange capacity of 140 meq./100g of air-dried clay was used as received.

Epoxy resin, Epon-828 from Shell Co. with an average molecular weight of 380 was used as received.



n = 0 (88%); n = 1 (10%); n = 2 (2%).

Long chain primary alkylamines $CH_3(CH_2)_{n-1}NH_2$, where n = 4, 6, 8, 10, 12, 16 and 18, secondary, tertiary and quaternary alkylammonium chloride or bromide ($CH_3(CH_2)_{17}NH_3^+$, $CH_3(CH_2)_{17}N(CH_3)H_2^+$, $CH_3$-$(CH_2)_{17}N(CH_3)_2H^+$ and $CH_3(CH_2)_{17}N(CH)_3^+$) salts were purchased from Aldrich Chemicals and used as received.

2. Preparation of Organoclays

The cation exchange reaction was carried out by mixing 500 ml of 0.05 M alkylammonium chloride ethanol:water (1:1) solution and 2.0 g of clay at 70 ~ 75 $^oC$ for 24 h,[27,30] The exchanged clays were washed with ethanol:water (1:1) several times until no chloride was detected with 1.0 M $AgNO_3$ solution and then air dried. Finally, the clays were ground and the particle size fraction of 40 ~ 50 μm was collected.

3. Intercalation Reaction

A 5 wt% onium ion exchanged clay (40 ~ 50 μm fraction) was uniformly dispersed in the Epon-828 monomer by mixing the clay at 75 $^oC$ for 30 minutes. About 0.02 g of the mixture was placed on a glass slide and

a thin film of the epoxy-clay complex was thereby prepared for X-ray diffraction measurements. Epoxy-clay intercalative complexes mixed at different temperatures were also obtained and measured by X-ray diffraction at room temperature.

4. Physical Measurements

Powder X-ray diffraction measurements were carried out for different epoxy-clay complexes. The scanning rate was $2^{o}$ $2\theta$ $min^{-1}$ from $1^{o}$ to $20^{o}$ 2 $\theta$. The diffractometer utilized was a Rigaku Rotaflex Ru-200BH rotating anode X-ray diffractometer, equipped with a Cu target with a curved crystal graphite monochromator as the radiation source (Cu $k\alpha$) and operated at 45 KV and 100 mA.

## C. Results and Discussion

Intercalation of epoxy resin monomers into the organoclay galleries can be observed by the basal spacing change in the X-ray diffraction patterns. The **Figure II 1** shows typical X-ray diffraction patterns of the organoclay before and after solvation by epoxy resin monomer. These patterns clearly demonstrate that after epoxy resin solvation, the initial diffraction peak due to the organoclay (17.6 Å) disappears, and new diffraction peaks at 34.1 Å and 17.1 Å appear. The 34.1 Å and 17.1 Å peaks correspond to the (001) and (002) diffractions of the epoxy resin solvated organoclay. X-ray diffraction results of epoxy intercalation into organoclays show that when organoclays are dispersed in the epoxy resin, a series of distinct diffraction peaks corresponding $d_{00l}$ diffraction can be observed. This indicates that the epoxy resin solvated organoclays retain a highly ordered layer stacking structure.

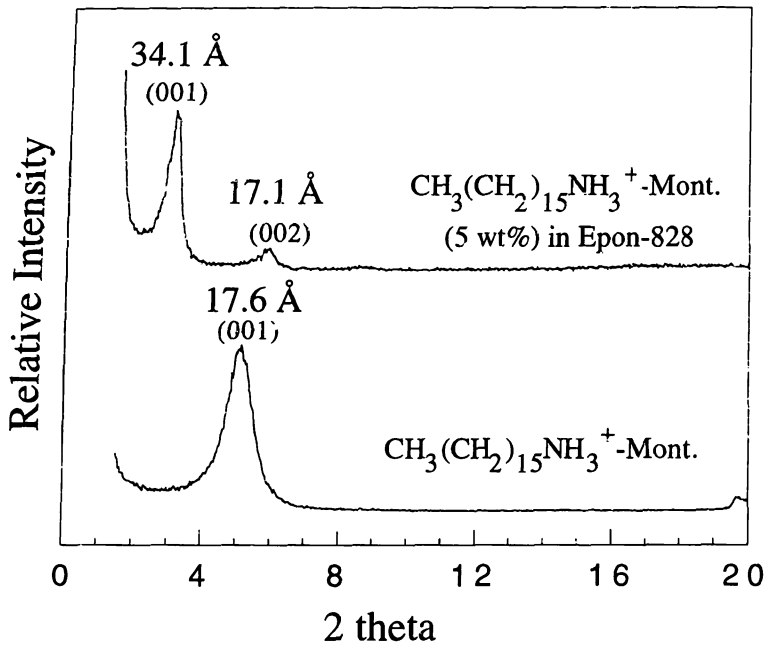



**Figure II 1**. X-ray diffraction patterns of a typical intercalation of epoxy resin monomers into organoclays.

1. Reaction time Effect

The solvation process of the organoclay in the epoxy resin includes the dispersion of the clay in the liquid resin and penetration of the epoxy monomer into the clay galleries. The time needed for the epoxide-organoclay system to reach an equilibrium is important for nanocomposite preparation. Therefore the effect of reaction time on the swelling behavior of the alkylammonium exchanged clays by the epoxy monomer was studied. Interestingly, the basal spacing of $CH_3(CH_2)_{15}NH_3^+$-montmorillonite clay in the epoxy resin monomer at 75 $^oC$ is almost time independent, as shown in **Figure II 2**. In other words, the epoxy monomer migrates into the clay galleries immediately when the epoxy comes in contact with the clay. This is believed to be caused by the organophilic nature of the long chain alkylammonium cation exchanged clays.

2. Reaction Temperature Effect

Reaction temperature determines the viscosity of the reaction system and reactant molecule mobility. We studied the effect of temperature on the intercalation of epoxy monomer into $CH_3(CH_2)_{15}NH_3^+$-montmorillonite clay from room temperature to 105 $^oC$. The reaction time is 15 min for each temperature. If the temperature is higher than 105 $^oC$, the epoxy monomer turns to undergo self-polymerization. The basal spacings of the intercalated $CH_3(CH_2)_{15}NH_3^+$-montmorillonite at different temperatures are listed in **Table II 1**.

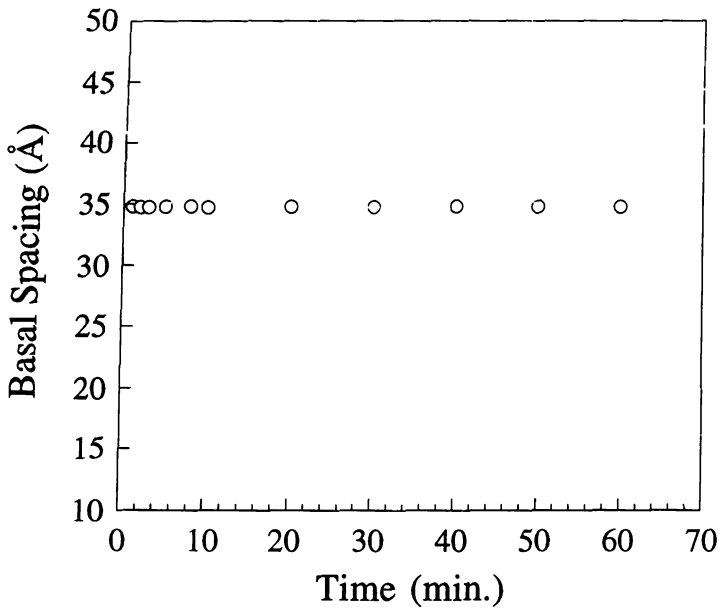



**Figure II 2.** Time dependence of epoxy resin intercalation into $CH_3(CH_2)_{15}NH_3^+$-montmorillonite (5 wt%) at 75 °C.

**Table II 1.** Basal spacing of $CH_3(CH_2)_{15}NH_3^+$-montmorillonite in Epon-828 at different temperatures

| Temperature ($^oC$) | $d_{001}$, Å |
|---|---|
| $CH_3(CH_2)_{15}NH_3^+$-Mont. only | 17.6 |
| 25.0 | 18.3 |
| 50.0 | 33.7 |
| 75.0 | 34.4 |
| 90.0 | 37.1 |
| 105.0 | 37.6 |

The results of the clay basal spacings at different temperatures indicate that the organoclays do not swell or the epoxy resin does not penetrate the clay galleries at 25 $^oC$, simply due to the high viscosity of the epoxy monomer at low temperatures. However, when the epoxy resin is heated to about 50 $^oC$, the viscosity of the resin decreases drastically and penetration into the clay galleries can be observed. The basal spacing increases very slightly from 50 $^oC$ to 105 $^oC$. It may be due to the fact that the mobility of epoxy monomer increases with increasing temperature. Therefore, there are more epoxy monomers in the clay galleries at higher than at lower

temperatures. The electrostatic forces between the intergallery cations and the negatively charged clay layers limit the expansion of the gallery region.

3. Effect of Gallery Cation Chain Length

Organoclays with different chain length cations and layer charge densities have different chain orientations in the air-dried state. For a clay with a certain layer density, with increasing chain length the cation orientation changes from lateral monolayer to lateral bilayer to paraffin structures. Organoclays with different chain length alkylammonium ions are expected to have different affinity to monomer resins. In order to investigate the dependence of swelling on chain length of the exchanged alkylammonium cations, a series of alkylammonium ions was used as the intergallery cations. **Table II 2** shows that the basal spacing of the epoxy monomer intercalated clay increases significantly with increasing chain length. According to Lagaly's results,[31] the initial orientation of long chain alkylammonium cations is dependent on both the chain length and the clay layer charge. Basal spacings for $CH_3(CH_2)_{n-1}NH_3^+$-montmorillonite (n = 4, 8, 10, 12, 16 and 18) solvated by the epoxy resin are compared with those for the pristine air-dried clays. Upon solvation (intercalation) by the epoxy resin monomers, the gallery spacings increase. Assuming that the gallery cations reorient from their original monolayer or bilayer orientations to a vertical orientation relative to the clay layer after the epoxy solvation, we calculated the basal spacings from the relationship $d_{001}$ = 12.8 Å+ (n - 1)*1.27 Å+ 3.0 Å, where 12.8 Å is the basal spacing for $NH_4^+$-montmorillonite, 3.0 Å for the -$CH_3$ end group of the alkyl chain and (n - 1) * 1.27 Å is the contribution due to the -$CH_2$- chain segments, when all the segments adopt *trans.* configurations.[32] For $CH_3(CH_2)_3NH_3^+$-

montmorillonite, the observed basal spacing is smaller than the calculated value, due to the low hydrophobicity of the relatively short alkyl chain. For montmorillonite with alkyl chains of 8 or more carbon numbers, the basal spacing of the epoxy solvated organoclay is slightly larger than or almost equal to the calculated values for a vertical onium ion orientation. The size of the epoxy monomer estimated from computer modeling is 14.6 Å x 4.4 Å x 3.5 Å. Therefore, for $CH_3(CH_2)_3NH_3^+$-montmorillonite, there is one monolayer of epoxy intercalated into the clay gallery, and for the alkyl chain longer than 8, there are multiple layers of epoxy monomers inside the galleries. This indicates that access of the epoxy monomer to the gallery is mediated by the chain length of the gallery cations.

Epoxy resin solvation in montmorillonites with primary, secondary, tertiary and quaternary alkylammonium species having the same alkyl chain length of 18 including: $CH_3(CH_2)_{17}NH_3^+$, $CH_3(CH_2)_{17}N(CH_3)H_2^+$, $CH_3$-$(CH_2)_{17}N(CH_3)_2H^+$ and $CH_3(CH_2)_{17}N(CH)_3^+$ was studied to confirm the chain length control on the epoxy resin solvation degree. The basal spacing results are listed in **Table II 3**. Although these montmorillonites have different basal spacings before epoxy solvation, because of the bulky -$CH_3$ groups, the epoxy solvated clays have essentially the same basal spacing which is controlled by the $C_{18}$ long alkyl chain.

**Table II 2.** Basal Spacings ($d_{001}$, Å) of Alkylammonium Exchanged Montmorillonite.

| Gallery Cations | Cation Orientation[a] | Air-Dried | Epoxy Solvated | Calculated Value[b] |
|---|---|---|---|---|
| $CH_3(CH_2)_3NH_3^+$ | monolayer | 13.5 | 16.5 | 19.6 |
| $CH_3(CH_2)_7NH_3^+$ | monolayer | 13.8 | 27.2 | 24.7 |
| $CH_3(CH_2)_9NH_3^+$ | monolayer | 13.8 | 30.0 | 27.2 |
| $CH_3(CH_2)_{11}NH_3^+$ | bilayer | 15.6 | 31.9 | 29.8 |
| $CH_3(CH_2)_{15}NH_3^+$ | bilayer | 17.6 | 34.1 | 34.9 |
| $CH_3(CH_2)_{17}NH_3^+$ | bilayer | 18.0 | 36.7 | 37.4 |

a. Orientation of the alkylammonium ion under air-dried conditions.

b. Basal spacings are calculated assumed the gallery cation adopts a vertical orientation relative to the layer. $d_{001}$= 12.8 + 3.0 + (n - 1) x 1.27 (Å), where 12.8 Å is the $d_{001}$ of $NH_4^+$-montmorillonite, 3.0 Å is the size of -$CH_3$ end group and 1.27 Å is the distance increase upon adding one -$CH_2$- group in the chain.[32]

**Table II 3.** Basal Spacings ($d_{001}$, Å) of Air-Dried Organoclays and Their Epoxy-Solvated Analogues (75 °C).

| Gallery Cations ( -montmorillonite ) | Air-Dried | Epoxy Solvated |
|---|---|---|
| $CH_3(CH_2)_{17}NH_3^+$ | 18.0 | 36.7 |
| $CH_3(CH_2)_{17}N(CH_3)H_2^+$ | 18.1 | 36.2 |
| $CH_3(CH_2)_{17}N(CH_3)_2H^+$ | 18.7 | 36.7 |
| $CH_3(CH_2)_{17}N(CH_3)_3^+$ | 22.1 | 36.9 |

4. Effect of Clay Layer Charge Density

The gallery cation orientation in an organoclay is determined by not only the alkyl chain length, but also the layer charge density of the clay. With constant cation alkyl chain length, increasing the layer charge density changes the orientation of the cations from lateral bilayer to paraffin structure.[31] In order to further confirm that the chain length controls the epoxy solvation to the organoclay galleries, 2:1 layered silicates with different charged densities were selected. The basal spacings of hectorite, montmorillonite, fluorohectorite and vermiculite having alkylammonium cation, $CH_3(CH_2)_{15}NH_3^+$ and their epoxy resin solvated analogues are given in **Table II 4**.

Even though, the initial orientations of alkylammonium cations of these clays is different, the observed data for the epoxy resin solvated clays show a very similar orientation (basal spacing) after being solvated by the epoxy monomer. The gallery height is about 25 Å for all the clays studied, which is about the length of the $C_{16}$ alkyl chain. This indicates that different clays with the same exchangeable cation show the same pattern of swelling. Therefore, it is reasonable to conclude that the gallery height of the swollen clay is determined mainly by the chain length of the intergallery cation rather than the clay layer charge density.

**Table II 4**. Basal Spacings of Air-dried Organoclays Containing $CH_3(CH_2)_{15}NH_3^+$ as Exchanged Cations in Their Dry States and Solvated State by the Epoxy Resin, Epon-828.

| Clay ($CH_3(CH_2)_{15}NH_3^+$-) | Charge Density ($e^-/O_{20}(OH)_4$) | Cation Orientation | Air Dried Clay (Å) | Epoxy Solvated (Å) | Layer Expanding (Å) | Gallery Height (Å) |
|---|---|---|---|---|---|---|
| Hectorite | 0.66 | bilayer | 18.0 | 35.3 | 17.3 | 25.7 |
| Montmorillonite | 0.86 | bilayer | 17.6 | 34.1 | 16.5 | 24.5 |
| Fluorohectorite | 1.20 | paraffin | 28.0 | 33.7 | 5.7 | 24.1 |
| Vermiculite | 1.60 | paraffin | 28.6 | 34.9 | 6.3 | 25.3 |
| Rectorite | 0.70 | bilayer | 29.4 | 45.1 | 15.7 | 25.1 |

On the basis of our observations, a model is proposed to explain the swelling of onium exchanged clay by the epoxy monomers (**Figure II 2**). When the epoxy molecules are intercalated in the clay galleries, the orientation of the intergallery cations changes from their initial states (in general, long chain alkylammonium cations lie parallel to or stand up at an angle to the clay layers[31]) to a perpendicular position. It is also possible that the gallery cations stand up as a result of the solvation by epoxy monomers within the gallery region. Therefore, the gallery height is determined by the chain length of the interlayer alkylammonium cations.

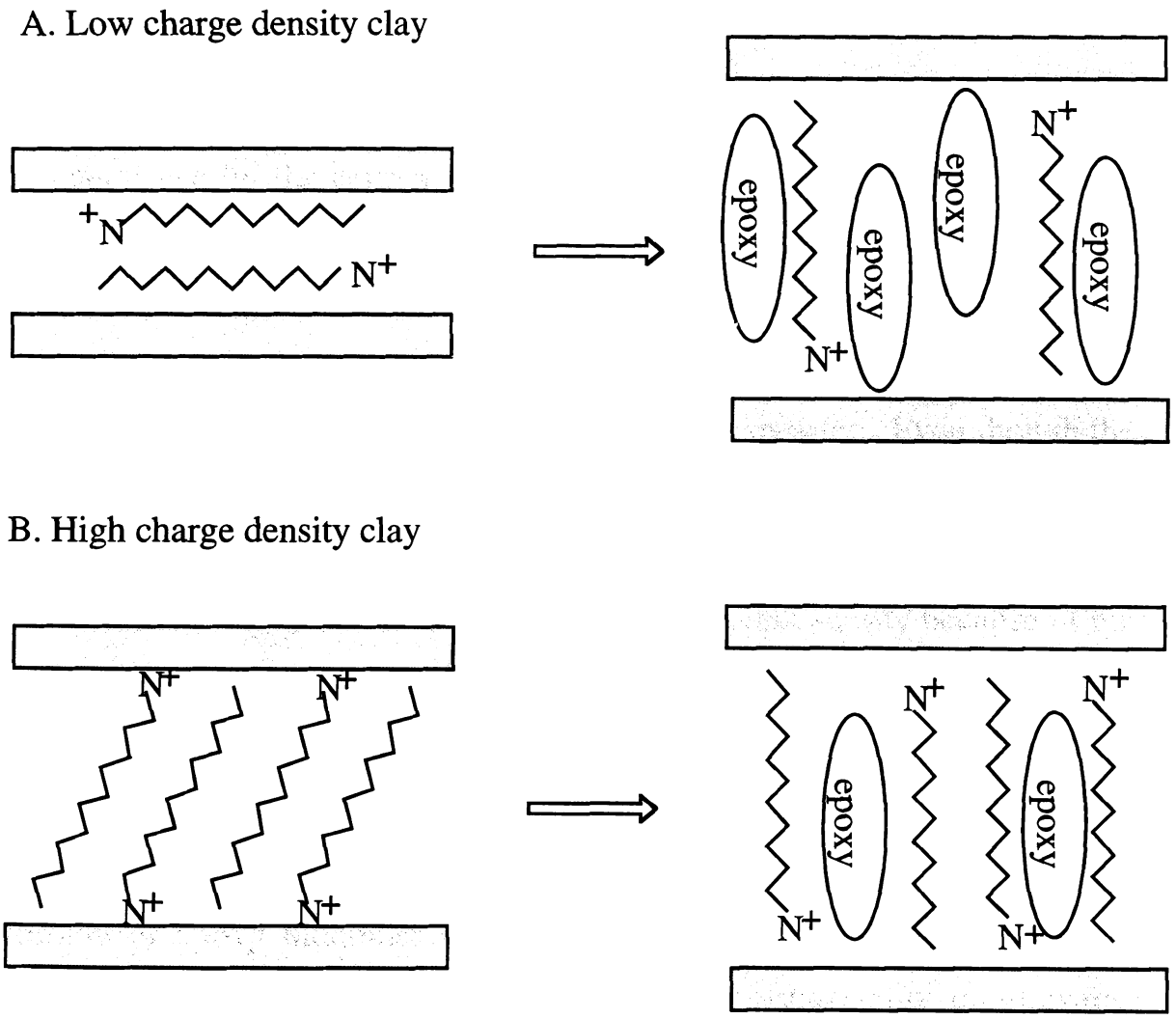



**Figure II 3**. Proposed model for the swelling of alkylammonium exchanged clay by Epon-828. A: low charge density clay with a lateral bilayer structure and B: high charge density clay with paraffin structure. Regardless of the initial charge density of the clay and orientation of the gallery alkylammonium cations, the final gallery height is determined by the vertical orientation of the organocations in the solvated intercalates.

## D. Conclusion

The solvation (swelling) of organoclays by the epoxy resin, Epon-828, is determined by the resin viscosity and hydrophobicity of the clays. The extent of solvation of organoclays by the epoxy resin monomer is dependent on the chain length of the intergallery cations. Organoclays solvated by the epoxy resin having different gallery heights provide a variety of precursors for the preparation of nanoscale polymer-clay composites. Even though the clays with different layer charge densities but with the same intergallery cations show the same swelling properties, the amount of epoxy monomers that enter the clay galleries is expected to be different simply because of the different amount of alkylammonium ions in the gallery. The higher the concentration of alkylammonium cations, the lower the number of epoxy monomers that can penetrate the gallery because of the stuffing effect. The gallery expansion after intercalation by epoxy resin monomers indicates the amount of epoxy monomer in the clay galleries. This provides different precursors for the preparation of nanoscale polymer-clay composites. Therefore, by judicial choice of the gallery cations as well as the layer charge density of the clay it is possible to control the extent of swelling and the amount of epoxy monomer in the clay galleries. These factors could provide an excellent method of manipulation of the epoxy-clay composite composition and thereby control the thermal and mechanical properties of the resulting nanocomposites.

## E. References

1. G.M. Whitesides, J.P. Mathias, C.T. Seto, *Sci.*, **254**, 1312 (1991).

2. T.A. Werpy, L.J. Michot, T.J. Pinnavaia, *ACS Symp. Ser.*, **427**, 119 (1990).

3. E.P. Giannelis, *JOM*, **44**, 28 (1992).

4. V. Mehrotra, E.P. Giannelis, *Solid State Ionics*, **51**, 115 (1992).

5. E. Ruiz-Hitzky, *Adv. Mater.*, **5**, 334 (1993).

6. Y. Fukushima, S. Inagaki, *J. Inclu. Phenom.*, **5** , 473 (1987).

7. Y. Fukushima, A. Okada, M. Kawasumi, T. Kurauchi, O. Kamigaito, *Clay Miner.* **23**, 27 (1988).

8. A. Usuki, M. Kawasumi, Y. Kojima, A. Okada, T. Kurauchi, O. Kamigaito, *J. Mater. Res.*, **8**, 1174 (1993).

9. A. Usuki, Y. Kojima, M. Kawasumi, A. Okada, Y. Fukushima, T. Kurauchi, O. Kamigaito, *J. Mater. Res.*, **8**, 1179 (1993).

10. Y. Kojima, A. Usuki, M. Kawasumi, A. Okada, Y. Fukushima, T. Kurauchi, O. Kamigaito, *J. Mater. Res.*, **8**, 1185 (1993).

11. A. Usuki, T. Mizutani, Y. Fukushima, M. Fujimoto, K. Fukumori, Y. Kojima, N. Sato, T. Kurauchi, O. Kamigaito, U.S. Patent 4,889,885 (1988).

12. K. Yano, A. Usuki, A. Okada, T. Kuraychi, O. Kamigaito, *Polymer Preprints*, **32**, 65 (1991).

13. K. Yano, A. Usuki, A. Okada, T. Kuraychi, O. Kamigaito, *J. Polym. Sci: Polym. Chem.*, **31**, 2493 (1993).

14. P.D. Kaviratna, T. Lan, T.J. Pinnavaia, *Polymer Preprints*, **35-1**, 788 (1994).

15. T. Lan, P.D. Kaviratna, T.J. Pinnavaia, *Polymer Preprints*, **35-1**, 823 (1994).

16. T. Lan, P.D. Kaviratna, T.J. Pinnavaia, *Proceedings of ACS, Div. of Polymeric Materials: Science and Engineering (PMSE)*, **71**, 527 (1994).

17. T.J Pinnavaia, *Sci.*, **220**, 365 (1983).

18. K. Norrish, *Disc. Faraday Soc.*, **18**, 120 (1954).

19. R.K. Hawkins, P.A. Egelstall, *Clays Clay Miner.*, **28**, 19 (1980).

20. Y. Fukushima, *Clays Clay Miner.*, **32**, 320 (1984).

21. A. Weiss, *Angew. Chem. Internat. Ed.*, **2**, 134 (1963).

22. A. Weiss, *Clays Clay Miner.*, **10**, 191 (1963).

23. Y. Fukushima, Surfactant in Solutions, 6, 1697, Proc. 5th Int. Sym. On surfactant in Solution, Bordeaux, France, Eds., Mittal, Bothorel, M. P. Plenum Publishing Co. New York, (1984).

24. Y. Fukushima, *Nippon Kinzoku Gakkai Kaiho*, **29**, 125 (1990).

25. S. Landau, Ph. D. Thesis, "Physical and Catalytic Properties of Hydroxy-Metal Intercalateed Smectite Minerals" Chemistry Department, Michigan State University, (1985).

26. J.M. Millsand, M.A. Zwarich, *Clays Clay Miner.*, **20**, 169 (1972).

27. Chi-Li Lin, Ph. D. Thesis "Organoclays as Triphase Catalysts" Chemistry Department, Michigan State University, (1988).

28. J. Butrulle, T.J. Pinnavaia, "Characterization of Catalytical Materials" I.E. Wachs, Ed. Butterworth-Heinemann, Boston, 149 (1992).

29. J. Guan, E. Min, Z. Yu, Proc. 9th Congr. Cata., Calgary, Canada, Vol. 1, ed. M. Phillips and M. Ternan, Chem. Inst. Canada, Ottawa, 104 (1988).

30. Chi-Li, Lin; T, Lee; T.J. Pinnavaia, *ACS Symp. Ser.*, **499**, 145 (1992).

31. G. Lagaly, *Solid State Ionics*, **22**, 43 (1986).

32. G. Lagaly, K. Beneke, A. Weiss, *American Mineralogist*, **60**, 642 (1975).

# CHAPTER III

## Mechanistic Studies of the Formation of Polyether - Clay Exfoliated Nanocomposites with Epoxide Self-Polymerization in Acidic Smectite Clays

### A. Introduction

Nanoscopic materials have recently attracted the attention of the scientific community because of their promising novel and unique properties.[1-5] Clays and related complex layered oxides have been recognized as potentially useful filler materials because of their high aspect ratios (10-2000) and platy morphology.[6] In order to realize the high aspect ratio of a single clay layer, new methods should be investigated to expand the clay gallery height to a relatively large value compared with the 10 Å thickness of a single clay layer.

Intercalation[7-9] of polymers and *in situ* intercalative polymerization[10-14] of monomers within the clay galleries has been reported. Seminal work on polymer-clay composites by Toyota researchers has led to the discovery of several nanoscale polymer-clay hybrid composites, including systems based on the dispersion of ω–amino acid and alkylammonium exchanged forms of montmorillonite in thermoplastic semicrystalline nylon-6,[15-18] thermoset epoxy[19] and polyimide polymers.[20,21] The properties of polymer-clay hybrids such as mechanical and thermal stabilities, are generally far superior to those of the pristine polymer or conventional composite materials.

A new type of polymer-clay nanocomposite has been prepared by the spontaneous self-polymerization of an epoxy resin, the diglycidyl ether of bisphenol A (DGEBA), and the concomitant delamination (exfoliation) of acidic forms of montmorillonite at elevated temperatures.[22-24] The polyether-clay nanocomposite has the 10 Å-thick clay layers dispersed uniformly in the polyether matrix. The acidic smectite clays are prepared by ion exchange reaction of the pristine montmorillonite with $H^+$, $NH_4^+$ and protonated ω-amino acid $[H_3N(CH_2)_{n-1}COOH]^+$, as well as protonated amines such as, $[H_3N(CH_2)_nNH_3]^{2+}$, $[H_3N(CH_2)_nNH_2]^+$, and $[CH_3(CH_2)_{n-1}NH_3]^+$, (n = 6 and 12). It has been reported that the epoxide polymerization-clay delamination temperature (PDT) is dependent upon both the clay basal spacings and acidity of clay gallery cations.[24] Higher acidity and larger basal spacings lower the PDT. The mechanism of the polymer-clay nanocomposite formation, especially the path way of clay exfoliation, is unknown. An understanding of the polyether-clay nanocomposite formation mechanism is essential in order to synthesize other novel polymer-clay nanocomposites. After studying the intercalation of the epoxy monomers into organoclays, intercalated epoxy-clay complexes were selected for studying the mechanism of polyether-clay nanocomposite formation. Our results clearly indicate that the acidity of the clay gallery cation plays a major role in catalyzing the epoxy self-polymerizations, especially the intragallery polymerization. Kinetics of the epoxy self-polymerization elucidates the mechanism of the formation of polyether-clay nanocomposites. In DSC studies, two distinct exotherm features associated with the epoxy polymerization - clay delamination reactions have been observed. The lower temperature process is attributed to the polymerization of the epoxide on the internal gallery surfaces where the proton

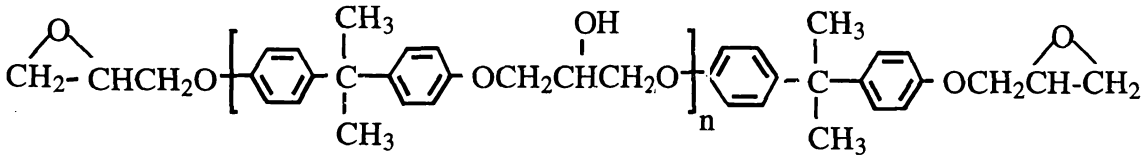
concentration is at a maximum. Polymerization of the epoxide monomer on the external surfaces of the clay particles is responsible for the higher temperature reaction. Owing to the powder form of the polyether-clay nanocomposites, they are not acceptable as structural materials.

## 2. Experimental

### 1. Materials

Natural montmorillonite from Wyoming was obtained from the Source Clay Mineral Depository, University of Missouri, Columbia. The mineral was purified by sedimentation to exclude particles larger than 2 μm, followed by removal of carbonates by using pH5 acetate buffer solution and elimination of iron oxide by employing sodium hydrosulfate. The unit cell of montmorillonite is $Na_{0.86}[Mg_{0.86}Al_{5.14}(Si_{8.00})O_{20}(OH)_4]$, with a cation exchange capacity of 88 meq./100g.[25]

Epoxy resin, Epon-828 was obtained from Shell Co. with an average molecular weight of 380.



n = 0 (88%); n = 1 (10%); n = 2 (2%).

Long chain primary alkylamines $CH_3(CH_2)_{n-1}NH_2$, where n = 4, 6, 8, 10, 12, 16 and 18, were purchased from Aldrich Chemicals and used as received.

The cation exchange reaction was carried out by using 500 ml of 0.05 M alkylammonium chloride ethanol:water (1:1) solution and 2.0 g of clay at 70 ~ 75 °C for 24 h,[26,27] The exchanged clays were washed with ethanol:water (1:1) several times until no chloride was detected with 1.0 M

$AgNO_3$ solution and air dried. Finally, the clays were ground and the 40 ~ 50 μm fraction was collected.

2. Polyether-Clay Nanocomposite Formation

An epoxy resin-clay mixture was prepared prior to the composite formation. 10 wt% of onium ion exchanged clay (40 ~ 50 μm fraction) was dispersed in Epon-828 monomer uniformly by mixing the clay at 75 $^{o}C$ for 30 minutes. The nanocomposites were synthesized by heating the epoxy resin-clay mixture in a beaker to the epoxy polymerization-clay exfoliation temperature at a heating rate of around 10 $^{o}C\ min^{-1}$. As the temperature increased, the epoxy resin-clay mixture turned more viscous and finally a liquid-to-powder transformation of the mixture took place within one minute. The liquid-to-powder transformation is an exothermic reaction, which could increase the reaction system temperature up to 50 $^{o}C$. The exact reaction temperatures were determined by differential scanning calorimetry (DSC).

3. Physical Measurements

FTIR spectra were obtained on an IBM Single Beam FTIR-44 spectrometer. Liquid and solid spectra were obtained by placing the liquid sample on a KBr plate or by pressing the solid sample into a KBr pellet.

X-ray powder diffraction patterns were recorded on a Rigaku Rotaflex Ru-200BH rotating anode X-ray diffractometer. The diffractometer was equipped with a Cu-$K_\alpha$ radiation source with a curved crystal graphite monochromater and was operated at 45 KV and 100 mA.

DSC measurements were carried out on a Du Pont 910 differential scanning calorimeter at desired heating rates with $N_2$ as the purging gas. The samples of epoxy resin-clay mixtures for DSC analysis were hermetically sealed in aluminum sample pans.

## C. Results and Discussion

### 1. X-ray Diffraction Studies on Polyether-Clay Nanocomposites

The reaction of the epoxy resin, Epon-828, with the acidic forms of montmorillonite at temperatures in the range 150 - 300 °C resulted in the polymerization of the epoxy resin and the concomitant delamination of the clay structure.[22-24] At the polymerization-delamination temperature a dramatic liquid-to-powder transformation occurred which increased the bulk volume of the reaction mixture by a factor of 4 - 6. The first evidence of clay delamination is the absence of $d_{00l}$ X-ray reflections after the reaction (**Figure III 1**). By comparing the X-ray diffraction pattern (c) with (a) and (b), we notice that after the liquid-to-powder transformation the product does not have a $d_{001}$ of either the original clay or the epoxy solvated clay. However, the diffraction peaks of the clay ($d_{011}$) at 4.52 Å and ($d_{060}$) at 1.50 Å are observed in the product. The existence of clay ($d_{011}$) (4.52 Å) reflections suggests that the clay 2-D structure remains intact after the nanocomposite formation. X-ray diffraction patterns for the clay, the epoxy-clay complex and the polyether-clay nanocomposite at high angle diffraction ($d_{060}$) also indicate the clay 2-D structure has not been destroyed after the nanocomposite formation.

The absence of the $d_{00l}$ reflection in the reaction product indicates that the clay stacking order along the z-direction has been disrupted in the composite formation process. The dispersion of the clay in the polyether matrix is no longer in a tactoid fashion as in conventional and intercalated polymer composites (**Chapter I**). In other words, an exfoliated nanocomposite with 10 Å-thick single clay layers dispersed at the molecular

level in a polyether matrix has been achieved. Further studies on the product by TEM (Transmission Electron Microscopy), FTIR and DSC confirm this conclusion.

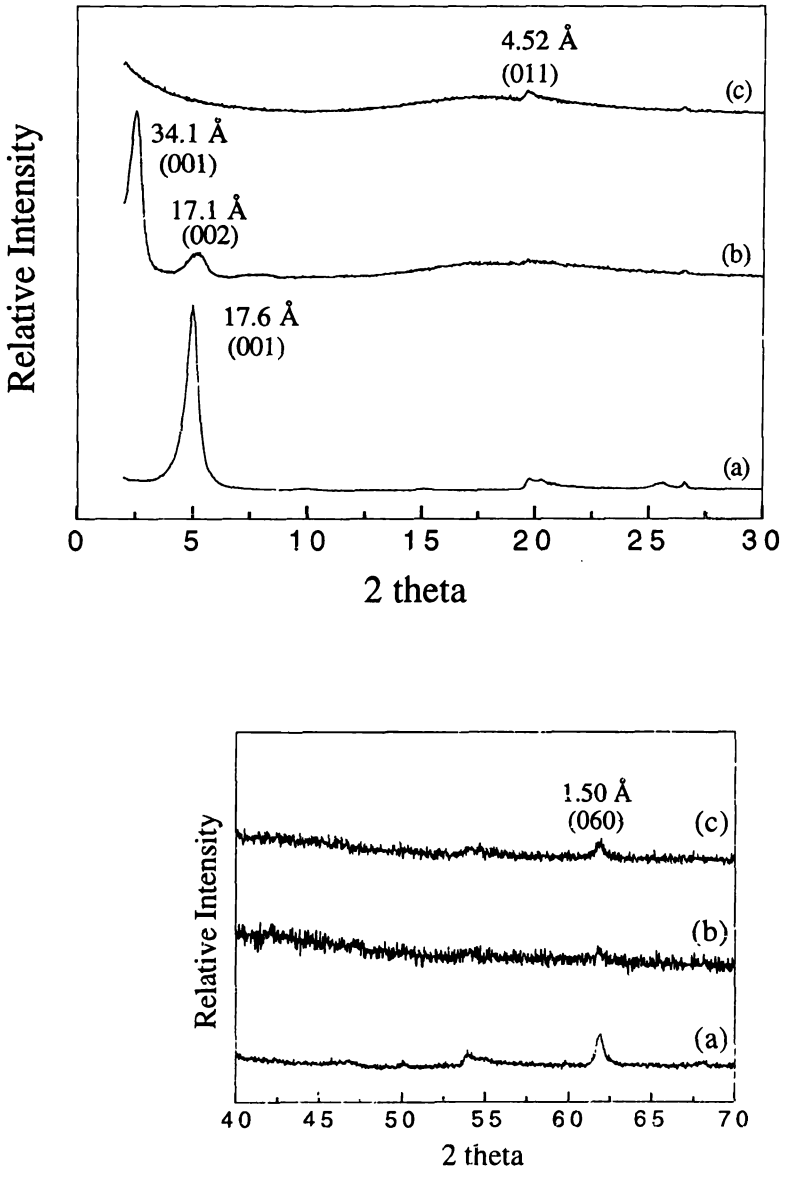
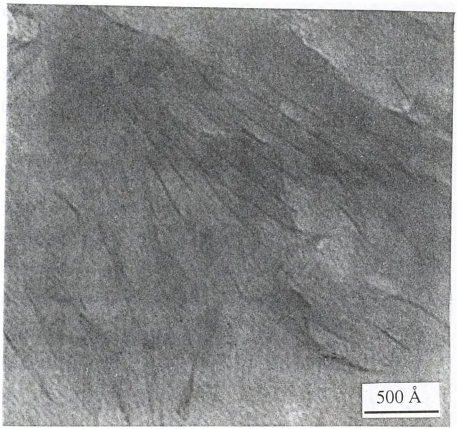



**Figure III 1.** X-ray diffraction patterns for (a) $CH_3(CH_2)_{15}NH_3^+$-montmorillonite air-dried at 25 °C; (b) $CH_3(CH_2)_{15}NH_3^+$-montmorillonite (5 wt%) intercalated with Epon-828; and (c) reaction product of Epon-828 with $CH_3(CH_2)_{15}NH_3^+$-montmorillonite (5 wt%) upon heating to 200 °C.

## 2. TEM Studies of Polyether-Clay Nanocomposites

In order to determine the clay layer separation in the polyether matrix, TEM images have been recorded of thin-sections of the polyether-clay nanocomposites. TEM of the polyether-clay nanocomposite with 5 wt% of $CH_3(CH_2)_{15}NH_3^+$-montmorillonite is shown in **Figure III 2**. The dark lines are the cross-sections of the 10 Å-thick silicate layers. The TEM micrograph reveals that the clay tactoids have been expanded by the polymer into accordion-like packets in which the interlayer spacing is up to 500 Å. Also the morphology of the exfoliated clay particles in the composite reflects the initial stacking of the clay layers. This TEM micrograph is quite similar to those observed from polyether-clay nanocomposites synthesized with ω-amino acid exchanged montmorillonites.[24]

**Figure III 2**. TEM image of polyether-clay nanocomposite formed by epoxy self-polymerization in the presence of 5 wt% of $CH_3(CH_2)_{15}NH_3^+$-montmorillonite.


500 Å

3. FTIR Studies on Polyether-Clay Nanocomposites

Although the formation of the polyether-clay nanocomposites has been reported.[22-24] The FTIR spectra associated with the reactants and products have not been shown. We used FTIR to observe the presence of the epoxide ring in order to monitor the epoxy polymerization process. The characteristic absorption bands of the epoxy resin in the IR region at 916 and 1184 $cm^{-1}$ represent the epoxide ring vibration and H-benzene ring in-plane deformation, respectively.[28,29] FTIR spectra of the epoxy resin-acidic clay reaction products are presented in **Figure III 3**. It is very clear that after the liquid-to-powder transformation of the mixture, the 916 $cm^{-1}$ epoxide ring band disappears, whereas the 1184 $cm^{-1}$ H-benzene ring band remains. The disappearance of the epoxide absorption peak in the FTIR results indicates that the epoxide groups undergo ring-opening polymerization to form a polyether upon heating.

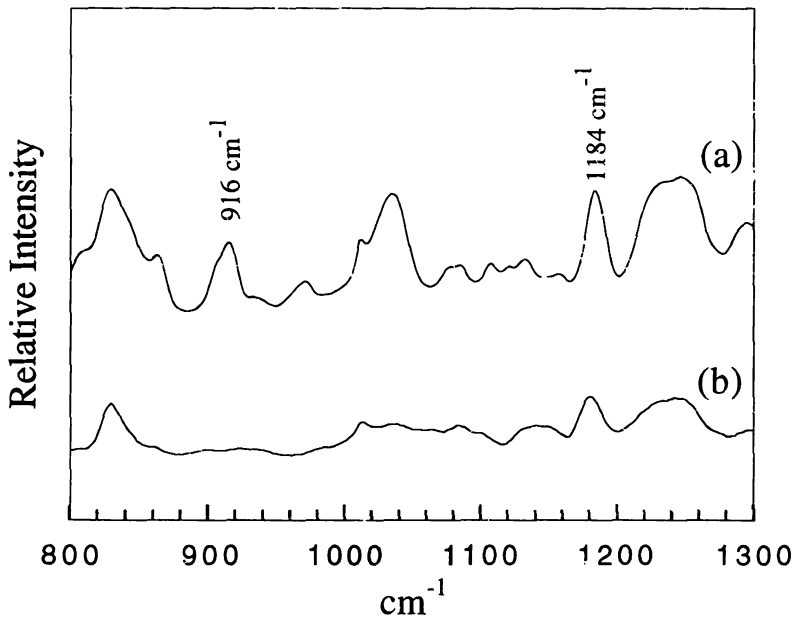



**Figure III 3**. FTIR spectra of (a) Epoxy resin (Epon-828) and (b) Reaction product between Epon-828 and $CH_3(CH_2)_{15}NH_3^+$-montmorillonite (5 wt%) upon heating to 200 $^oC$.

3. DSC Studies of Nanocomposite Formation

Differential scanning calorimetry is used to measure the difference in energy input of a substance and a reference material as a function of temperature. As the energy change in the epoxy-polymerization clay delamination is very significant, DSC is suitable to determine the reaction onset temperature and enthalpy changes. Previous results[24] have shown that delamination temperature is dependent on the heating rates and the initial basal spacing of the clay. We have systematically studied the dependence on the reaction onset temperature of the different alkylammonium montmorillonite clays, heating rates and clay loadings to reach a full understanding of the reaction mechanism.

DSC measurements were carried out to study the self-polymerization of epoxy in the presence of alkylammonium exchanged montmorillonite clays. The epoxy-clay mixtures were heated at a constant rate, and with increasing temperature, the enthalpy changes associated with the reaction corresponding to the temperature were recorded. It was very interesting to note that two exotherms were observed in the DSC profiles (**Figure III 4**). The epoxide polymerization-clay delamination temperature is determined from the onset temperature of the first peak. The onset temperature is derived from the intersection of the initial tangent and the final tangent of the DSC curve (inset in **Figure III 4**). The changes in enthalpy obtained by integrating the two exothermic peaks are listed in **Table III 1**. By varying the heating rate of the measurement, we observed a shift of the polymerization reaction peak temperatures (**Figure III 5**).

**Table III 1.** Onset Temperatures and Enthalpy Changes Associated with the Polyether-Clay Nanocomposite Formation for Different Alkylammonium Montmorillonite Clay Systems.

| Gallery Cation (-montmorillonite)* | $T_{onset}$ ($^{o}C$) | $\Delta H$** ($KJmol^{-1}$) |
|---|---|---|
| $CH_3(CH_2)_7NH_3^+$ | 185.0 | 480.0 |
| $CH_3(CH_2)_9NH_3^+$ | 170.0 | 473.9 |
| $CH_3(CH_2)_{11}NH_3^+$ | 151.0 | 458.8 |
| $CH_3(CH_2)_{15}NH_3^+$ | 144.0 | 477.0 |
| $CH_3(CH_2)_{17}NH_3^+$ | 136.0 | 495.3 |

* The clay content is 5 wt% and heating rate is 5 $^{o}Cmin^{-1}$.

**The enthalpy changes have been normalized by clay weight percentage.

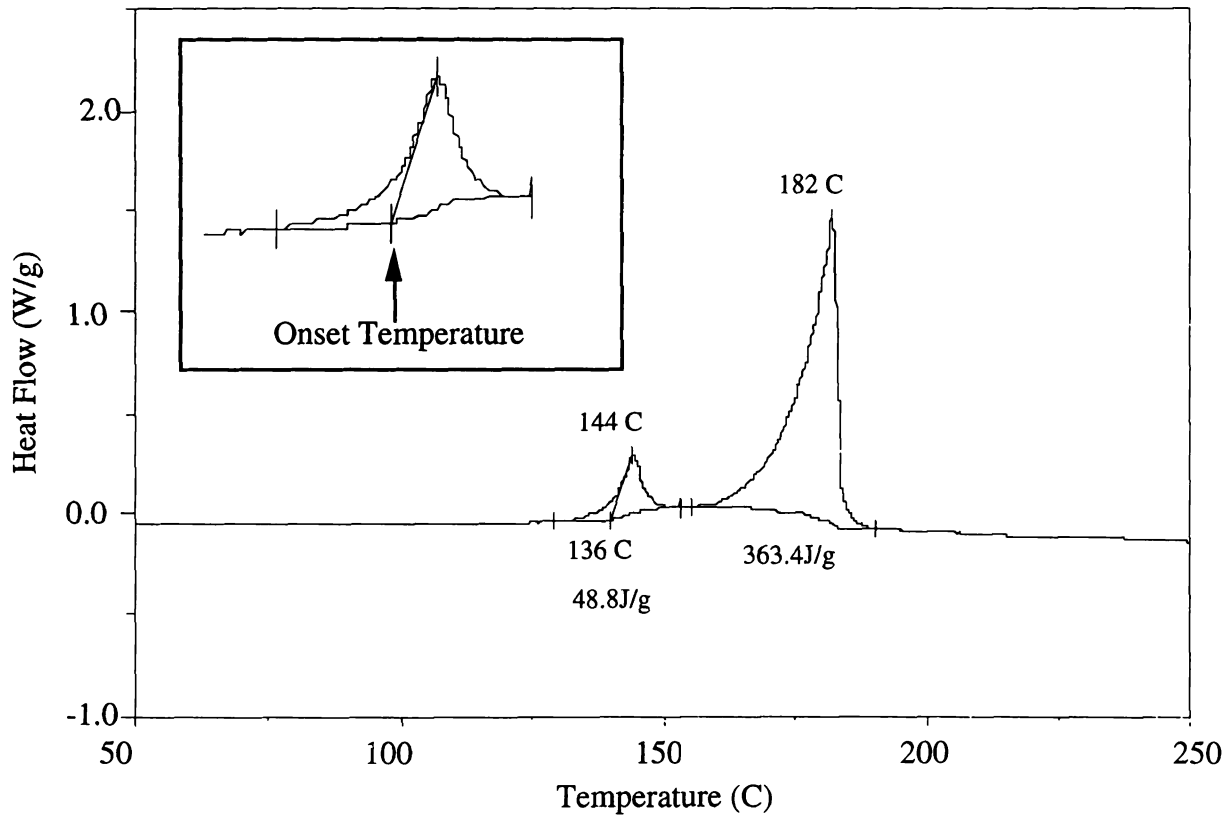
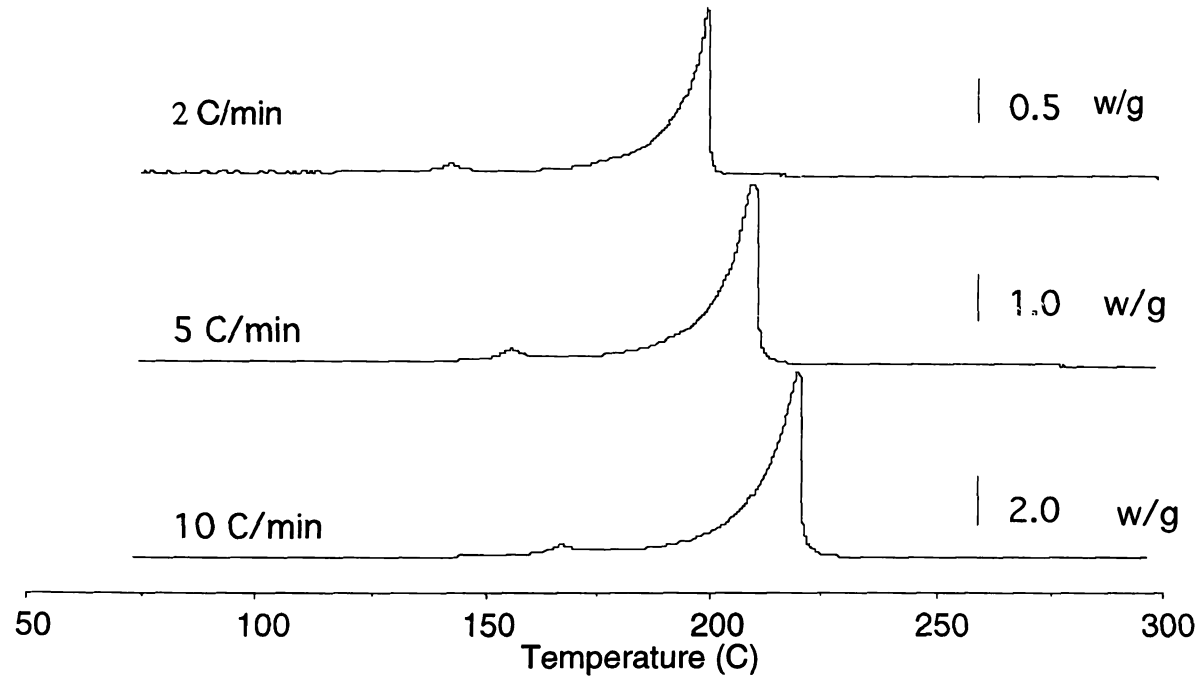


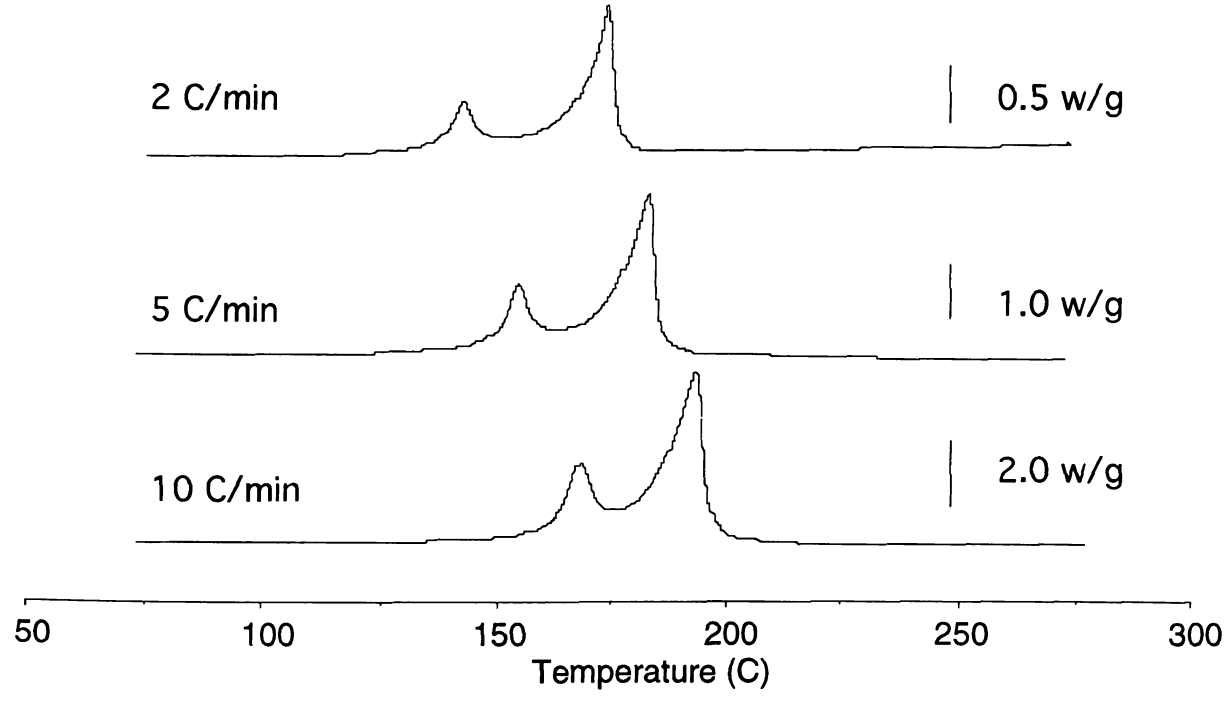

**Figure III 4**. DSC curve for the polymerization of Epon-828 epoxy resin in the presence of 3 wt% $CH_3(CH_2)_{17}NH_3^+$-montmorillonite at a heating rate of 5 $^oCmin^{-1}$. The inset defines the reaction onset temperature.

The two exothermic peaks associated with the polymerization - delamination process may provide incisive insight in the reaction mechanism. The dependence of the enthalpy changes associated with the first peak and the second peak, on the clay loading in the reaction system, as well as the dependence of reaction peak positions on the experimental heating rate was expected. DSC studies of the epoxy-clay systems with different $CH_3(CH_2)_{17}NH_3^+$-montmorillonite contents and different heating rates have been carried out (**Figure III 5**).

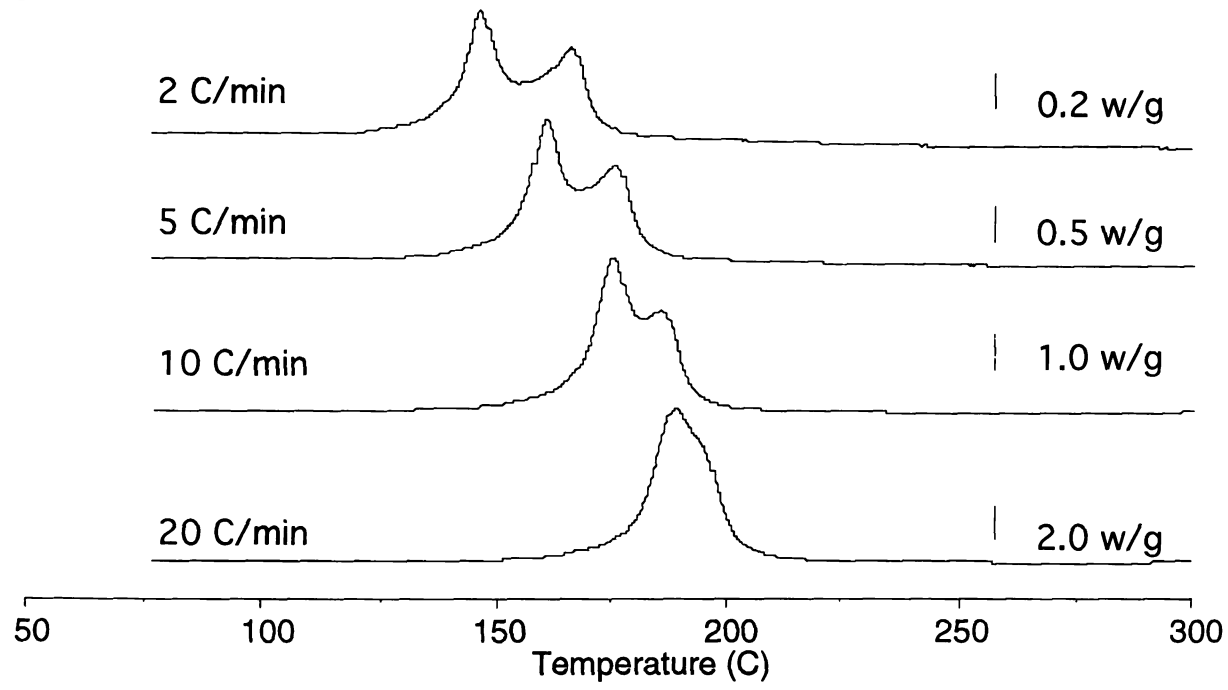
A


2 C/min
0.5 w/g
5 C/min
1.0 w/g
10 C/min
2.0 w/g
50
100
150
200
250
300
Temperature (C)

B


2 C/min
0.5 w/g
5 C/min
1.0 w/g
10 C/min
2.0 w/g
50
100
150
200
250
300
Temperature (C)

C




D

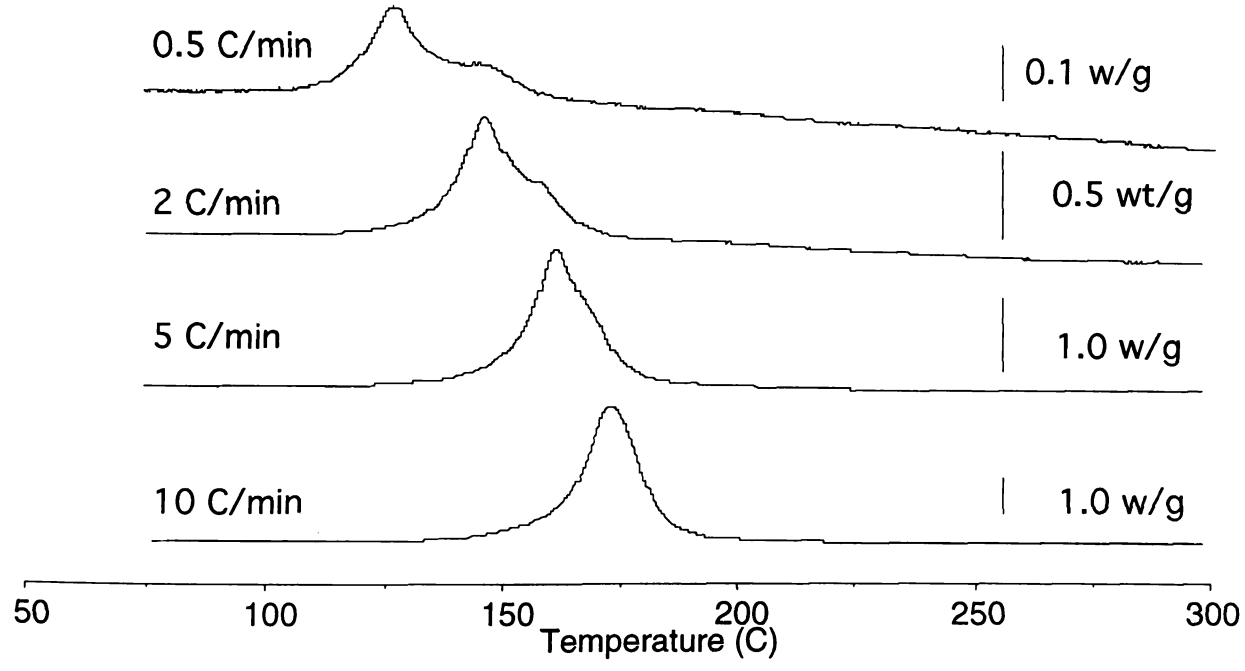



**Figure III 5**. DSC curves for the polymerization of Epon-828 epoxy resin in the presence of $CH_3(CH_2)_{17}NH_3^+$-montmorillonite at different heating rates. The clay loadings are (A) 1 wt%, (B) 5 wt%, (C) 10 wt%, and (D) 15 wt%.

From the DSC curves presented above (**Figure III 5**), it is observed that for the epoxy-clay systems with different clay loadings (1 - 15 wt%), the two exothermic peaks are significant. With increasing clay loading from 1 % to 15 %, the separation of the two exothermic peaks appears to be smaller. The separation of the two peaks is more distinguishable when a slow heating rate is applied. For example, for the reaction system with 10 % clay at a heating rate of 20 $^{o}C\ min^{-1}$, only one peak is observed, but for the same system at a heating rate of 2 $^{o}C\ min^{-1}$, two peaks are seen. This is due to the higher resolution of DSC at a lower applied heating rate. The peak temperatures of the two exothermic peaks also shift with different heating rates. The activation energies that are associated with the two exothermic peaks have been calculated and will be discussed later. However, the onset temperatures of the polymerization-delamination for different clay loadings are essentially the same (**Figure III 6**). It is interesting to observe that the reaction enthalpy values associated with the two peaks change with the different clay loading. By integration, the enthalpy change data associated with the two exothermic peaks, ($\Delta H_1$, $\Delta H_2$) and total enthalpy changes ($\Delta H_1 + \Delta H_2$) are obtained and listed in **Table III 2**. The result is that the percentage of the enthalpy change associated with the first peak ($\Delta H_1$) in the total enthalpy change ($\Delta H_1 + \Delta H_2$) increases linearly with increasing clay loadings (**Figure III 7**).

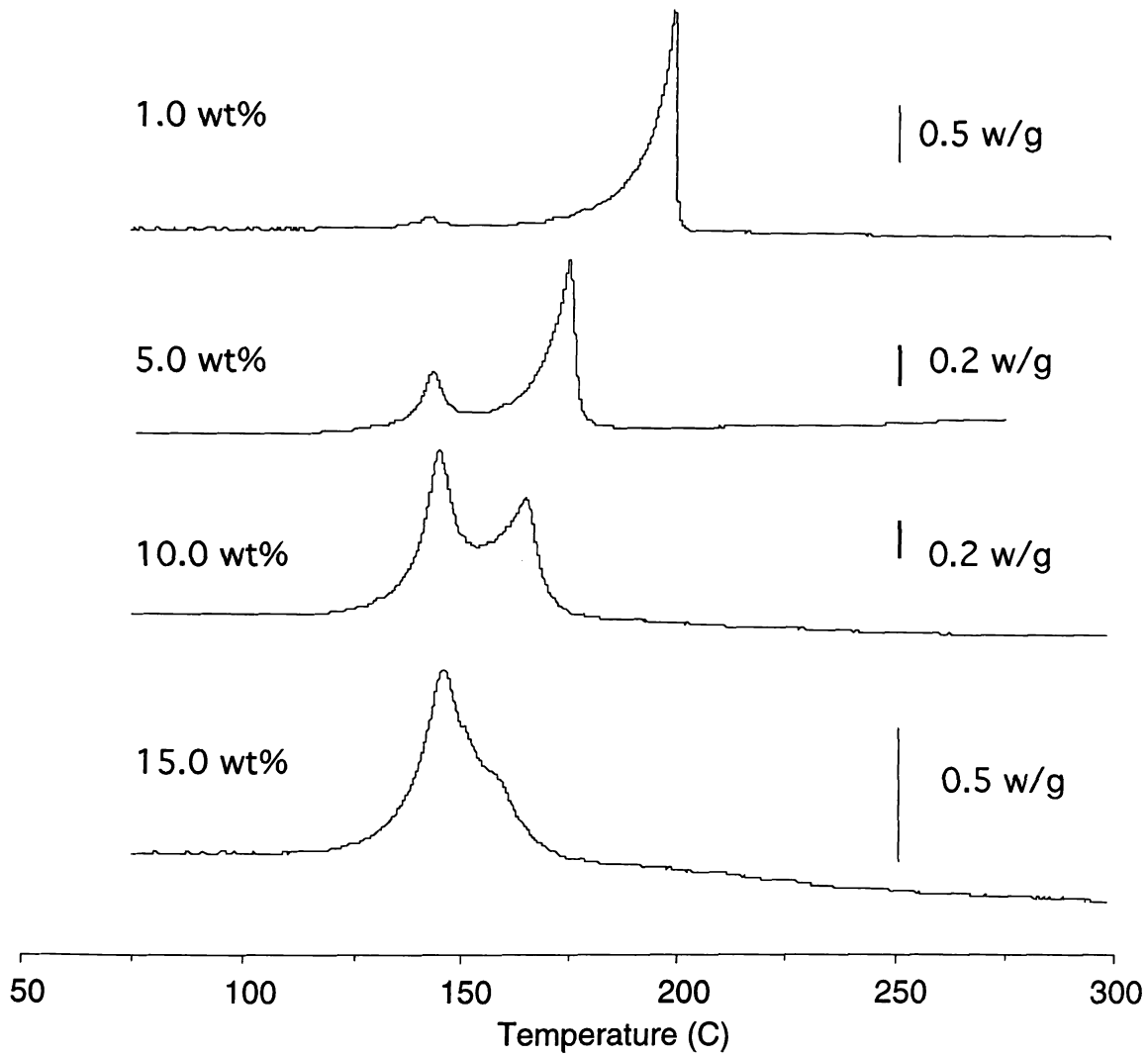



**Figure III 6**. DSC curves for the polymerization of Epon-828 epoxy resin in the presence of different loadings of $CH_3(CH_2)_{17}NH_3^+$-montmorillonite at a heating rate of 2 $^oC$/min.

**Table III 2.** The Enthalpy Changes Associated with the Two Exothermic Peaks ($\Delta H_1$ and $\Delta H_2$), and the Percentage of the 1st Peak's ($\Delta H_1$) in the Total $\Delta H$ *vs.* the wt% of Clay in the Epon-828 - $CH_3(CH_2)_{17}NH_3^+$-Montmorillonite Reaction Systems with Different Clay Loadings.

| Clay wt% | $\Delta H_1$ ($Jg^{-1}$) | $\Delta H_2$ ($Jg^{-1}$) | $\Delta H_1 + \Delta H_2$($Jg^{-1}$) | $\Delta H_1$ (%) |
|---|---|---|---|---|
| 1.0 | 14.1 | 448.3 | 462.4 | 3.2 |
| 2.0 | 39.2 | 373.0 | 412.2 | 9.5 |
| 3.0 | 48.8 | 363.4 | 412.2 | 11.5 |
| 4.0 | 62.6 | 305.9 | 368.5 | 16.9 |
| 5.0 | 73.4 | 255.4 | 328.8 | 22.3 |
| 10.0* | 8.4* | 7.9* | 16.3* | 51.5 |
| 15.0* | 11.5* | 4.8* | 16.3* | 71.0 |

* The $\Delta H$ value is a relative value.

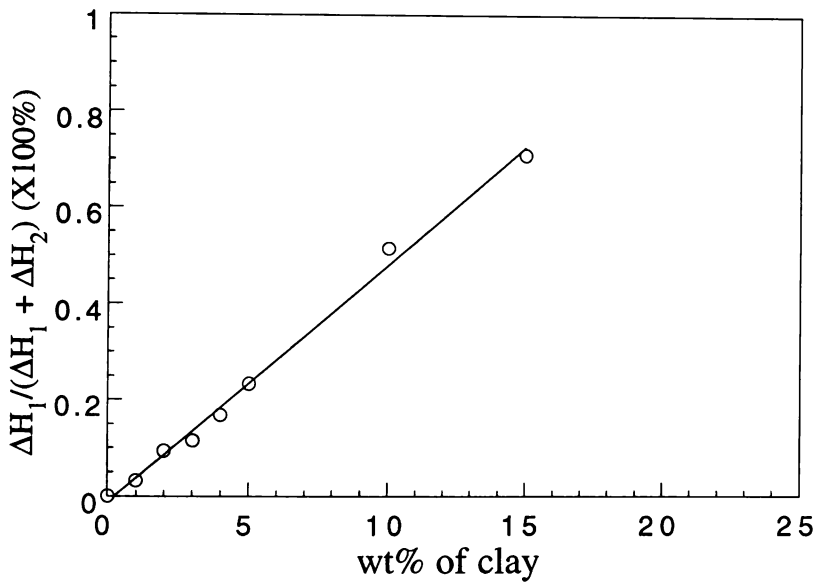



**Figure III 7.** Dependence of $\Delta H_1$ percentage in the total enthalpy change upon the clay loading.

Kinetic information, such as the activation energy ($E_a$) associated with the polymerization of epoxy resin in the presence of acidic clays, can be determined by the ASTM method E-698, using the following equation:

$$\ln\phi = \frac{-Ea}{RT_{exo}} + B \qquad \text{III.1}$$

Where $\phi$ is the heating rate, $T_{exo}$ (K) is the temperature at exotherm maximum and B is a constant. The $\ln\phi$ and $1/T_{exo}$ values from our experiments show excellent linear relationship. **Figure III 8** shows one typical of example of these.

The activation energy data for the reaction systems with different clays and different clay loadings are listed in **Tables III 3** and **III 4**. It is interesting to notice that the activation energy values associated with the first exothermic peaks are essentially the same (within experimental error) and independent of the chain length and the clay loading. This turns out to be true also for the second exothermic peaks. The two exotherms therefore, are characteristic of the reactions and reflect the mechanism of the epoxy self-polymerization and clay delamination processes.

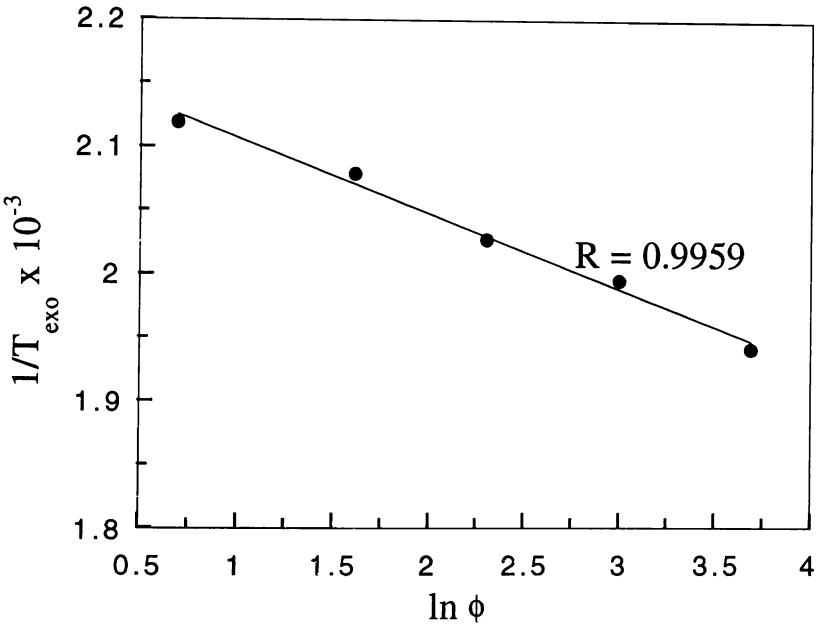



**Figure III 8.** Linear curve fitting of $1/T_{exo}$ *vs.* lnϕ for the second DSC peak in the epoxy polymerization reaction in the presence of 5 wt% $CH_3(CH_2)_{17}NH_3^+$-montmorillonite.

**Table III 3**. Activation Energies Associated with the Two Exothermic Peaks in the Self-Polymerization of Epon-828 in the Presence of Different Alkylammonium Montmorillonite Clays at 5 wt% Clay Loading.

| Gallery Cation | $E_{a1}$ (KJmol$^{-1}$) | $E_{a2}$ (KJmol$^{-1}$) |
|---|---|---|
| $CH_3(CH_2)_7NH_3^+$ | 76 ± 9 | 127 ± 4 |
| $CH_3(CH_2)_9NH_3^+$ | 82 ± 2 | 133 ± 9 |
| $CH_3(CH_2)_{11}NH_3^+$ | 84 ± 2 | 131 ± 3 |
| $CH_3(CH_2)_{15}NH_3^+$ | 82 ± 1 | 120 ± 5 |
| $CH_3(CH_2)_{17}NH_3^+$ | 91 ± 2 | 135 ± 4 |

**Table III 4.** Activation Energies Associated with the Two Exothermic Peaks in the Self-Polymerization of Epon-828 in the Presence of Different Loadings of $CH_3(CH_2)_7NH_3^+$-montmorillonite.

| Clay Percentage (wt%) | $E_{a1}$ ($KJmol^{-1}$) | $E_{a2}$ ($KJmol^{-1}$) |
|---|---|---|
| 1.0 | $91 \pm 2$ | $136 \pm 1$ |
| 2.0 | $90 \pm 4$ | $137 \pm 1$ |
| 3.0 | $85 \pm 8$ | $139 \pm 13$ |
| 4.0 | $80 \pm 2$ | $131 \pm 5$ |
| 5.0 | $76 \pm 9$ | $127 \pm 4$ |

**Table III 5.** Activation Energies Associated with the Two Exothermic Peaks in the Self-Polymerization of Epon-828 in the Presence of Different Loadings of $CH_3(CH_2)_{17}NH_3^+$-montmorillonite.

| Clay Percentage (wt%) | $E_{a1}$ (KJmol$^{-1}$) | $E_{a2}$ (KJmol$^{-1}$) |
|---|---|---|
| 1.0 | 89 ± 4 | 134 ± 11 |
| 5.0 | 91 ± 2 | 135 ± 4 |
| 10.0 | 89 ± 3 | 146 ± 10 |
| 15.0 | 93 ± 6 | * |

* The 2nd peak can not be resolved.

From the relationship of the percentage of $\Delta H_1$ in $\Delta H_1 + \Delta H_2$, it is expected that with increasing organoclay content in the reaction system, there would be only one exothermic peak in the DSC profiles, if the reaction system reaches equilibrium. We used Epon-828 with 50 wt% of $CH_3(CH_2)_{15}NH_3^+$-montmorillonite to prepare a high clay loading organoclay-epoxy complex at 75 °C for 1 week. Indeed, the DSC curve of this complex shows only one exothermic peak (**Figure III 9**), and the $\Delta H$ after normalization is 177 $KJmol^{-1}$, which is close to the enthalpy data in **Table III 1**. The polymerization-delamination reaction of this complex was carried out at 200 °C for 1 h. X-ray diffraction patterns of this complex and the product obtained by heating show that the clay in the epoxy solvated complex has $d_{001}$ at 34.4 Å before heating, which is consistent with epoxy resin solvated $CH_3(CH_2)_{15}NH_3^+$-montmorillonite (**Chapter II**), and an exfoliated clay after heat treatment (**Figure III 10**). The 2-D structure of the clay plates in the reaction product is confirmed by the X-ray diffraction $d_{011}$ peak at 4.52 Å (inset). This result agrees with those obtained from previous epoxy-clay systems that contain relatively low clay loadings.

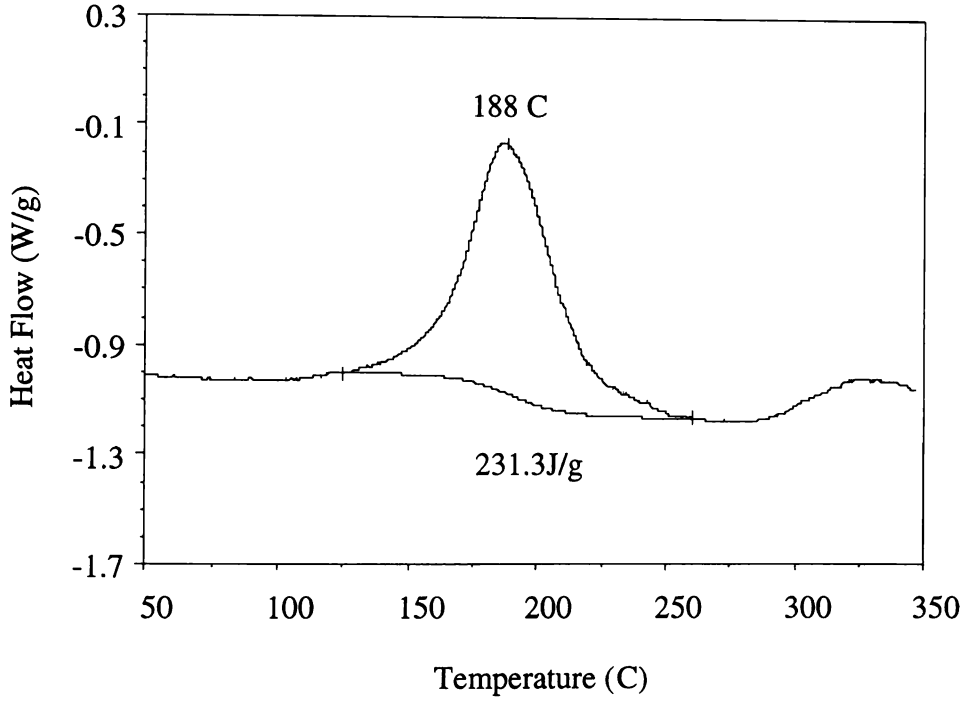



**Figure III 9**. DSC curve for the Epon-828 self-polymerization in the presence of 50 wt% of $CH_3(CH_2)_{17}NH_3^+$-montmorillonite at a heating rate of 2 $^oC$/min.

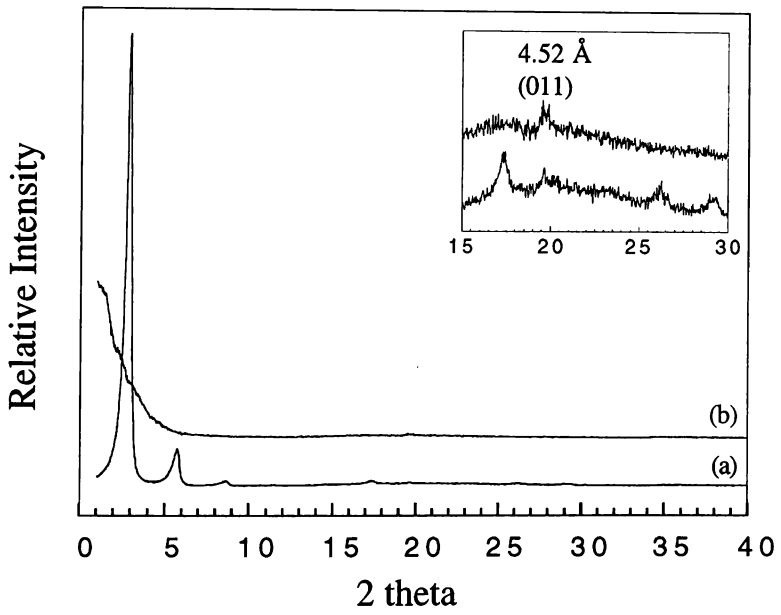



**Figure III 10**. X-ray diffraction patterns of (a) Epon-828 solvated $CH_3(CH_2)_{17}NH_3^+$-montmorillonite complex with 50 wt% of clay (b) Reaction product obtained by heating the Epon-828 solvated $CH_3(CH_2)_{17}NH_3^+$-montmorillonite complex (50 wt%) at 200 $^oC$ for 1 h.

5. Studies on Reaction Intermediates

In order to reveal the mechanism of the epoxy self-polymerization and clay delamination, we studied the reaction intermediate that was obtained after the first exothermic peak. The DSC curve of $CH_3(CH_2)_{17}NH_3^+$-montmorillonite reaction with epoxy (**Figure III 11**) indicates that the first exothermic reaction starts at around 130 $^oC$. Therefore, the reaction intermediate was obtained by heating the mixture of $CH_3(CH_2)_{17}NH_3^+$-montmorillonite (5 wt%) and Epon-828 at heating rate 2 $^oC\ min^{-1}$ to 135 $^oC$ and maintaining the temperature at 135 $^oC$ for one hour. After the reaction at 135 $^oC$ for 1 h, the epoxy-clay mixture turned from a liquid into a gel form without significant volume expansion.

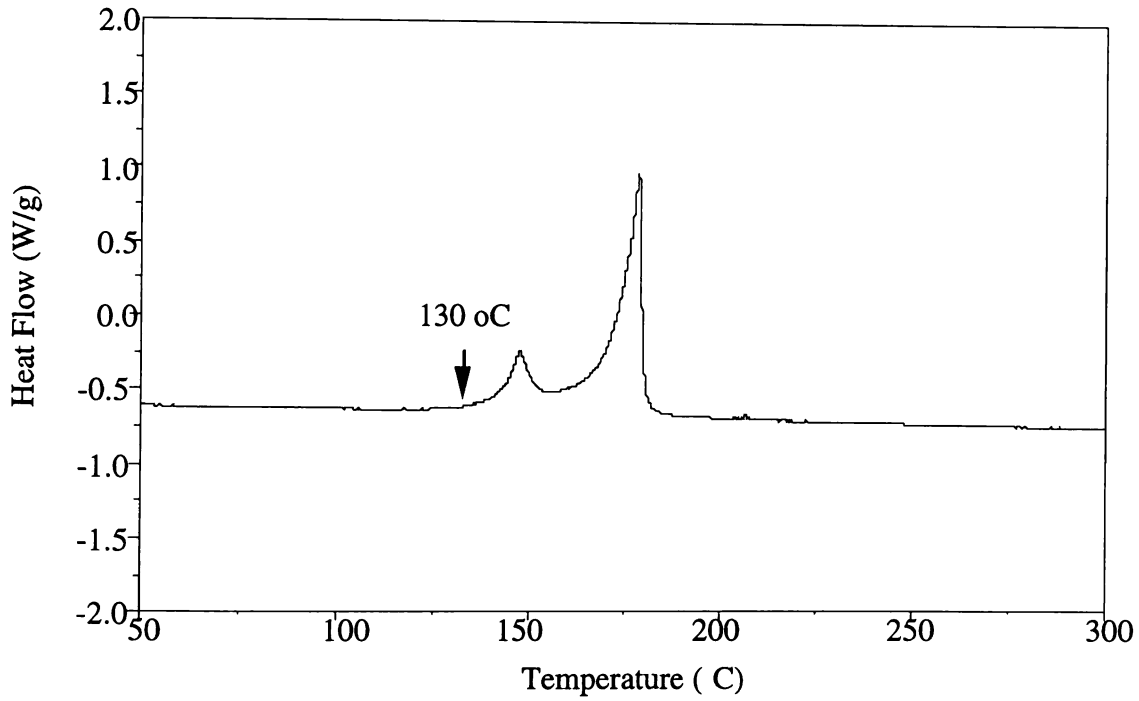



**Figure III 11**. DSC curve of Epon-828 self-polymerization in the presence of $CH_3(CH_2)_{17}NH_3^+$-montmorillonite (5 wt%) at 2 $^oC$/min.

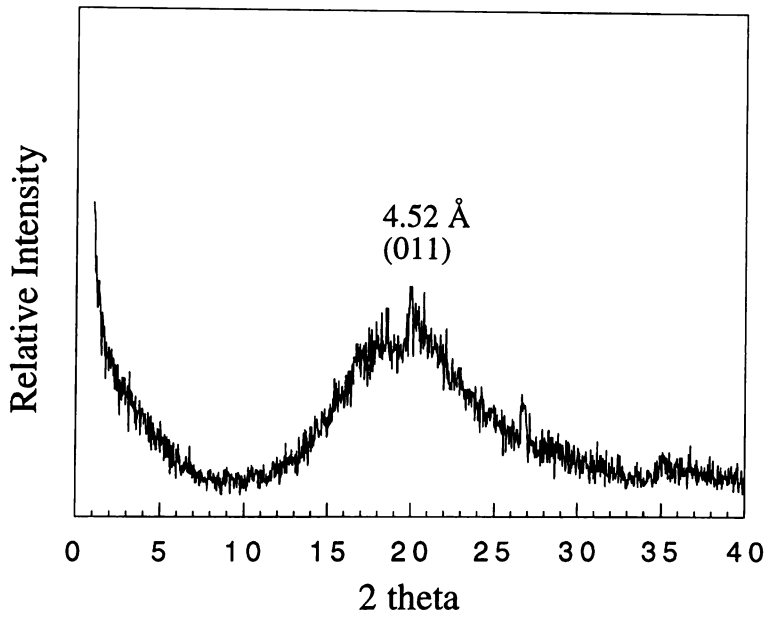



**Figure III 12.** X-ray diffraction pattern of the reaction intermediate of Epon-828 with $CH_3(CH_2)_{17}NH_3^+$-montmorillonite (5 wt%) at 135 $^oC$ for 1 h.

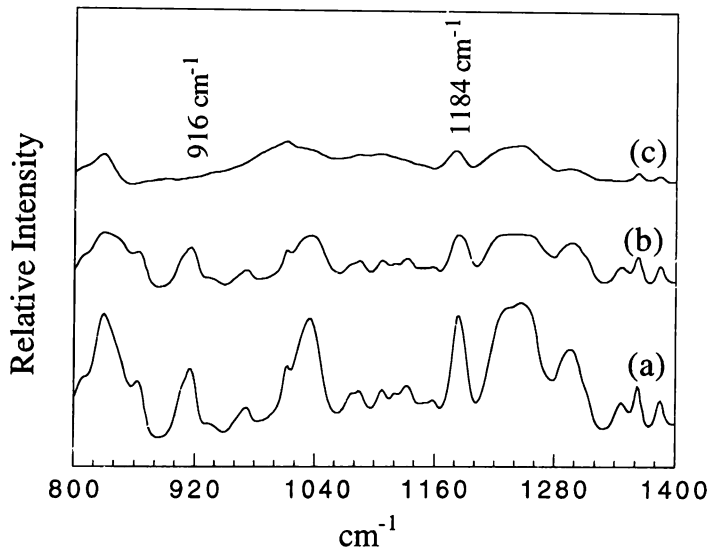



**Figure III 13.** FTIR of (a) Epon-828 solvated $CH_3(CH_2)_{17}NH_3^+$-montmorillonite (5 wt%) (b) Reaction intermediate of $CH_3(CH_2)_{17}NH_3^+$-montmorillonite with Epon-828 at 135 $^oC$ for 1h, and (c) Polyether-$CH_3(CH_2)_{17}NH_3^+$-montmorillonite nanocomposite.

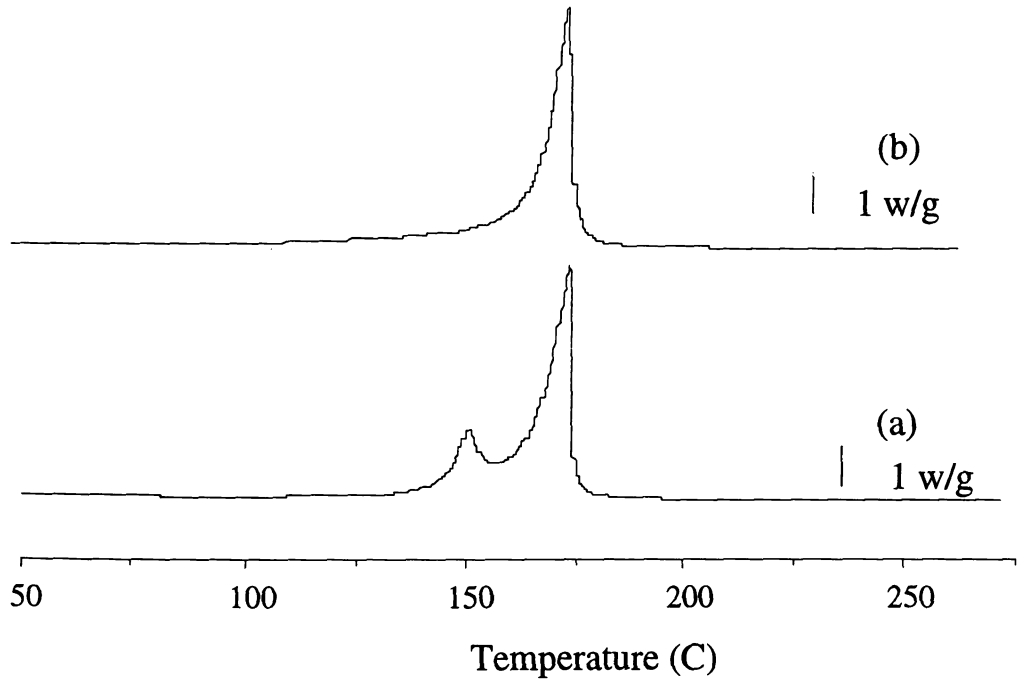



**Figure III 14.** DSC curves of Epon-828 self-polymerization in the presence of $CH_3(CH_2)_{17}NH_3^+$-montmorillonite (5 wt%).

(a) original mixture, (b) reaction intermediate after the reaction at 135 $^oC$ for 1 h.

**Table III 6.** Activation Energies of Epon-828 Self-Polymerization Reaction in the Presence of Different Clays at 1-Step and 2-Step Reactions.

| clay (-montmorillonite) | $E_{a1}$ ($KJmol^{-1}$) | $E_{a2}$ ($KJmol^{-1}$) | $E_{a2}^*$ ($KJmol^{-1}$) |
|---|---|---|---|
| $CH_3(CH_2)_7NH_3^+$ | $76 \pm 9$ | $131 \pm 8$ | $175 \pm 5$ |
| $CH_3(CH_2)_9NH_3^+$ | $82 \pm 2$ | $133 \pm 8$ | $172 \pm 6$ |
| $CH_3(CH_2)_{11}NH_3^+$ | $84 \pm 2$ | $131 \pm 3$ | $135 \pm 4$ |
| $CH_3(CH_2)_{17}NH_3^+$ | $84 \pm 2$ | $127 \pm 4$ | $125 \pm 5$ |

* $E_{a2}^*$ is obtained from the reaction intermediate.

6. Reaction Mechanism

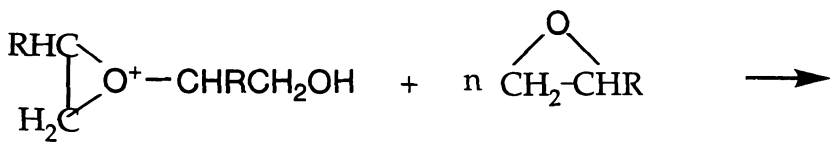
The reaction intermediate was characterized by X-ray diffraction, FTIR and DSC. The X-ray diffraction result (**Figure III 12**) shows no $d_{001}$ reflection. The FTIR result (**Figure III 13**) shows the presence of epoxy groups in the reaction intermediate with the presence of the 916 $cm^{-1}$ epoxy ring vibration, indicating that the reaction intermediate contains un-polymerized epoxy groups. In the DSC result, (**Figure III 14**) the first exothermic peak basically disappeared, which suggest the monomer groups associated with the first exothermic peak have undergone self-polymerization after the reaction at 135 $^{o}C$ for 1 h. From different heating rate measurements, the activation energy associated with the second peak has been obtained. Similar experiments have been conducted for different chain length alkylammonium exchanged montmorillonite clays and the activation energy data are listed in **Table III 6**. By comparing the second activation energy obtained from direct reaction and reaction of the intermediate, we find that the $E_{a2}$ of the reaction intermediate is slightly larger than that for direction reaction. A possible explanation is presented here: for the reaction intermediate there is little mobile phase as observed from its gel-like morphology, therefore for the second reaction, more diffusional energy is required compared with the direct reaction observed when the sample is heated continuously in the DSC cell. This observation suggests that the second reaction possesses a diffusion controlled step.

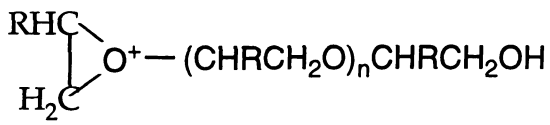
These $E_a$ and $\Delta H$ results suggest therefore, that there is a two-step reaction mechanism involved in the formation process of these nanocomposites. From the dependence of the enthalpy upon the

concentration of clay in the reaction mixture and the intercalation results given in the **Chapter II**, it is concluded that the first exothermic reaction is the intra-gallery epoxy self-polymerization and the second is the extra-gallery epoxy self-polymerization.

Primary amines are commonly used as curing agents for epoxy resin polymerization owing to the reaction of the amine group with the epoxide ring.[31,32] However, the concentration of onium ions in the organoclay is limited, e.g., for 5 wt% of clay, the equivalence of onium ions to the epoxide groups is only 1.4 %. Thus, the protonated amines in the organoclay galleries act primarily as acid catalysts rather than as curing agents. The acid-catalytic role of the onium ions can be represented by the following reaction equations:







Upon heating, the proton associated with the primary amine undergoes disassociation and initiates self-polymerization of the epoxy

monomers inside the clay galleries. Because of the acidity of the alkyl ammonium ions in the clay galleries, the inner-gallery epoxide monomers may start self-polymerization at the lower temperature. The onset temperature of the reaction depends on the alkylammonium chain length. With increasing alkylammonium chain length, more epoxide monomers are able to enter the clay gallery as concluded from epoxy intercalation chemistry into organoclays, and the onset temperature is lowered. The total enthalpy is essentially the same for each different reaction system, since the energy is associated with the consumption of the epoxide group only.

On the basis of the $E_a$ and $\Delta H$ results a model for the nanocomposite formation mechanism is proposed (**Figure III 15**). There are two major steps involved, the first step is the intra-gallery epoxy self-polymerization and the second is the extra-gallery epoxy self-polymerization. The epoxy resin monomers solvate the organoclay galleries at 75 $^{o}C$ and with increasing temperature the epoxy monomers intercalated inside the clay galleries undergo self-polymerization by the catalytic reaction of the acidic protons associated with the alkylammonium cations. After this step, the reaction intermediate forms a gel without significant volume increase. Upon further heating of the reaction intermediate, the outer-gallery epoxy monomers overcome the energy barrier to diffusion and migrate into the clay gallery and polymerize. The reaction is complete when all the mobile monomers enter the clay galleries and undergo polymerization. The migration of the extra-gallery epoxy resin monomers into the clay galleries impedes the continuity of polymer chain formation between different clay tactoids and introduces interfaces between polyether-clay nanocomposite aggregates. In other words, the structure of the polyether-clay

nanocomposite is based on the original clay tactoids. Due to the phase separation (polymer discontinuity) of the final polymer-clay tactoids, the final composites have a powder texture. The voids between the different polyether-clay composite aggregates contribute to the volume increase observed during the final nanocomposite formation. The diffusion energy barrier is reflected in the second activation energy, which explains the reason that the second activation energies are always greater than the first one.

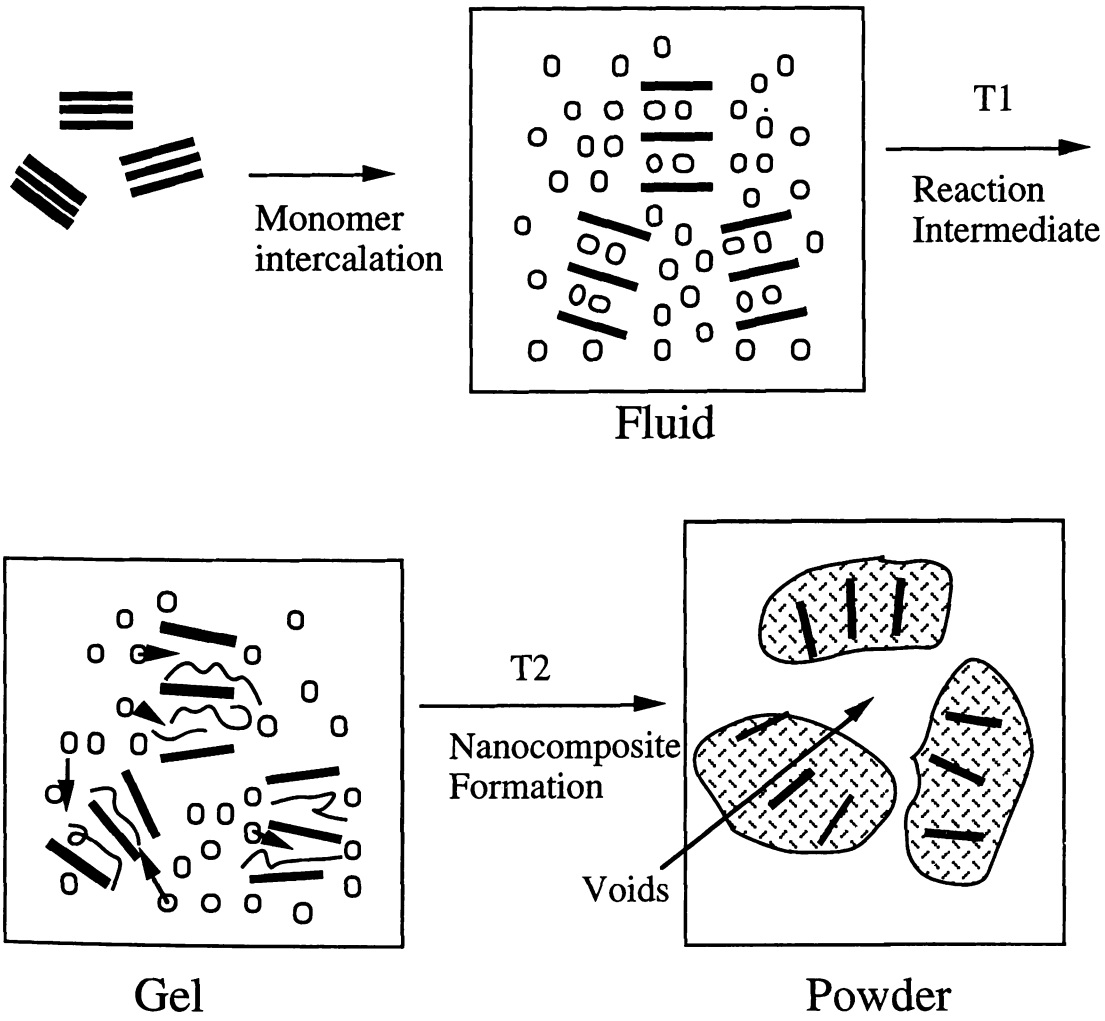



**Figure III 15.** Proposed reaction mechanism for the polyether-clay nanocomposite formation.

## D. Conclusion

Polyether-clay nanocomposites have been synthesized by use self-polymerization of epoxy monomer in the galleries of alkylammonium exchanged montmorillonites. The organoclays intercalated by the epoxy monomers performed as precursors. The catalytic activity of the acidic clay plays an important role in the polymerization-delamination process. The intra-gallery self-polymerization is earlier and faster than the extra-gallery polymerization. The intra-gallery polymerization provides a unique and promising route to the synthesis of different polymer-clay nanocomposites.

## E. References

1. G.M. Whitesides, J.P. Mathias, C.T. Seto, *Sci.*, **254**, 1312 (1991).

2. T.A. Werpy, L.J. Michot, T.J. Pinnavaia, *ACS Symp. Ser.*, **427**, 119 (1990).

3. Giannelis, E. P. *JOM*, **44**, 28 (1992).

4. E. Ruiz-Hitzky, *Adv. Mater.*, **5**, 334 (1993).

5. B.M. Novak, *Adv. Mater.*, **5**, 422 (1993).

6. T.J Pinnavaia, *Sci.*, **220**, 365 (1983).

7. B.K.G. Theng, Formation and Properties of Clay-polymer Complexes; Elsevier: New York, (1979).

8. E. Ruiz-Hitzky, P. Aranda, *Adv. Mater.*, **2**, 545 (1990).

9. R.A. Vaia, H. Ishii, E.P. Giannelis, *Chem. Mater.*, **5**, 1694 (1993).

10. C. Kato, K. Kuroda, M. Misawa, *Clays Clay Miner.*, **27**, 129 (1979).

11. M. Ogawa, K. Kuroda, C. Kato, *Clay Science*, **7**, 243, (1989).

12. T.J. Bandosz, J. Jagiello, K.A.G. Amankah, J.A. Schwarz, *Clay Miner.*, **27**, 435 (1992).

13. Y. Sugahara, S. Yoshiyuki, T. Sugiyama, T. Nagayama, K. Kurado, C. Kato, *Nippon Seramikkusu Kyokai Gakujutsu Ronbunshi*, **100**, 413 (1992).

14.P.B. Messersmoth, E.P. Giannelis, *Chem. Mater.*, **5**, 1064 (1993).

15. Y. Fukushima, S. Inagaki, *J. Inclu. Phenom.* **5**, 473 (1987).

16. Y. Fukushima, A. Okada, M. Kawasumi, T. Kurauchi, O. Kamigaito, *Clay Miner.*, **23**, 27 (1988).

17. A. Usuki, M. Kawasumi, Y. Kojima, A. Okada, T. Kurauchi, O. Kamigaito, *J. Mater. Res.*, **8**, 1174 (1993).

18. A. Usuki, Y. Kojima, M. Kawasumi, A. Okada, Y. Fukushima, T. Kurauchi, O. Kamigaito, *J. Mater. Res.*, **8**, 1179 (1993).

19. A. Usuki, T, Mizutani, Y. Fukushima, M. Fujimoto, K. Fukumori, Y. Kojima, N. Sato, T. Kurauchi, O. Kamigaito, U.S. Patent 4,889,885, (1988).

20. K. Yano, A. Usuki, A. Okada, T. Kuraychi, O. Kamigaito, *Polymer Preprints*, **32-1**, 65 (1991).

21. K. Yano, A. Usuki, A. Okada, T. Kuraychi, O. Kamigaito, *J. Polym Sci: Polym. Chem.*, **31**, 2493 (1993).

22. P.D. Kaviratna, T. Lan, T.J. Pinnavaia, *Polymer Preprints*, **35-1**, 788 (1994).

23. T.J. Pinnavaia, T. Lan, P.D. Kaviratna, M.S. Wang, Clay-Polymer Nanocomposites: Polyether and Polyimide Systems. MRS Symposium, Paper N-2.8 April, (1994).

24. M.S. Wang, T.J. Pinnavaia, *Chem. Mater.*, **6**, 468 (1994).

25. J. Butrulle, T.J. Pinnavaia, "Characterization of Catalytical Materials" I.E. Wachs, Ed. Butterworth-Heinemann, Boston, 149 (1992).

26. Chi-Li Lin, Ph. D. Thesis "Organoclays as Triphase Catalysts" Chemistry Department, Michigan State University, (1988).

27. Chi-Li, Lin; T, Lee; T.J. Pinnavaia, ACS Symp. Ser. **499**, 145 (1992).

28. E. Mertzel, J.L. Koenig, "Epoxy Resins and Composites II, Advances in Polymer Science", **Vol. 75**, K. Dusêk ed. Springer-Verlag, New York, p73-113 (1985).

29. D.W. Schiering, J.E. Katon, L.T. Drzal, V.B. Gupta, *J. Apply. Polym. Sci.*, **34**, 2367 (1987).

30. J.M. Barton, "Epoxy Resins and Composites I, Advances in Polymer Science", **Vol. 72**, K. Dusêk ed. Springer-Verlag, New York, p111-115 (1985).

31. C.A. May Ed. Epoxy Resins, Marcel Dekker, New York, (1988).

32. T. Kamon, H. Furukawa, "Epoxy Resins and Composites II, Advances in Polymer Science", **Vol. 80**, K. Dusêk ed. Springer-Verlag, New York, p173-203 (1986).

# CHAPTER IV

## Synthesis, Characterization and Mechanical Properties of Glassy Amine-Cured Epoxy-Clay Nanocomposites

### A. Introduction

Attempts to prepare hybrid organic-inorganic composites have been reported recently. The primary goal in such work is to achieve unique combinations of properties from both the organic and inorganic components.[1-4] The properties of the hybrid organic-inorganic composite materials are greatly influenced by the degree of mixing between the different phases and the dispersion of the inorganic component in the organic matrix. Such dispersion is mostly desired in the nanometer scale, creating the so-called nanocomposites.

Clay minerals such as kaolin,[5,6] talc,[7,8] mica[9-11] and smectite clays have been used as fillers in thermoplastic and thermoset polymer matrices. The natural abundance and low cost of layered clay minerals are advantageous in the use of these materials. The platy nature and two-dimensional aspect ratios of clay single layers indicate that they are analogues to fibers in polymer matrices. However, these clay minerals usually exist as aggregated layered tactoids, and the aspect ratios of such aggregates are normally less than 20, which limits the clay minerals to acting as fillers instead of reinforcement in the polymer matrices. Recent studies[11] on clay-epoxy composites indicate that surface treatment of the clays determines the filling limits, dispersion and composite tensile strength.

These results also show that smectite clays and muscovite mica reduce the tensile strength but enhance the tensile moduli of epoxy resin Epon-828 cured with meta-phenylenediamine.

Smectite clay minerals are members of a broad class of layered silicates with 2:1 mica-like layer lattice structure.[12] The negative charge on the silicate layer which arises from isomorphous substitution within the various layers is balanced by intergallery exchange cations. For mica, the interlayer cations ($K^+$) are non-exchangeable due to the very high layer charge density; this limits the intergallery chemical modification of mica for intercalation or delamination. Because of the moderate layer charge densities of smectite clays, the intergallery cations can be exchanged by inorganic, organic and complex cations. Therefore, the intergallery region of smectite clay plays an important role in the delamination of the 10 Å-thick layers. When smectite clays have organic cations as the gallery ions, the surface properties of the clay also change from hydrophilic to hydrophobic, which enhance the affinity between the inorganic components and organic matrices. The unique structural features of smectite clays make them potential inorganic components in the synthesis of hybrid organic-inorganic composites.

The intercalation of small organic molecules and some polymers into smectite clay galleries has been known for some time.[13] In the intercalated clay-polymer hybrids (intercalated nanocomposite), the clays exist in a tactoid form, where a monolayer or multilayers of polymers, the nanophase, are accommodated within the clay galleries. The layer separation of the clay is independent of the clay loading in such a hybrid system. The intercalated clay-polymer nanocomposites have been synthesized through direct polymer

intercalation,[14] indirect polymer intercalation which is associated by solvent molecules[13] and *in situ* intercalative polymerization of monomers in the clay galleries.[15-17] Owing to the spacial restriction within the gallery region, intercalated polymer-clay nanocomposites exhibit impressive properties such as conductivity[18] and gas permeability.[19]

When the 10 Å-thick silicate layers are dispersed as single layers in polymer matrices, the polymer-clay hybrids can be described as exfoliated polymer-clay nanocomposites. The first report of a hybrid having the exfoliated polymer-clay nanocomposite structure was nylon-6-montmorillonite described by Toyota researchers.[20,21] This hybrid material exhibited greatly improved mechanical properties and thermal stability.[22-24] The driving force for the exfoliation of the clay tactoids was concluded to be the energy released during the polymerization of ε-caprolactam, the monomer of nylon-6.[20] Exfoliated polyether-clay nanocomposites have been prepared by the self-polymerization of an epoxy resin in the galleries of acidic alkylammonium ion exchanged forms of montmorillonite in our laboratory.[25-27] Owing to their powder texture, these polyether-clay nanocomposites were not suitable for mechanical measurements. It is a very challenging project to implant the existing 10Å-thick silicate layers of the smectite clays into a continuous polymer matrix by overcoming the electrostatic attraction between the silicate layers and intergallery cations.

Epoxy resins are commonly used as matrices for high performance fiber reinforced composites. Various resins, curing agents and curing catalysts are available to meet different property requirements. Cured epoxy resins possess low cure shrinkage, high mechanical strength, thermal stability and good chemical and electrical resistance. In this chapter, we

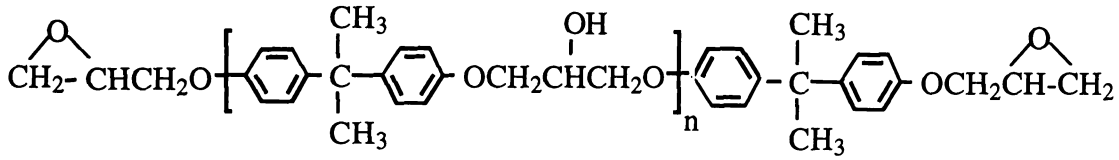
report the synthesis of amine-cured epoxy-clay exfoliated nanocomposite and demonstrate that the single clay layer functions as fibers in the epoxy matrix which enhances the mechanical properties. Meta-phenylenediamine (mPDA) has been used as curing agent for Epon-828. The epoxy resins cured with mPDA possess a glass transition temperature ($T_g$) around 150 $^oC$, and they are rigid solids at room temperature. The synthetic approaches to novel epoxy-clay nanocomposites and their mechanical performance will be discussed.

## B. Experimental

### 1. Materials

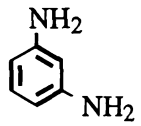
Natural California hectorite and Wyoming montmorillonite were obtained from the Source Clay Mineral Depository, University of Missouri, Columbia. These minerals were purified by sedimentation to exclude particles larger than 2 μm, followed by removal of carbonates by using pH5 acetate buffer solution and elimination of iron oxide with sodium hydrosulfate. The unit cell formula of hectorite is $Na_{0.67}[Li_{0.67}Mg_{5.33}(Si_{8.00})O_{20}(OH)_4]$,[28,29] with a cation exchange capacity 73 meq./100g of air-dried clay.[30] The unit cell of montmorillonite is $Na_{0.86}[Mg_{0.86}Al_{5.14}(Si_{8.00})O_{20}(OH)_4]$, with a cation exchange capacity of 88 meq./100g.[30] Texas vermiculite from the Source Clay Minerals Repository was used after grinding to particle sizes less than 46 μm (325 mesh). Rectorite was obtained from Bao-Tou,[31] China and purified in the same manner as described for hectorite. The chemical composition of rectorite is $[(Na_{0.72}K_{0.02}Ca_{0.05})(Ca_{0.24}Na_{0.07})](Al_{4.00}Mg_{2.00})$-$[Si_{6.58}Al_{1.12}]O_{22}$, with a cation exchange capacity of 60 meq./100 g of air-dried clay. Synthetic fluorohectorite, $Li_{1.60}[Li_{1.60}Mg_{4.40}(Si_{8.00})O_{20}F_4]$, was obtained from Corning Glass, Corning, New York, with a particle size larger than 2 μm and a cation exchange capacity of 140 meq./100 g.

Epoxy resin, Epon-828 was obtained from Shell Co. with an average molecular weight of 380.



n = 0 (88%); n = 1 (10%); n = 2 (2%).

Meta-phenylenediamine (mPDA) was used as a curing agent for the epoxy resin:



Long chain primary alkylamines $CH_3(CH_2)_{n-1}NH_2$, where n = 4, 6, 8, 10, 12, 16 and 18,. and secondary, tertiary and quaternary alkylammonium chloride/bromide ($CH_3(CH_2)_{17}NH_3^+$, $CH_3(CH_2)_{17}N(CH_3)H_2^+$, $CH_3(CH_2)_{17}N(CH_3)_2H^+$ and $CH_3(CH_2)_{17}N(CH)_3^+$) salts were purchased from Aldrich Chemicals and used as received.

Cation exchange reaction was carried out by using 500 ml of 0.05 M alkylammonium chloride ethanol:water (1:1) solution and 2.0 g of clay at 70 ~ 75 °C for 24 h,[32,33] The exchanged clays were washed with ethanol:water (1:1) several times until no chloride was detected with 1.0 M $AgNO_3$ solution and air dried. Finally, the clays were ground and collected the particle size of the 40 ~ 50 μm fraction was retained.

2. Synthesis of mPDA-Cured-Epoxy-Clay Nanocomposites

Initially, a mixture of epoxy-clay was obtained by mixing the desired amount of clay with the epoxy resin at 75 $^{o}$C. The equivalent of mPDA 14.5 wt% (stoichiometric amount) of Epon-828, was added to the epoxy-clay mixture. The epoxy-clay-mPDA complex was then outgassed in a vacuum oven (~ 25 torr) for a short period of time. The degassed composition was transferred into a silicone rubber mold for curing. The processing condition is controllable for the composite with clay content less than 10 wt%. We studied the dependence of the nanocomposite formation on the curing conditions, such as temperature and time. We discovered that the best curing conditions for amine-cured epoxy-clay exfoliated nanocomposite formation was at 75 $^{o}$C for 2 h and at 125 $^{o}$C for an additional 2 h. These optimum curing conditions for exfoliated nanocomposite formation were applied to all amine-cured epoxy-clay nanocomposite preparations reported in this chapter except where stated otherwise.

3. Physical Measurements

X-ray diffraction patterns were obtained by using a Rigaku X-ray diffractometer with a rotating anode (Cu) and a curved graphite monochromater. Samples for X-ray diffraction were prepared by crushing the epoxy-clay composite specimens and collecting the particle size range of 150 μm to 180 μm.

Transmission electron micrographs (TEM) were obtained with a JEOL-100CX microscope, operated with an acceleration voltage of 100 kV. The crushed epoxy-clay composite samples were encapsulated with the

embedding agent, Hard-Spurr, which was allowed 48 h at 60 $^{o}$C to polymerize. The embedded sample was ultrathin sectioned by using a microtome equipped with a glass knife. The thin-sections ranged from 600 Å to 900 Å thick.

4. Tensile Testing of Epoxy-Clay Nanocomposites

The tensile strengths and moduli of our new epoxy-clay nanocomposites were measured according to ASTM method 3039 by using a UTS system. The specimens had dimensions of 1.50 x 4.00 x 25.40 $mm^3$, with a deviation of thickness of 0.01 mm. Tensile testing was performed at ambient temperature with a strain rate of 0.51 mm/min. The maximum failure strength and Young's modulus of the tested sample were obtained from the stress-strain curve. At least 5, usually 5 - 8, specimens were measured for each sample and the average data and the standard deviation were plotted.

## C. Results and Discussion

### 1. Effect of Curing Temperature on Nanocomposite Formation

Different curing conditions affect the degree of curing of amine-cured epoxy composites.[34] Four curing cycles have been examined as preliminary studies. The X-ray diffraction patterns of amine-cured epoxy-clay composites with 5 wt% $CH_3(CH_2)_{15}NH_3^+$-montmorillonite cured at different conditions are shown in **Figure IV 1**. The primary evidence for exfoliated nanocomposite formation is the absence of Bragg scattering. It is very clear that composites prepared at 75 °C for 4 h, then at 140 °C for 4 h have Bragg diffraction peaks at 32 and 34 Å, respectively. Although the diffraction peaks are not as sharp as those of the original clay, they are distinguishable from the diffraction background. The composites prepared at 75 °C for 2 h followed by 125 °C for an additional 2 h and those prepared at 100 °C for 4 h do not have diffraction peaks. We can therefore infer that composites prepared at 2 h each at 75 °C followed by 125 °C and 100 °C, 4 h, have exfoliated structures, whereas those cured at 75 °C for 4 h and 140 °C for 4 h, possess intercalated structures. As the optimum curing condition for the reaction between Epon-828 and mPDA,[34] we selected that in which the sample was heated 2 h at 75 °C followed by an additional 2 h at 125 °C, as our epoxy-clay composite curing cycle.

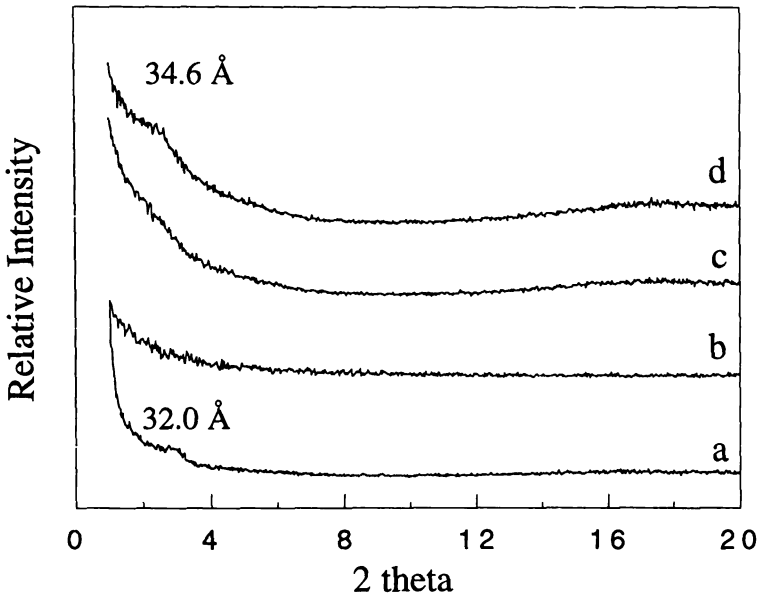



**Figure IV 1.** X-ray diffraction patterns of amine-cured epoxy-clay composites containing 5 wt% $CH_3(CH_2)_{15}NH_3^+$-montmorillonite at the following curing conditions, (a) 75 °C, 4 h (b) 75 °C, 2 h and 125 °C 2 h (c) 100 °C, 4 h (d) 140 °C 4 h.

2. Effect of Gallery Cation Chain Length on Nanocomposite Formation

In **Chapter II**, we studied the effect of epoxy resin solvation of the organoclay containing different chain length alkylammonium gallery cations. Here, we use such epoxy solvated organoclay as the precursor to epoxy-clay nanocomposites.

Powder X-ray diffraction patterns of epoxy-clay composites containing 5 wt% of various alkylammonium montmorillonite clays are shown in **Figure IV 2**. For the composites formed with $CH_3(CH_2)_7NH_3^+$-, $CH_3(CH_2)_{11}NH_3^+$- and $CH_3(CH_2)_{15}NH_3^+$-montmorillonite, there is no Bragg scattering observed, indicative that exfoliated epoxy-clay nanocomposites have been achieved. The layer separation is larger than the largest possible detectable $d_{001}$ value of 90 Å (2 theta = 1.0°), and clay layers are assumed to be dispersed uniformly inside the amine cured epoxy matrix. For $CH_3(CH_2)_3NH_3^+$-montmorillonite, a diffraction at 16.6 Å is observed and indicates that a monolayer of epoxy-amine polymer is formed inside the clay gallery, and is therefore an intercalated nanocomposite. Thus, for montmorillonites with alkylammonium cation chain lengths larger than 8 carbon atoms, exfoliated nanocomposites can be obtained, whereas those interlayered by shorter alkylammonium cations only afford intercalated nanocomposites. A TEM image of an exfoliated epoxy-clay nanocomposite with 5 wt% $CH_3(CH_2)_{15}NH_3^+$-montmorillonite is shown in **Figure IV 3**. The dark lines are the intersections of 10 Å-thick silicate sheets. The clay layer separations are in the range 50 Å to 150 Å, which is significantly different from the basal spacing of the uncured epoxy solvated $CH_3(CH_2)_{15}NH_3^+$-montmorillonite.

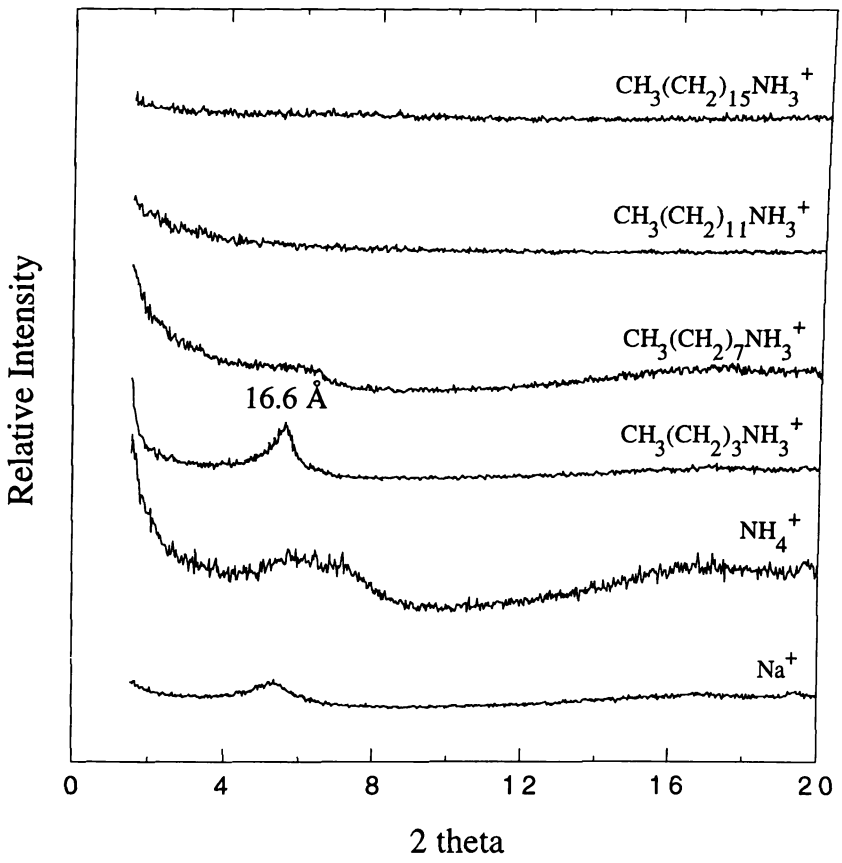
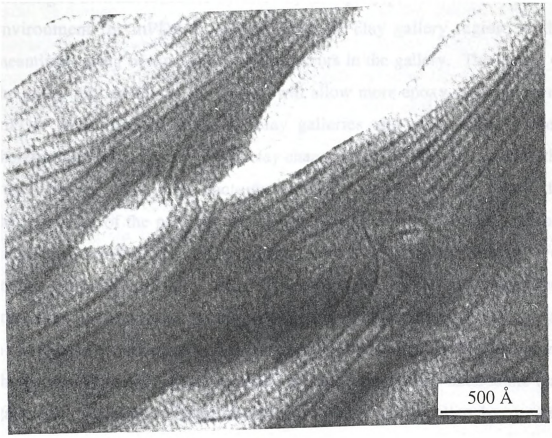



**Figure IV 2**. X-ray diffraction patterns of epoxy-clay composite materials formed by the polymerization of a DGEBA resin, Epon-828, with stoichiometric amount of mPDA as a curing agent in the presence of various cation exchanged forms of montmorillonite. The exchange ions are identified for each diffraction pattern.

**Figure IV 3**. TEM of amine(mPDA)-cured epoxy-clay exfoliated nanocomposite with $CH_3(CH_2)_{15}NH_3^+$- montmorillonite (5wt%).


500 Å

A preliminary explanation is presented for the aforementioned observations: The large basal spacing of long chain alkylammonium exchanged montmorillonites solvated by the epoxy provides a hydrophobic environment for mPDA to migrate into the clay gallery region; in the meantime curing of epoxy and mPDA occurs in the gallery. The curing of the epoxy and mPDA in the gallery will allow more epoxy monomers and mPDA molecules to enter the clay galleries and polymerize further, therefore the basal spacing of the clay changes from its solvated value to the cured value. The clay tactoids exfoliate simultaneously when the thermosetting of the polymer matrix occurs. The extent of the clay tactoid exfoliation parallels the degree of thermoset of the polymer matrix. For montmorillonite with short chain alkylammonium ions as the intergallery ions, even upon swelling, the basal spacing is not large enough for more than a monolayer of monomer units to migrate into its gallery region, therefore, the polymerization of the epoxy and mPDA occurs mainly outside the clay galleries. Inorganic forms of montmorillonite are swollen by organic monomers in a very limited way, because of their hydrophilic nature, and the polymerization of monomer in the gallery is therefore impossible. Thus, conventional phase-separated composites were obtained for $Na^+$- and $NH_4^+$-montmorillonites. The swelling property of clay in an organic monomer controls the initial layer expansion prior to the complete clay exfoliation in a polymer matrix.

3. Effect of Clay Layer Charge Density on Nanocomposite Formation

Other clays such as hectorite, fluorohectorite and vermiculite with the same exchanged cation, $CH_3(CH_2)_{15}NH_3^+$, exhibit similar swelling properties in the presence of Epon-828. The orientation of the intergallery ions of these clays changes from the initial state of lateral bilayer or paraffin orientations to a perpendicular position in the gallery region upon solvation by the epoxy resin. The motivation for using these clays is that they can have the same gallery cation, but different concentrations of gallery cations because of their different layer charge densities. Different performances of these clays in the formation of epoxy-clay nanocomposites are therefore expected.

X-ray powder diffraction patterns of mPDA-cured epoxy-clay composites containing 5 wt% loading of $CH_3(CH_2)_{15}NH_3^+$-hectorite, -montmorillonite, -fluorohectorite and -vermiculite are shown respectively in **Figure IV 4**. For hectorite and montmorillonite, the absence of $d_{001}$ diffraction peaks indicates that the clays exfoliate in the epoxy matrix. The X-ray diffraction pattern of the composite with fluorohectorite shows broad diffraction peaks with a basal spacing of 35-37 Å. This indicates that the layer separation of fluorohectorite is increased in the matrix from its uncured epoxy solvated state, but that it maintains a tactoid structure. For vermiculite there is a very strong $d_{001}$ diffraction with a very well defined basal spacing of 36 Å. These results suggest that clays with high layer charge density form only intercalated, not exfoliated nanocomposites.

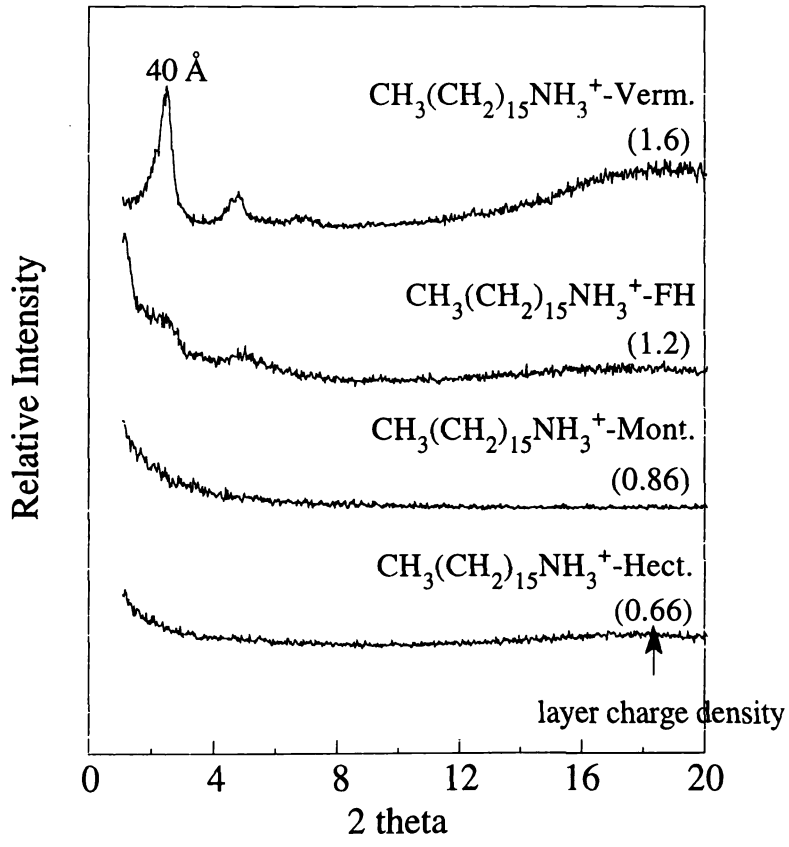



**Figure IV 4**. X-ray diffraction patterns of amine-cured epoxy-clay composite materials formed by the polymerization of a DGEBA resin, Epon-828, with stoichiometric amount of mPDA as a curing agent in the presence of $CH_3(CH_2)_{17}NH_3^+$ exchanged different layer charge density clays. Layer charge density values (meq./g) are given in parentheses.

TEM images of epoxy-clay composites containing 5 wt% $CH_3(CH_2)_{15}NH_3^+$ exchanged hectorite, fluorohectorite and vermiculite are shown in **Figure IV 5A, 5B, and 5C** respectively. These pictures display the distribution of clay layers in the continuous amine-cured epoxy matrix. The TEM of the composite with hectorite is very similar to that of montmorillonite (**Figure IV 3**.), but with shorter silicate plates. The separations between two layers are in the range 60 ~ 200 Å. The TEM of the fluorohectorite composite shows that some of the silicate layers still retain an ordered-layered structure with a basal spacing of around 40 Å which contributes to the X-ray diffraction, while others show a layer distance in the range 50~140 Å. The TEM of the vermiculite composite shows a very well ordered crystalline layered silicate structure with a basal spacing of about 40 Å, consistent with the X-ray diffraction result.

**Figure IV 5**. TEM images of amine-cured epoxy-clay nanocomposite with clay content of 5 wt%. Exfoliated epoxy-clay nanocomposite structure obtained with (A) $CH_3(CH_2)_{15}NH_3^+$-hectorite. Intercalated epoxy-clay nanocomposite structure obtained with (B) $CH_3(CH_2)_{15}NH_3^+$-fluorohectorite and (C) $CH_3(CH_2)_{15}NH_3^+$- vermiculite.

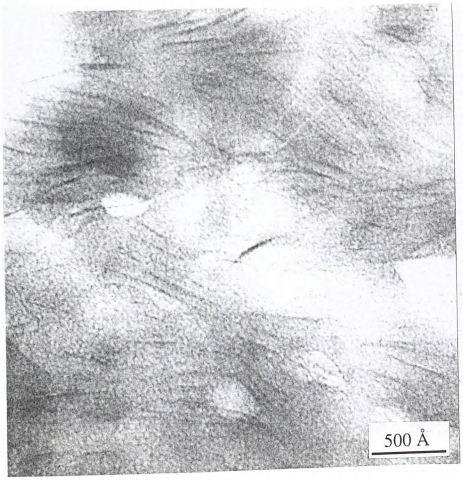

500 Å

**Figure IV 5**. (B) Intercalated epoxy-clay nanocomposite structure obtained with $CH_3(CH_2)_{15}NH_3^+$- fluorohectorite

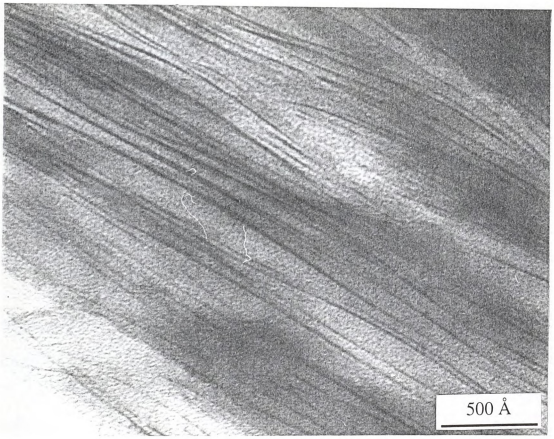
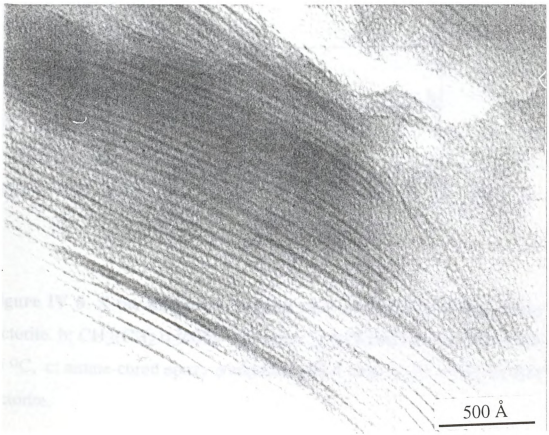

500 Å

**Figure IV 5**. (C) Intercalated epoxy-clay nanocomposite structure obtained with $CH_3(CH_2)_{15}NH_3^{+}$- vermiculite.


500 Å

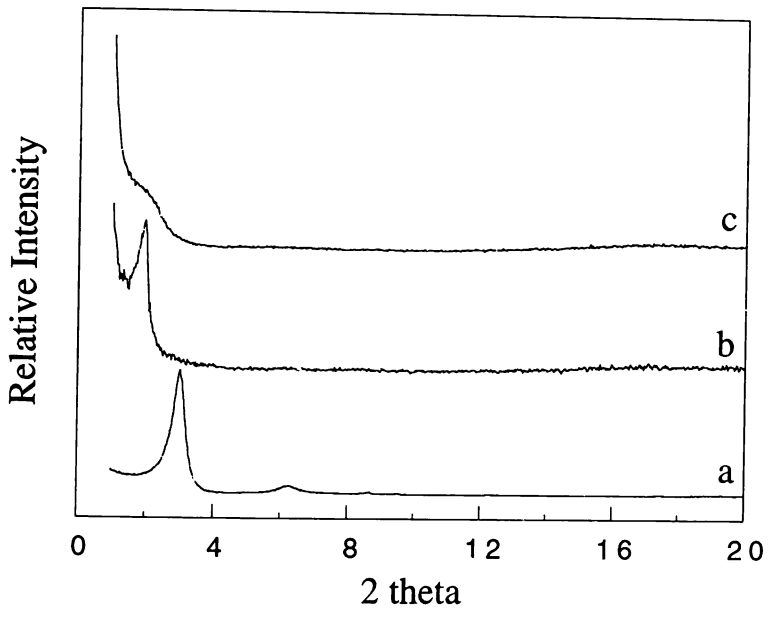
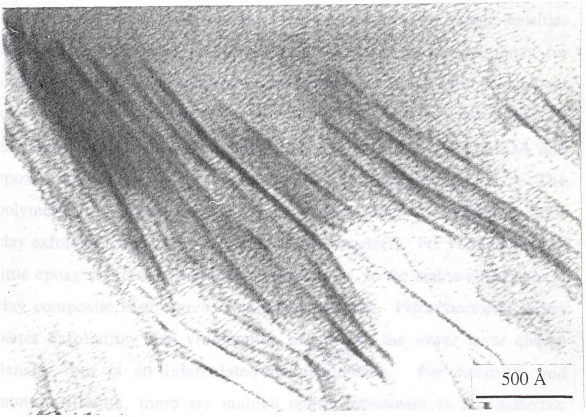



**Figure IV 6**. X-ray diffraction patterns of a: pristine $CH_3(CH_2)_{15}NH_3^+$-rectorite. b: $CH_3(CH_2)_{15}NH_3^+$-rectorite, (5 wt%) solvated by Epon-828 at 75 $^oC$, c: amine-cured epoxy composite with 5 wt% of $CH_3(CH_2)_{15}NH_3^+$-rectorite.

Rectorite is a regularly interstratified clay and its layer thickness is ~ 20 Å, with CEC of 60 meq./100g, therefore the layer charge density is between those of montmorillonite and fluorohectorite. Indeed, the X-ray diffraction patterns of amine-cured epoxy-rectorite indicate that the composite is an exfoliated nanocomposite structure. TEM shows (**Figure IV 7**) the distribution of the rectorite layers in the amine-cured epoxy matrix. The distribution is similar to that of hectorite. The layer thickness of rectorite is 20 Å, twice that of the normal smectite clays (10 Å). Therefore, in the TEM image, the dark lines, cross-sections of single rectorite layers are thicker than those of montmorillonite, hectorite and fluorohectorite.

**Figure IV 7**. TEM of amine-cured epoxy-clay exfoliated nanocomposite with $CH_3(CH_2)_{15}NH_3^+$- rectorite (5wt%).

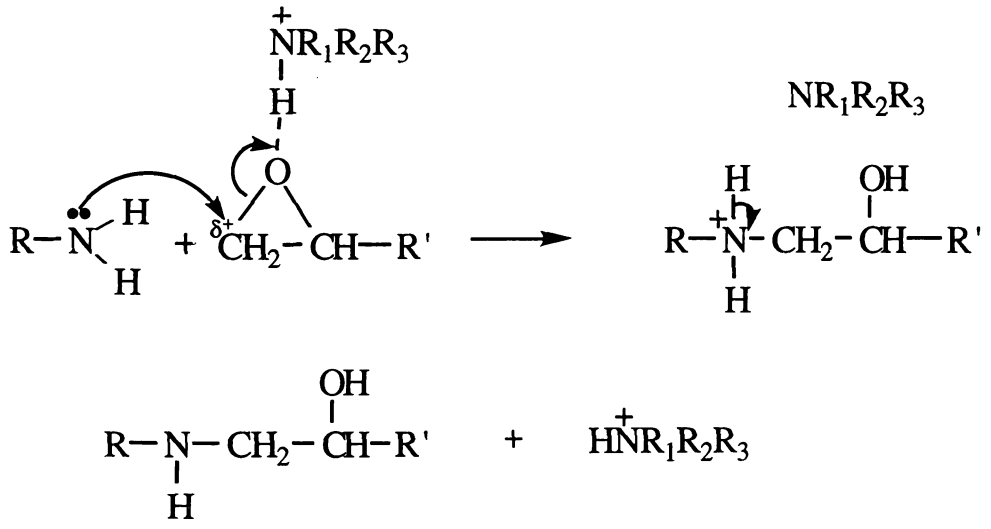

500 Å

The X-ray diffraction and TEM results of these amine-cured epoxy-clay composites show that the layer charge density of clays plays a very important role in clay tactoid exfoliation during the thermosetting process of thermoset polymers. Clays with a low to moderate layer charge densities such as hectorite and montmorillonite are very good candidates for exfoliated epoxy-clay nanocomposite formation. They exhibit excellent swelling properties in organic monomers and less amounts of alkylammonium ions in the gallery provide more space for mPDA and epoxy monomers to be accommodated in the clay gallery. The polymerization of monomers in the clay gallery is the basic driving force for clay exfoliation due to the migration of the monomers. For vermiculite, too little epoxy resin is present inside the galleries, so the amine-cured epoxy-clay composite is an intercalated nanocomposite. Fluorohectorite shows better exfoliation than vermiculite, because of the lower layer charge density, but is an intercalated nanocomposite. For hectorite and montmorillonite, there are enough epoxy monomers in the galleries, therefore exfoliated nanocomposites are achieved.

Some morphological properties of the pristine clay such as the length (width) of the clay plates (2-dimensional) are retained after composite formation. The exfoliation process makes the clay distribute randomly in the polymer matrix, but with locally ordered structure. "Ordered" means that the original clay tactoid structure still exists, but with irregular and much larger layer separation distances. The unique structure of the exfoliated epoxy-clay composites are expected to alter the mechanical properties of the material.

4. Effect of Gallery Cation Acidity on Nanocomposite Formation

Brönsted acids are known to catalyze epoxy-amine polymerization reactions.[35-37] Acid catalysis is also expected for our amine-cured epoxy-clay composite systems, because alkylammonium ions are present in the clay galleries.



**Scheme IV 1.** Catalytic Ring Opening of Epoxy by Acidic Onium ion

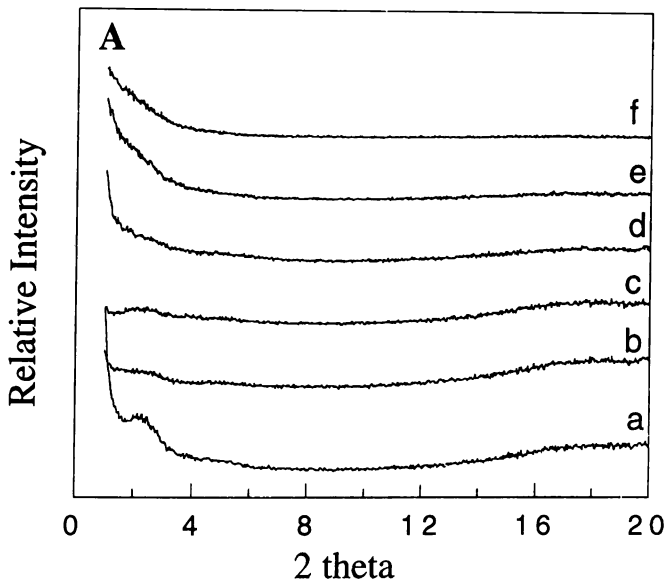
The following alkylammonium cations were used to study the catalytic effects on epoxy-clay nanocomposite formation; $CH_3(CH_2)_{17}NH_3^+$, $CH_3(CH_2)_{17}N(CH_3)H_2^+$, $CH_3(CH_2)_{17}N(CH_3)_2H^+$ and $CH_3(CH_2)_{17}N(CH)_3^+$. For these clays, the extent of the epoxy monomer intercalation into the clay galleries is essentially the same because intercalation of epoxy monomers into the organo clay gallery is dependent on the chain length of the intergallery cations (**Table IV 1**). X-ray diffraction patterns of the clays in the epoxy-amine curing process indicate

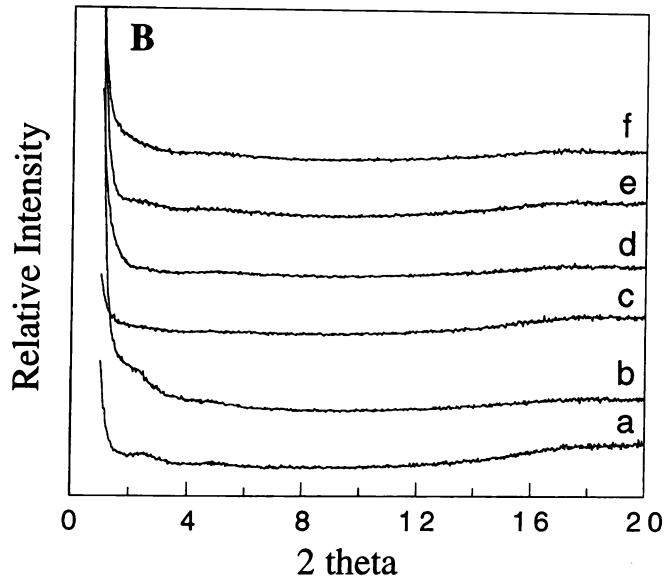
that clay exfoliation is dependent on the acidity of the gallery cations (**Figure IV 8**).

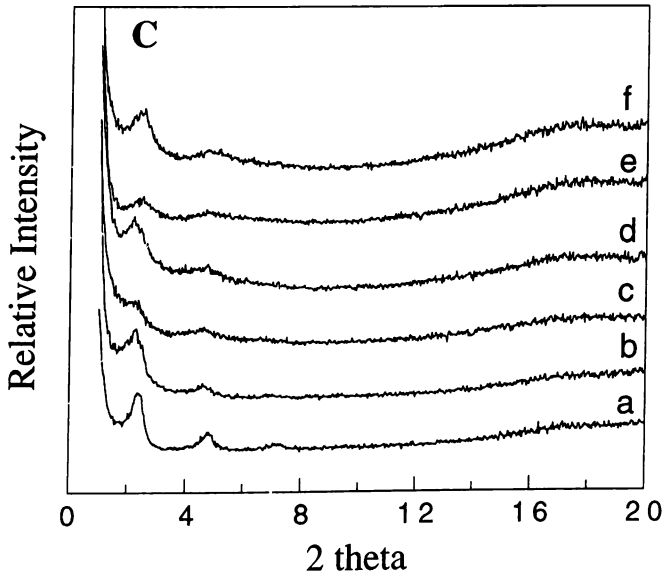
**Table IV 1.** Basal Spacings of Air-Dried Organoclays and Their Epoxy-Solvated Analogues (75 °C).

| Gallery Cations ( -montmorillonite ) | Air-Dried $d_{001}$, Å | Epoxy Solvated $d_{001}$, Å |
|---|---|---|
| $CH_3(CH_2)_{17}NH_3^+$ | 18.0 | 36.7 |
| $CH_3(CH_2)_{17}N(CH_3)H_2^+$ | 18.1 | 36.2 |
| $CH_3(CH_2)_{17}N(CH_3)_2H^+$ | 18.7 | 36.7 |
| $CH_3(CH_2)_{17}N(CH_3)_3^+$ | 22.1 | 36.9 |

**Figure IV 8** shows that montmorillonite clays with different acidities perform differently in the composite formation process. For high acidity clays with primary and secondary alkylammonium cations, (A) and (B), the $d_{001}$ of the clays disappears in a short curing time. For low and non-acidic clays with tertiary and quaternary alkylammonium exchange cations, the final composites still show $d_{001}$ diffraction peaks. These results indicate that the acidity of the gallery cations plays an important role in the epoxy-clay nanocomposite formation. The X-ray diffraction results for amine-cured epoxy-clay composites with these clays, (**Figure IV 9**), indicate that clays with primary and secondary onium ions form exfoliated nanocomposites, while those with tertiary and quaternary onium ions retain the clay tactoid structure, typical of intercalated nanocomposites.


A
f
e
d
c
b
a
Relative Intensity
0
4
8
12
16
20
2 theta


B
f
e
d
c
b
a
Relative Intensity
0
4
8
12
16
20
2 theta


C
f
e
d
c
b
a
Relative Intensity
0
4
8
12
16
20
2 theta

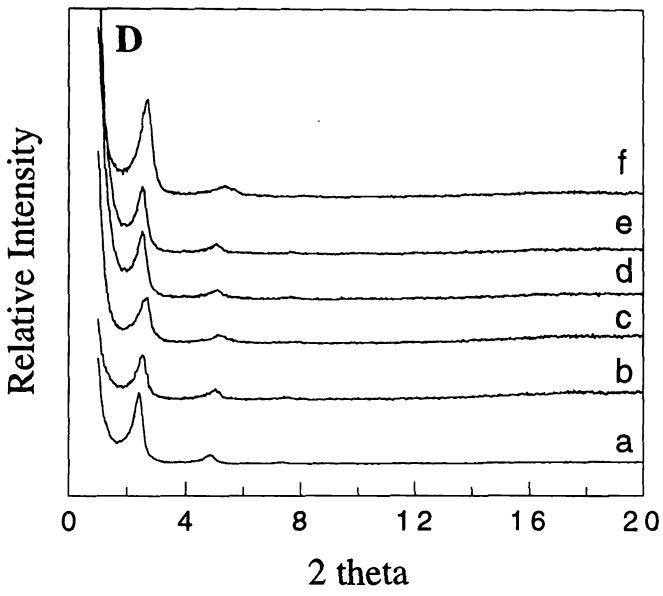



**Figure IV 8**. X-ray diffraction patterns of different organoclays in the amine-cured epoxy-clay (5 wt%) nanocomposite formation process.

A: $CH_3(CH_2)_{17}NH_3^+$; B: $CH_3(CH_2)_{17}NH_2(CH_3)^+$;

C: $CH_3(CH_2)_{17}NH(CH_3)_2^+$; D: $CH_3(CH_2)_{17}N(CH_3)_3^+$

a: 75 °C, 5 min. b: 75 °C, 1 h.

c: 75 °C, 2 h. d: 75 °C, 2 h plus 125 °C, 5 min.

e: 75 °C, 2 h plus 125 °C, 1 h. f: 75 °C, 2 h plus 125 °C, 2 h.

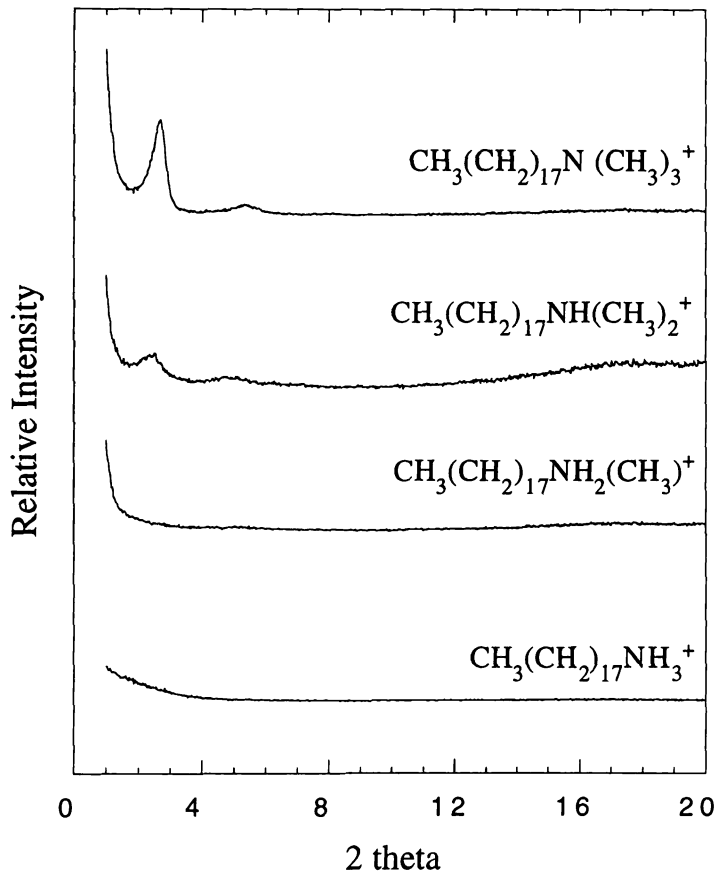



**Figure IV 9**. X-ray powder diffraction patterns of amine-cured epoxy-clay nanocomposites formed from montmorillonite clays (5 wt%) containing primary, secondary, tertiary and quaternary onium ions with a n-C18 chain.

The protons of the onium ions can be released to form a free proton, which is a good catalyst for epoxy polymerization.[32-34] The acidity of these onium ions is in the order, $RNH_3^+ > RNH_2(CH_3)^+ > RNH(CH_3)_2^+$ and there is no acidic proton associated with $RN(CH_3)_3^+$. The higher the acidity of the intergallery cations, the better the catalytic properties, and hence, the faster the epoxy polymerization reaction. When the polymerization rate of monomers in the intergallery region is higher than that outside the gallery, the monomer molecules residing outside of the gallery migrate into the gallery and undergo polymerization under the concentration gradient control. This process overcomes the electrostatic forces between the clay layers and the intergallery ions, allowing the clay tactoids to exfoliate. The migration of monomers into the gallery will continue until the monomers outside of the gallery form a network, which eventually freezes the clay layer expansion. Therefore, we begin to understand the dependence of exfoliated nanocomposite formation on the curing temperature. Under higher initial curing temperatures like 140 $^oC$, the polymerization reaction rate between epoxy and amine molecules is so fast that the epoxy-amine molecules in the outer gallery form a network which stops the clay layers from expanding, whereas under mild initial curing temperature, an exfoliated nanocomposite can be prepared.

5. Mechanical properties of mPDA-cured epoxy-clay nanocomposites

Mechanical properties such as tensile strength and modulus for the epoxy-clay nanocomposites have been studied. For the amine-cured epoxy matrix, the tensile strength is 90 MPa and tensile modulus is 1.1 GPa. A comparison of the exfoliated and intercalated nanocomposites show that the

exfoliated nanocomposites exhibit enhanced mechanical performance (**Table IV 2** and **Figure IV 10**).

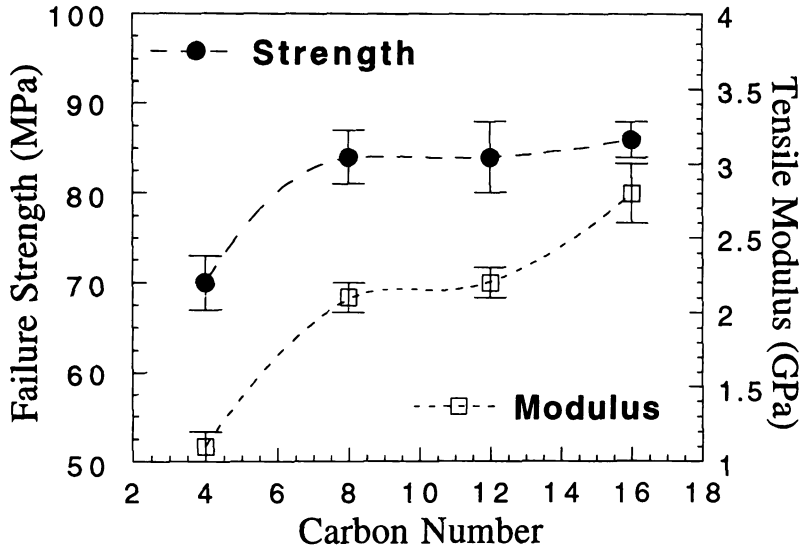



**Figure IV 10**. Tensile strength and modulus of amine-cured epoxy-clay nanocomposites with clay loading of 2 wt%.

**Table IV 2.** Mechanical Properties of Epoxy-Clay Nanocomposites Containing 1.0 wt% of $CH_3(CH_2)_{15}NH_3^+$-Clays.

| Clay Samples (1 wt%) | Failure Strength (MPa) | Tensile Modulus (GPa) |
|---|---|---|
| no clay | 90 ± 3 | 1.10 + 0.03 |
| Laponite | 83 ± 2 | 1.59 ± 0.04 |
| Hectorite | 94 ± 2 | 1.65 ± 0.03 |
| Montmorillonite | 92 ± 5 | 1.49.± 0.03 |
| Fluorohectorite | 73 ± 3 | 1.55 ± 0.06 |

**Figure IV 10** shows the dependence of tensile strength and modulus of the epoxy-clay nanocomposite on the chain length of the clay gallery cations. It is very interesting to note that the tensile strength and modulus of amine-cured montmorillonite composites increase with increasing chain length of the gallery onium ions, . The longer the alkyl chain, the greater the layer separation becomes. Therefore, we conclude that the exfoliated nanocomposites show improved mechanical performance with increasing chain length of the gallery alkylammonium ions. The tensile strengths and moduli of epoxy-clay nanocomposite with different clays are listed in **Table IV 2**. For the exfoliated montmorillonite and hectorite nanocomposites, improved mechanical performance relative to the intercalated fluorohectorite nanocomposite is observed. However, the exfoliated epoxy-laponite nanocomposite shows a lower tensile strength than that of montmorillonite or hectorite. This result may be explained by the low aspect ratio of the silicate layers of laponite. Therefore, the relationship between composite mechanical properties and organoclay properties is complicated and depends both on the extent of exfoliation and on the aspect ratio of the clay layers. Adding the 10 Å-thick layer silicate in the amine-cured epoxy matrix increases the tensile strength and modulus because of the high tensile strength and modulus of the single silicate sheet. The mixing rule used in fiber reinforced polymer composites may be applicable here. If the clays exist in a tactoid form, there will be a boundary (phase separation) between clays and polymer matrices, although a monolayer of polymer may penetrate into the clay gallery. This may explain the better performance of exfoliated nanocomposites on the tensile properties. By increasing the content of the

clay

mech

D. C

prep

regi

the

synt

limi

Cat

mo

for

pol

im

cu

th

st

clay inside the amine-cured epoxy matrix, significant improvement of mechanical properties is expected.

**D. Conclusion**

Two types of amine-cured epoxy-clay nanocomposites have been prepared by tuning the polymerization rate inside/outside clay gallery regions. With linear long chain alkylammonium ions as intergallery cations, the uncured epoxy solvated clays act as very good precursors for the synthesis of nanocomposites. The layer charge density of the pristine clays limits the concentration of monomers within the intergallery region. Catalytic reactions on the monomer polymerization in the clay gallery allow more monomers to enter the galleries and undergo further polymerization to form a nanocomposite. This synthetic approach can be applied to other polymer-clay nanocomposite systems.

Tensile strengths and moduli of exfoliated nanocomposites are improved over those of the intercalated nanocomposites of the glassy amine-cured epoxy polymer matrix. The reinforcement of the polymer matrix by the individual clay 10 Å-thick layers is assumed to be due to the high bond strength within the 2-dimension silicate layers.

E. R

1. G

2. E

3. H

4. M

5. S

6. P

127

7. S

8. M

9. J

10.

11.

12

13

El

14

15

(1

## E. References

1. G.M. Whitesides, T.P. Mathias, C.T. Seto, *Science*, **254**, 1312 (1991).

2. E.P. Giannelis, *JOM*, **44**, 28 (1992).

3. H. Gleiter, *Adv. Mater.*, **4**, 474 (1992).

4. M.B. Novak, *Adv. Mater.*, **5**, 422 (1993).

5. S.N. Maiti, B.H. Lopez, *J. Apply. Polym. Sci.*, **44**, 353 (1992).

6. P. Godard, J.L Wertz, J.J. Biebuyck, J. P. Mercier, *Polym, Eng. Sci.*, **29**, 127 (1989).

7. S.N. Maiti, K.K. Sharma, *J. Mater. Sci.*, **27**, 313 (1992).

8. M. A. Ramos, J.P.V. Matheu, *Polym. Comps.*, **9**, 105 (1988).

9. J. P. Trotignon, L. Demdoum J. Verdu, *Composites*, **23**, 2563 (1992).

10. S. F. Xavier, J. M. Schultz, *J. Mater. Sci.*, **25**, 2428 (1990).

11. M.S. Wang, Ph.D. Thesis, Michigan State University, (1993).

12. T.J. Pinnavaia, *Science* , **220**, 365 (1983).

13. B.K.G. Theng, Formation and Properties of Clay-Polymer Complexes, Elsevier, New York, (1979).

14. R. A. Vaia, H. Ishii, E.P. Giannelis, *Chem. Mater.*, **5**, 1694 (1993).

15. C. Kato, K. Kuroda, M. Misawa, *Clays and Clay Minerals*, **27**, 129 (1979).

16. Y. Sugahara, T. Sugiyama, T. Nagayama, K. Kuroda, C. Kato, *J. of the Ceramic Society of Japan*, **100**, 413 (1992).

17. P.B. Messersmith, E.P. Giannelis, *Chem. Mater.*, **5**, 1064 (1993).

18. V. Mehrotra, E.P. Giannelis, *Solid State Communications*, **77**, 155 (1991).

19. T. Lan, P.D. Kaviratna, T.J. Pinnavaia, *Polymer Preprints*, **35-1**, 823 (1994).

20. Y. Fukushima, S. Inagaki, *J. Inclusion Phenomena*, **5**, 473 (1987).

21 Y. Fukushima, A. Okada, M. Kawasumi, T. Kurauchi, O. Kamigaito, *Clay Miner.*, **23** , 27 (1988).

22. A. Usuki, M. Kawasumi, Y. Kojima, A. Okada, T. Kurauchi, O. Kamigaito, *J. Mater. Res.*, **8**, 1174 (1993).

23. A. Usuki, Y. Kojima, M. Kawasumi, A. Okada, Y. Fukushima, T. Kurauchi, O. Kamigaito, *J. Mater. Res.*, **8**, 1179 (1993).

24. Y. Kojima, A. Usuki, M. Kawasumi, A. Okada, Y. Fukushima, T. Kurauchi, O. Kamigaito, *J. Mater. Res.*, **8**, 1185 (1993).

25. P.D. Kaviratna, T. Lan, T.J. Pinnavaia, *Polymer Preprints*, **35-1**, 788 (1994).

26. T.J. Pinnavaia, T. Lan, P.D. Kaviratna, M. Wang Clay-Polymer Nanocomposites: Polyether and Polyimide Systems. *MRS Symposium, Paper* N-2.8, (1994).

27. M. Wang, T.J. Pinnavaia, *Chem. Mater.*, **6**, 468 (1994).

28. S. Landau Ph. D. Thesis, "Physical and Catalytical Properties of Hydroxy-Metal Intercalated Smectite Minerals" Chemistry Department, Michigan State University, (1985).

29. J.M. Millsand, M.A. Zwarich, *Clays and Clay Miner.*, **20** 169 (1972).

30. J. Butrulle, T.J. Pinnavaia, "Characterization of Catalytical Materials" I.E. Wachs, Ed. Butterworth-Heinemann, Boston, 149 (1992).

31. J. Guan, E. Min, Z. Yu Proc. 9th Congr. Cata., Calgary, Canada, Vol. 1, ed. M. Phillips and M. Ternan, Chem. Inst. Canada, Ottawa, 104 (1988).

32. C.L. Lin; T. Lee, T.J. Pinnavaia, *ACS Symp. Ser.*, **499**, 145 (1992).

33. T. Lee, Ph. D. Thesis, Michigan State University, (1992).

34. D.W. Schiering, J.E. Katon, L.T. Drzal, V.B. Gupta, *J. Apply. Polym. Sci.*, **34**, 2367 (1987).

35. T. Kamon, H. Furakaw, in Epoxy Resins and Composites IV, Dusek, K. ed. *Advances in Polymer Science*, vol. **80**. Springer-Verlag, Berlin, 177 (1986).

36. J.M. Barton, in Epoxy Resins and Composites I, Dusek, K. ed. *Advances in Polymer Science*, vol. **72**. Springer-Verlag, Berlin, 120 (1985).

37. C.A. May, ed. Epoxy Resins, 2nd ed., Marcel Dekker, New York, (1988).

# Chapter V

## Synthesis, Characterization and Mechanical Properties of Novel Sub-Ambient $T_g$ Epoxy - Clay Nanocomposites

### A. Introduction

Hybrid organic-inorganic composites typically exhibit mechanical properties superior to those of their separate components. In order to optimize the performance properties of these materials it is usually desirable to disperse the inorganic components in the organic matrix on a nanometer length scale.[1-3] One successful approach to achieve such nanocomposites is the *in situ* polymerization of metal alkoxides in organic matrices *through* the sol-gel process. Inorganic components, especially silica, have been formed by the hydrolysis and condensation of a mononuclear precursor, such as tetraethoxysilane (TEOS), in many polymer systems.[4-8] Owing to the loss of volatile by-products formed in the hydrolysis/condensation reaction, it is difficult to control sample shrinkage after molding. More recently, however, novel non-shrinkage hybrids have been reported.[8]

Smectite clays and other layered inorganic materials that can be broken down into nanoscale building blocks are good alternatives to the sol-gel process for the preparation of organic-inorganic nanocomposites.[9] In general, the polymer-clay composites can be divided into three categories: conventional composites, intercalated nanocomposites and exfoliated nanocomposites. In a conventional composite, the clay tactoids exist in their original aggregated state with no intercalation of the polymer matrix into the

clay. In an intercalated nanocomposite the insertion of polymer into the clay structure occurs in a crystallographically regular fashion, regardless of the clay to polymer ratio. An intercalated nanocomposite normally is interlayered by only a few molecular layers of polymer and the properties of the composites typically resemble those of the ceramic host.[10-13] In contrast, in an exfoliated nanocomposite, the individual 10 Å-thick clay layers are separated in a continuous polymer matrix by average distances that depend on loading. Usually, the clay content of an exfoliated clay composite is much lower than that of an intercalated nanocomposite. Consequently, an exfoliated nanocomposite has a monolithic structure with properties related primarily to those of the of the starting polymer.

The exfoliation of smectite clays provides 10 Å-thick silicate layers with high in - plane bond strength and aspect ratios comparable to those found for fiber reinforced polymer composites. Exfoliated clay nanocomposites formed between organocation exchanged montmorillonites and thermoplastic nylon-6 have recently been described by Toyota researchers.[14-16] Clay exfoliation in the nylon-6 matrix gave rise to greatly improved mechanical, thermal and rheological properties, making possible new materials applications of this polymer.[17-18]

Epoxy-exfoliated clay nanocomposites formed with Epon-828 resin and meta-phenylenediamine as the curing agent have been prepared in our laboratory by using long chain alkylammonium-exchanged smectite clays.[19,20] The mechanical properties of the exfoliated nanocomposites, however, were only marginally improved relative to those of conventional composites. Due to the high glass transition temperature (~150 $^{o}$C) of the epoxy matrix, the composites are in a glassy state at room temperature.

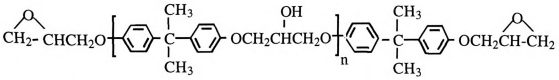
Greatly enhanced properties might be expected for exfoliated epoxy-clay nanocomposites with sub-ambient glass transition temperatures. Thus, it was of interest to examine the properties of an epoxy-clay nanocomposite in a rubbery state. On the basis of on our previous results that clays with different acidities may form intercalated and exfoliated epoxy-nanocomposites, we synthesized both intercalated and exfoliated sub-ambient glass transition temperature epoxy-clay nanocomposites and compared their tensile properties.

**B. Experimental**

1. Materials

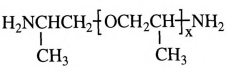
Natural hectorite, montmorillonite, rectorite and synthetic fluorohectorite clays were used as clay components in our epoxy-clay nanocomposites. The purification procedures used and the chemical formulas are given in **Chapter III** and **IV**. Long chain primary alkylamines $CH_3(CH_2)_{n-1}NH_2$, where n = 8, 10, 12, 18, and the quaternary alkylammonium $CH_3(CH_2)_{17}N(CH_3)_3Br$ salt were purchased from Aldrich Chemicals and used as received. These alkylammonium species were exchanged into clay galleries to prepare organoclays.

Epon-828 (Shell Co.) with an average molecular weight of 380 was used as epoxy resin.



n = 0 (88%); n = 1 (10%); n = 2 (2%).

The following polyetheramine (JEFFAMINE D2000, Texaco Co.) was used as the curing agent to achieve sub-ambient glass transition temperatures:



where x = 33.1 and the molecular weight is 2000.

2. Synthesis of JEFFAMINE-Epoxy-Clay Nanocomposite

Equivalent amounts of the epoxide resin (27.5 wt%) and the polyetheramine (72.5 wt%) were mixed at 75 $^{o}$C for 30 min. The desired amount of organoclay, from 2 to 23.2 wt%, was added to the epoxide-amine mixture and stirred for another 30 min. The clay-epoxide-amine complex was then outgassed in vacuum for 10 min and transferred into an aluminum mold for curing at 75 $^{o}$C for 3 h and then at 125 $^{o}$C for an additional 3 h.

3. Physical Measurements

X-ray diffraction patterns were obtained by using a Rigaku X-ray diffractometer with a rotating anode (Cu) and a curved graphite monochromater. Samples for X-ray diffraction were prepared by crushing the epoxy-clay composite specimens and collecting the particle size range of 150 μm to 180 μm.

Transmission electron micrographs (TEM) were obtained with a JEOL-100CX microscope, operated with an acceleration voltage of 100 kV. The crushed epoxy-clay composite samples were encapsulated with the embedding agent, Hard-Spurr, which was allowed 48 h at 60 $^{o}$C to polymerize. The embedded sample was ultrathin sectioned by using a microtome equipped with a glass knife. The thin-sections ranged from 600 Å to 900 Å thick.

4. Tensile Testing of Epoxy-Clay Nanocomposites

The tensile strengths and moduli of our new epoxy-clay nanocomposites were measured according to ASTM method 3039 by using a

UTS system. The specimens had dimensions of 1.50 x 4.00 x 25.40 $mm^3$, with a deviation of thickness of 0.01 mm. Tensile testing was performed at ambient temperature with a strain rate of 0.51 mm/min. The maximum failure strength and Young's modulus of the tested sample were obtained from the stress-strain curve. At least 5, usually 5 - 8, specimens were measured for each sample and the average data and the standard deviation were plotted.

## C. Results and Discussion

### 1. Preparation and Characterization of D2000-Epoxy Clay Nanocomposites

The synthetic route we applied in mPDA-epoxy system (**Chapter IV**) is not suitable for D2000-epoxy system because of the percentage of the epoxy resin in the matrix (27.5 wt%) compared with that of the mPDA case (85.5 wt%) is relatively low. The low percentage of epoxy resin makes the formation of the epoxy-clay complex very difficult especially for composites with high clay loading. The slow curing nature of D2000-epoxy reaction system allows us to blend epoxy and curing agent prior to solvation of the clay in the epoxy resin. As a preliminary experiment, solvation of JEFFAMINE D2000 to organoclays was carried out. In contrast to the epoxy resin solvation to the organoclay, there is no indication of the intercalation of D2000 into the organoclay galleries as judged by the X-ray diffraction patterns. The reason may be the non-capability between the ether linkage $-CH_2-O-CH_2-$ of the D2000 and the $-CH_2-$ segment of the alkyl chains. Also, no intercalation of the D2000-epoxy mixture into the organoclay was observed when the clay was added into the D2000-epoxy mixture. The changes of the basal spacing in the D2000-epoxy curing process were monitored at different reaction times.

We have observed that organoclays with different alkyl chain length perform differently in the mPDA-epoxy nanocomposite formation. Therefore, we examined the D2000-epoxy nanocomposite formation with $CH_3(CH_2)_{n-1}NH_3^+$-montmorillonite, where n= 8 and 18. X-ray diffraction patterns of the epoxy-clay composites containing $CH_3(CH_2)_7NH_3^+$- and $CH_3(CH_2)_{17}NH_3^+$-montmorillonite are shown in **Figure V 1**.

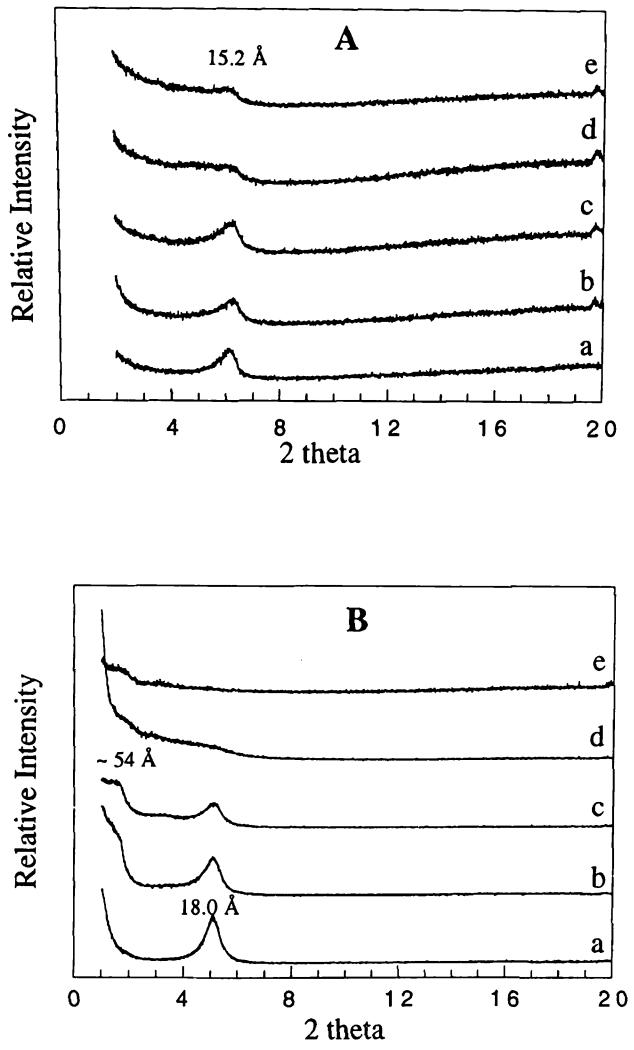



**Figure V 1.** X-ray diffraction patterns of (A) $CH_3(CH_2)_7NH_3^+$-montmorillonite and (B) $CH_3(CH_2)_{17}NH_3^+$-montmorillonite in stoichiometric mixtures of epoxide resin and polyetheramine curing agent after reaction under the following conditions: a: 75 °C, 10 min; b: 75 °C, 1h; c: 75 °C, 3 h; d. 75 °C, 3 h. and 125 °C, 1 h; e: 75 °C, 3 h. 125 °C, 3 h. The clay loading in each case was 10 wt%.

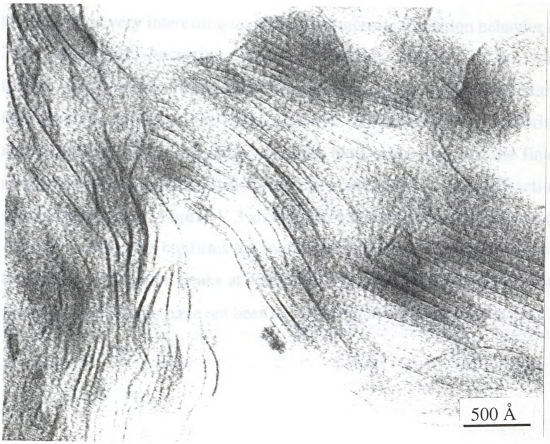
These diffraction patterns reveal the clay basal spacing changes which occur in the epoxy curing process. It is noteworthy that $CH_3(CH_2)_7NH_3^+$- and $CH_3(CH_2)_{17}NH_3^+$-montmorillonites respond differently to the epoxide-polyetheramine reaction mixture. For $CH_3(CH_2)_7NH_3^+$-montmorillonite (**Figure V 1** A), the initial basal spacing at 15.2 Å is retained throughout the curing process, but significant broadening and reduction of scattering intensity occur for this reflection at 125 °C. For $CH_3(CH_2)_{17}NH_3^+$-montmorillonite (**Figure V 1** B), the basal spacing increases with reaction time and temperature. A new diffraction line with basal spacing at 54 Å appears after curing at 75 °C for 3 h, while the intensity of the original clay diffraction line decreases. With further curing at 125 °C, the clay diffraction lines are too broad to be distinguishable. Therefore, for $CH_3(CH_2)_{17}NH_3^+$-montmorillonite, an exfoliated nanocomposite is achieved. In contrast, $CH_3(CH_2)_7NH_3^+$-montmorillonite is only partially exfoliated in the polymer matrix .

The formation of exfoliated clay nanocomposites is dependent on the nature of the alkylammonium exchanged clays. Longer linear alkyl chains facilitate the formation of the nanocomposite. Heating the $CH_3(CH_2)_{17}NH_3^+$-montmorillonite system at 75 °C causes the epoxide and amine to migrate into the clay galleries and form an intermediate with a 54 Å basal spacing. Upon additional heating, further polymerization is catalyzed by the acidic primary amine[23-25] and more epoxide and amine enters the galleries, leading to the formation of an exfoliated nanocomposite. Thus, the exfoliation of the clay is caused by intragallery polymer formation. In the case of $CH_3(CH_2)_7NH_3^+$-montmorillonite, the hydrophobicity of the galleries is relatively low, and the amount of intercalated epoxide and amine

is insufficient to achieve exfoliation. Therefore, only a portion of the clay is delaminated, as evidenced by the broadening and decreased scattering intensity of the 15.2 Å reflection, and the remainder of the clay retains its original basal spacing. Consequently, the final product in the case of $CH_3(CH_2)_7NH_3^+$-montmorillonite is a mixture of exfoliated and conventional clay composites.

A TEM image of the exfoliated D2000-epoxy clay nanocomposite has been obtained from the thin-sections of the composite sample to verify the exfoliation structure and study the special clay morphology in the polymer matrix. A typical TEM image of the epoxy-exfoliated clay nanocomposite containing $CH_3(CH_2)_{17}NH_3^+$-montmorillonite is shown in **Figure V 2**. The dark lines are the cross sections of the 10 Å-thick silicate layers. A face-face layer morphology is retained but the layers are irregularly separated by ~80 - 150 Å of polymer. This clay particle morphology is correlated with the absence of Bragg X-ray scattering. The TEM images and XRD patterns of the epoxy composite formed with $CH_3(CH_2)_{11}NH_3^+$-montmorillonite were essentially the same as those for the $CH_3(CH_2)_{17}NH_3^+$-montmorillonite system.

**Figure V 2.** TEM image of the D2000-epoxy clay nanocomposite containing 20 wt% $CH_3(CH_2)_{17}NH_3^+$-montmorillonite.


500 Å



As stated in **Chapter IV**, in the mPDA-epoxy system, hectorite and rectorite form exfoliated nanocomposite structures, and fluorohectorite, because of the high charge density, forms an intercalated nanocomposite structure. It is very interesting to study the composite formation behavior of $CH_3(CH_2)_{17}NH_3^+$-hectorite, fluorohectorite and rectorite in the sub-ambient epoxy matrix. In the D2000-epoxy system, we have observed the basal spacing changes in the curing process. For hectorite, and rectorite, results similar to those of montmorillonite have been obtained; the finial composites are exfoliated nanocomposites and their X-ray diffraction patterns are shown in **Figure V 3** and **Figure V 4,** respectively. The lack of a clay $d_{001}$ reflection confirms the formation of exfoliated nanocomposites. The in-plane diffraction peaks at 4.54 Å ($d_{011}$) and 1.60 Å ($d_{060}$) indicate the clay 2-D structures have not been destroyed in the exfoliation process.

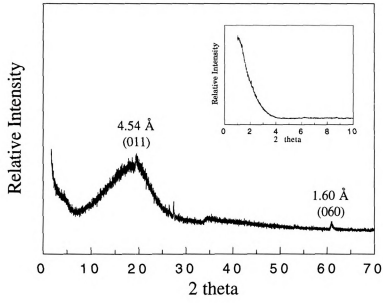



**Figure V 3.** X-ray diffraction pattern of D2000-epoxy composite containing 10 wt% of $CH_3(CH_2)_{17}NH_3^+$-rectorite. Inset is the enlarged region from 1 to 10°.

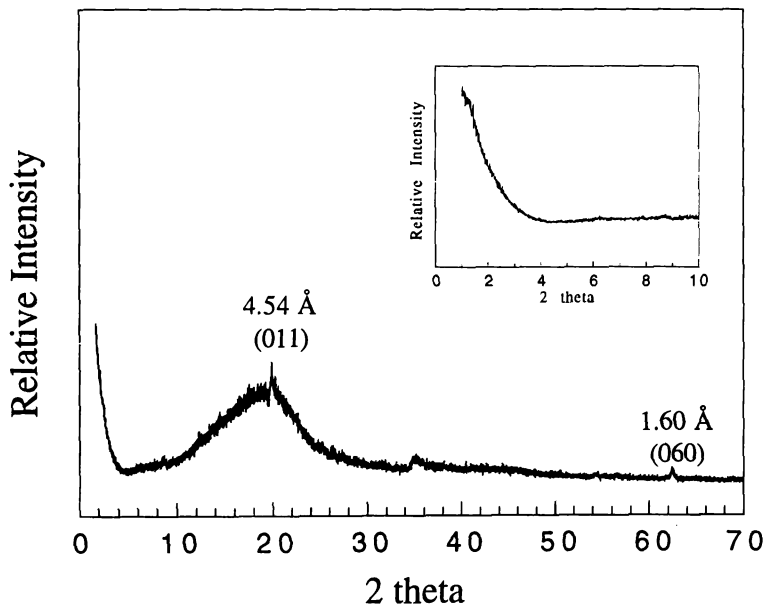



**Figure V 4.** X-ray diffraction pattern of D-2000-epoxy composite containing 10 wt% of $CH_3(CH_2)_{17}NH_3^+$-hectorite. Inset is the enlarged region from 1 to 10°.

The slow curing nature of D2000-epoxy system allows us to monitor the formation of the exfoliated nanocomposites. It is also very interesting to observe the formation of an intercalated nanocomposite. $CH_3(CH_2)_{17}NH_3^+$-fluorohectorite was selected for the intercalated nanocomposite formation experiment on the basis of our mPDA-epoxy results (**Chapter IV**). Changes of the basal spacing of $CH_3(CH_2)_{17}NH_3^+$-fluorohectorite in the formation of nanocomposites can be observed in **Figure V 5**. At 10 min reaction time (curve A), two phases were detected from the broadness of the diffraction peaks. The first is $CH_3(CH_2)_{17}NH_3^+$-fluorohectorite slightly solvated by D2000-epoxy, with $d_{001}$ at 38.7 Å and $d_{002}$ at 19.4 Å. The second is a more solvated phase, with $d_{001}$ at 56.0 Å and $d_{002}$ at 28.1 Å. After reaction at 75 $^oC$ for 1 h, the X-ray diffraction pattern (curve B) only shows one phase of fluorohectorite in the composite system and the $d_{00l}$ diffraction peaks ($l$ = 1 - 4) are 57.7 Å, 28.8 Å, 19.3 Å and 14.4 Å respectively. After reaction at 75 $^oC$ for 3 h, we find new diffraction lines; the previous diffraction lines has disappeared. These initially appeared to be no obvious relationship among the 55.5 Å, 34.9 Å and 26.5 Å diffraction peaks. But after considering the layer separation expansion with reaction time, we assigned these peaks as the $d_{002}$, $d_{003}$, and $d_{004}$ diffractions of the clay, the $d_{001}$ diffractions, which would be around 110 Å, can not be detected by our instrument. With further increasing reaction time and temperature, the line broadening of the previous diffraction lines can be seen in curve D and E in **Figure V 5**. A very well defined intercalated nanocomposite containing 10 wt% $CH_3(CH_2)_{17}NH_3^+$-fluorohectorite was obtained. With a different clay percentage, we observed similar diffraction patterns. The TEM image of an Epoxy-D2000 composite

containing 10 wt% $CH_3(CH_2)_{17}NH_3^+$-fluorohectorite (**Figure V 6**) indicates the layer separation is in the range of 100 Å, on the same order of the nanocomposite containing $CH_3(CH_2)_{17}NH_3^+$-montmorillonite. The morphology of the fluorohectorite in the matrix is similar to that we found in mPDA-cured epoxy composite (**Chapter IV**). The TEM result seems to agree with the 110 Å basal spacing assumption. The large particle size may help the fluorohectorite to remain the tactoid structure in the finial composite. Therefore, the D2000-epoxy composite with $CH_3(CH_2)_{17}NH_3^+$-fluorohectorite is an extensively intercalated nanocomposite.

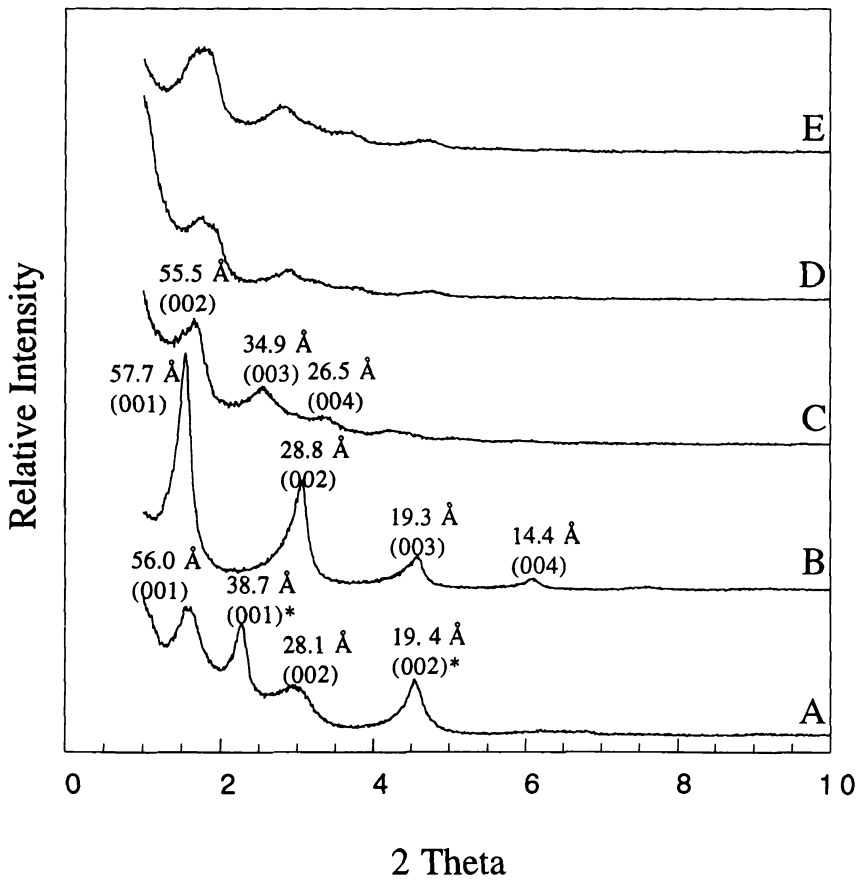
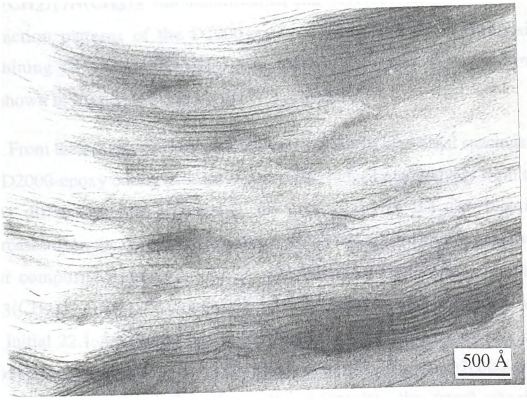



**Figure V 5.** X-ray diffraction patterns of $CH_3(CH_2)_{17}NH_3^+$-fluorohectorite in stoichiometric mixtures of epoxide resin and polyetheramine curing agent after reaction under the following conditions: A: 75 °C,10 min; B: 75 °C, 1h; C: 75 °C, 3 h; D: 75 °C, 3 h and 125 °C, 1 h; E: 75 °C, 3 h and 125 °C, 3 h. The clay loading in each case was 10 wt%.

**Figure V 6.** TEM image of the D2000-epoxy clay nanocomposite containing 10 wt% $CH_3(CH_2)_{17}NH_3^+$-fluorohectorite.


500 Å

Intercalated polymer-clay nanocomposites are expected to perform differently from exfoliated ones. In order to study their properties, we prepared the following intercalated nanocomposites by using non-acidic $CH_3(CH_2)_{17}N(CH_3)_3^+$-montmorillonite, and -fluorohectorite. The X-ray diffraction patterns of the D2000-epoxy solvated and cured composite containing $CH_3(CH_2)_{17}N(CH_3)_3^+$-montmorillonite, and -fluorohectorite are shown in **Figure V 7** and **Figure V 8** respectively.

From their X-ray patterns, a slight increase of the clay basal spacings in the D2000-epoxy curing process is observed. Judged qualitatively from the $d_{001}$ diffraction line broadening, the crystallinity of the clay tactoids decreases upon the composite formation. Good tactoid structure is preserved after composite formation. For the D2000-epoxy composite containing $CH_3(CH_2)_{17}N(CH_3)_3^+$-montmorillonite, the basal spacing increases from the initial 22.1 Å value to the 36. 4 Å value of the D2000-epoxy solvated state and to the 42.2 Å value in the finial composite. For the D2000-epoxy $CH_3(CH_2)_{17}N(CH_3)_3^+$-fluorohectorite composite, the basal spacing increases from initial the 29.3 Å value to 38.7 Å of the D2000-epoxy solvated state and remains at that value in the finial composite. Both $CH_3(CH_2)_{17}N(CH_3)_3^+$-montmorillonite and fluorohectorite formed typical intercalated nanocomposites.

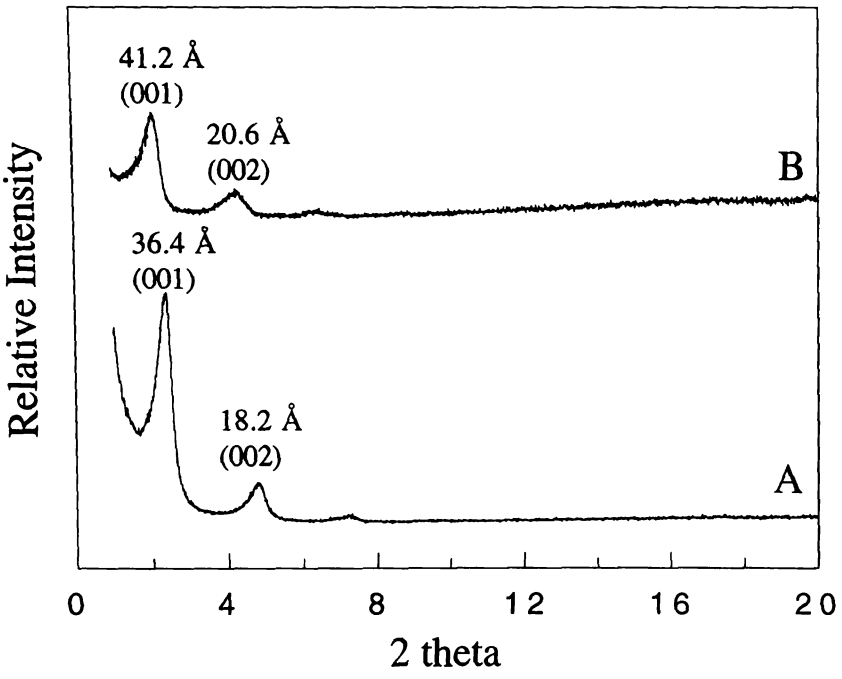



**Figure V 7.** X-ray diffraction patterns of D2000-epoxy solvated (A) and D2000-epoxy composite (B) with 10 wt% of $CH_3(CH_2)_{17}N(CH_3)_3^+$-montmorillonite.

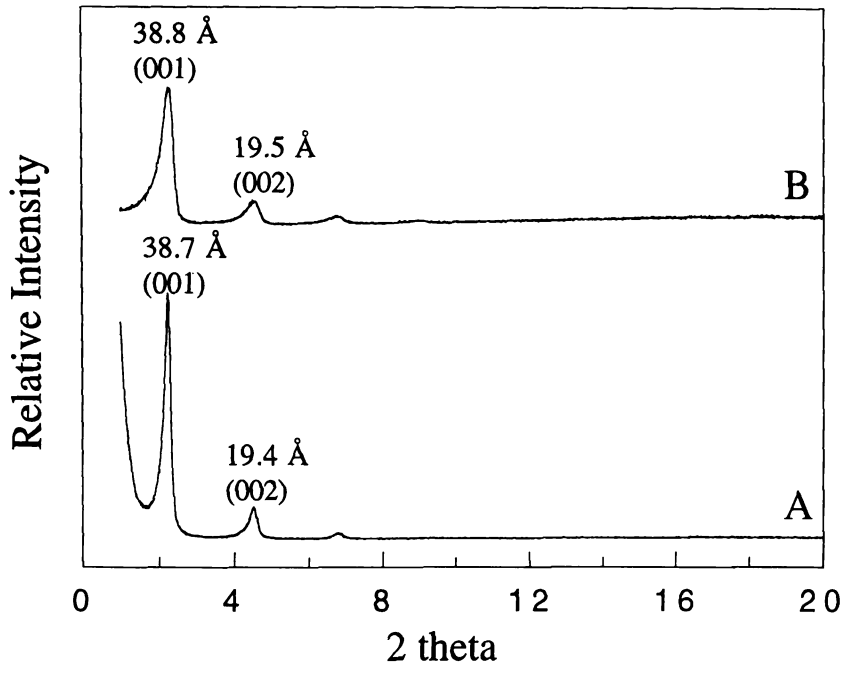



**Figure V 8.** X-ray diffraction patterns of D2000-epoxy solvated (A) and D2000-epoxy composite (B) with 10 wt% of $CH_3(CH_2)_{17}N(CH_3)_3^+$-fluorohectorite.

2. Mechanical Properties of D2000-Epoxy Clay Nanocomposites

The tensile strengths and moduli of our new epoxy-clay nanocomposites have been measured according to ASTM method 3039 by using a UTS system. The relationship between the alkylammonium cation chain length of the organoclay and the mechanical properties of the composites is illustrated in **Figure V 9** for loadings of 10 wt% $CH_3(CH_2)_{n-1}NH_3^+$-montmorillonite. The presence of the organoclay substantially increases both the tensile strength and the modulus relative to the pristine polymer. The mechanical properties increase with increasing clay exfoliation in the order $CH_3(CH_2)_7NH_3^+$- < $CH_3(CH_2)_{11}NH_3^+$- < $CH_3(CH_2)_{17}NH_3^+$-montmorillonite. In more exfoliated nanocomposites, 10 Å-thick clay single layers exhibit better reinforcement.

Dependence of the reinforcement of the epoxy-clay nanocomposites on clay loading has been studied. As shown in **Figure V 10**, the tensile strength and modulus for the $CH_3(CH_2)_{17}NH_3^+$-montmorillonite system increases nearly linearly with clay loading. More than a ten-fold increase in strength and modulus is realized by the addition of only 15 wt% (~ 7.5 vol%) of the exfoliated organoclay. It is noteworthy that the break elongation of the specimen in the tensile testing is fairly constant, and in the range of 50 ~ 60%.

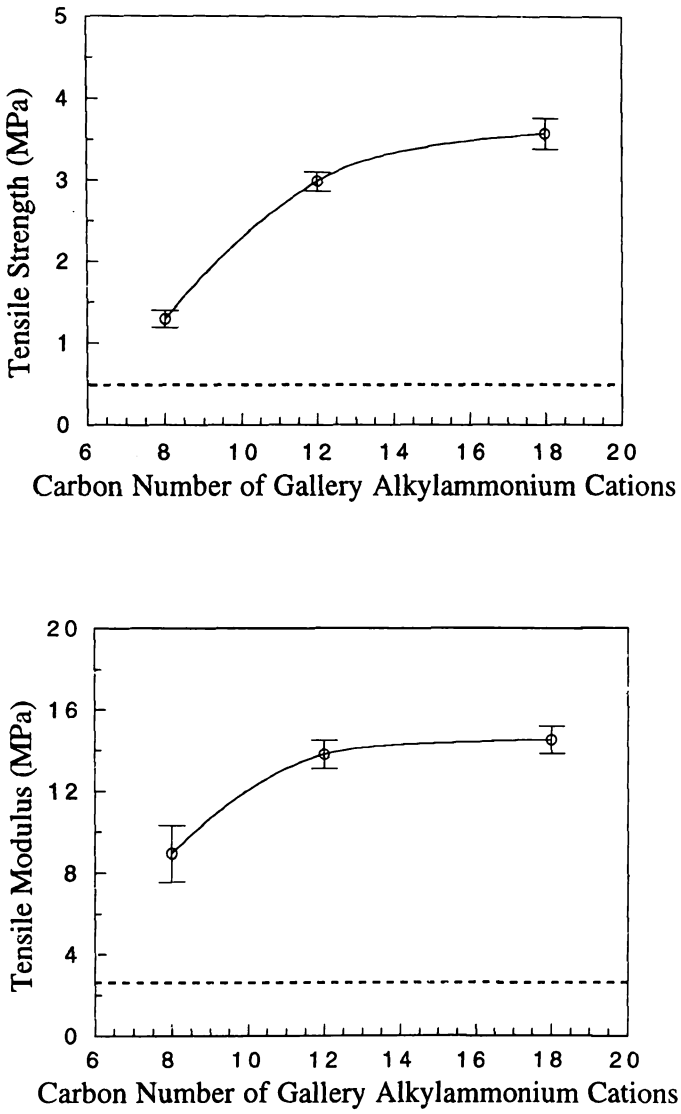



**Figure V 9.** Dependence of tensile strength and modulus of epoxy-organoclay composites on the chain length of the clay-intercalated alkylammonium ions. The clay loading in each case was 10 wt%. The dashed lines indicate the tensile strength and modulus of the polymer in absence of clay.

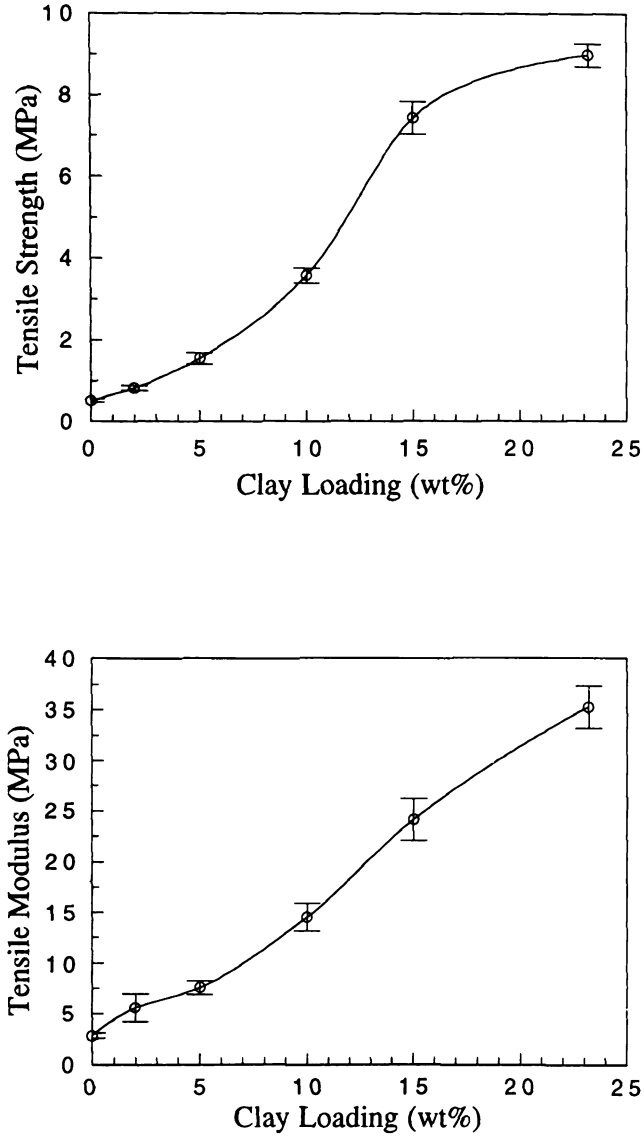



**Figure V 10.** Dependence of tensile strength and modulus on clay loading for D2000-epoxy-$CH_3(CH_2)_{17}NH_3^+$-montmorillonite nanocomposites.

Tensile properties of the exfoliated D2000-epoxy-clay nanocomposites containing different charge density clays have been measured for comparison of the reinforcing effect. From the tensile strength and modulus data (**Table V 1**) of the nanocomposites with different layer density clays, we find that tensile strength and modulus increase with clay loading (from 5 to 10 wt%) for all the clays. It is very interesting to notice that the tensile strengths and moduli for the nanocomposites having exfoliated structures, such as $CH_3(CH_2)_{17}NH_3^+$-montmorillonite, hectorite and rectorite, are very close. Whereas, for the intercalated nanocomposite having $CH_3(CH_2)_{17}NH_3^+$-fluorohectorite, its tensile strengths and moduli are relatively lower than those of the exfoliated ones at the same clay loading.

**Table V 1.** Tensile Strengths and Moduli of D2000-Epoxy Clay Composites with $CH_3(CH_2)_{17}NH_3^+$- Exchanged Montmorillonite, Hectorite, Rectorite and Fluorohectorite at 5 and 10 wt% Clay Loading.

| Clay | Tensile Strength (MPa) | | Modulus (MPa) | |
|---|---|---|---|---|
| $CH_3(CH_2)_{17}NH_3^+$- | 5 wt% | 10 wt% | 5 wt% | 10 wt% |
| montmorillonite | 1.55 ± 0.13 | 3.57 ± 0.18 | 7.59 ± 0.42 | 14.5 ± 0.6 |
| hectorite | 1.51 ± 0.09 | 2.94 ± 0.18 | 8.28 ± 0.67 | 14.5 ± 0.6 |
| rectorite | 1.52 ± 0.12 | 3.20 ± 0.20 | 6.90 ± 0.67 | 13.1 ± 0.6 |
| fluorohectorite | 1.17 ± 0.08 | 2.54 ± 0.11 | 9.66 ± 0.67 | 15.2 ± 0.6 |

We further studied the mechanical performance of D2000-epoxy clay nanocomposites that have exfoliated and intercalated structures. Tensile properties of $CH_3(CH_2)_{17}NH_3^+$- and $CH_3(CH_2)_{17}N(CH_3)_3^+$-montmorillonites at different clay loadings are given in **Figure V 11**. Both tensile strengths and moduli of the intercalated and exfoliated nanocomposites increase with increasing of the clay content in the composites. It is interested to notice that the tensile strengths and moduli of intercalated and exfoliated nanocomposites have very close values at low clay loading ($\leq$ 5 wt%). At high clay loading, (> 5 wt%), the exfoliated nanocomposites exhibit a much greater reinforcing effect than that of the intercalated ones.

$CH_3(CH_2)_{17}NH_3^+$- and $CH_3(CH_2)_{17}N(CH_3)_3^+$- fluorohectorite have basal spacing at 110 Å and 38.8 Å in D2000-epoxy matrix, respectively. It is interesting to compare the mechanical properties of intercalated nanocomposites which have different clay layer separation. From **Figure V 12**, the increasing trends of tensile strengths and moduli with increasing clay loading can be identified. We also find that the reinforcement effect on the tensile strength and modulus by the larger basal spacing clay is greater than those of low basal spacing clay.

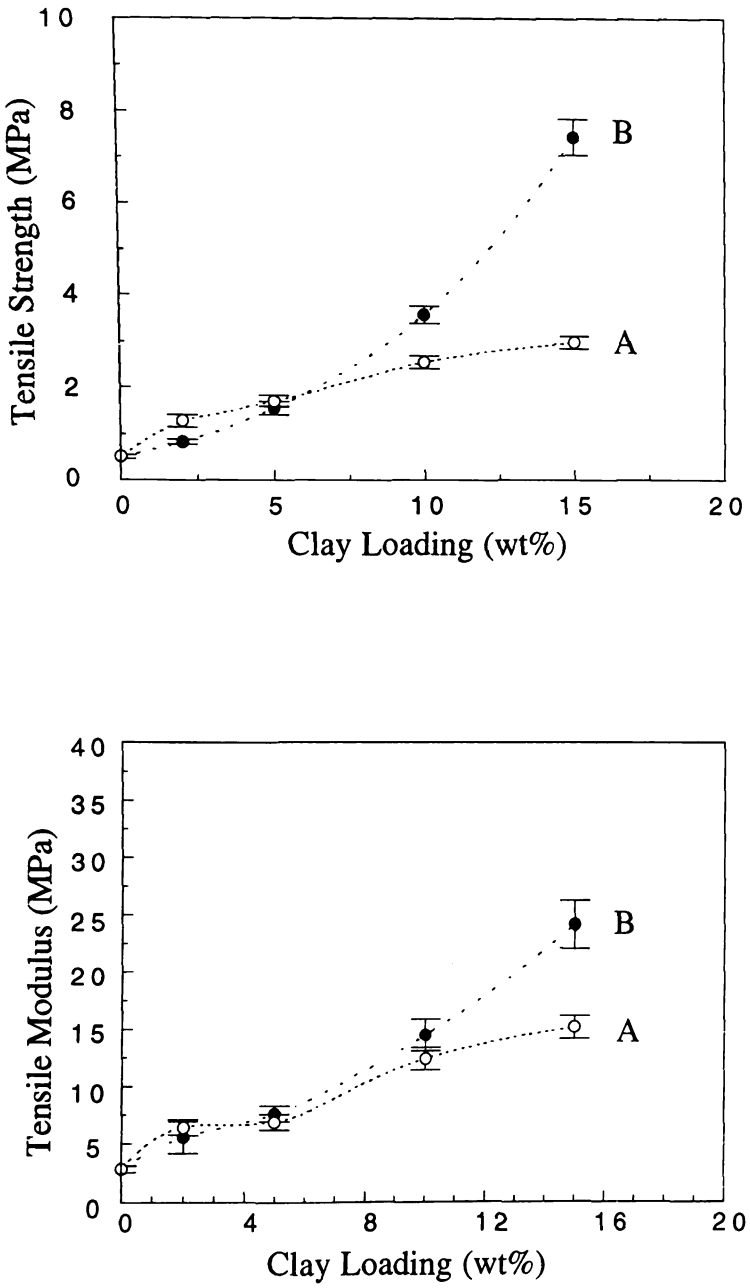



**Figure V 11.** Comparison of tensile strengths and moduli of intercalated nanocomposites containing $CH_3(CH_2)_{17}N(CH_3)_3^+$-montmorillonite (curve A) and exfoliated nanocomposites containing $CH_3(CH_2)_{17}NH_3^+$-montmorillonite (curve B).

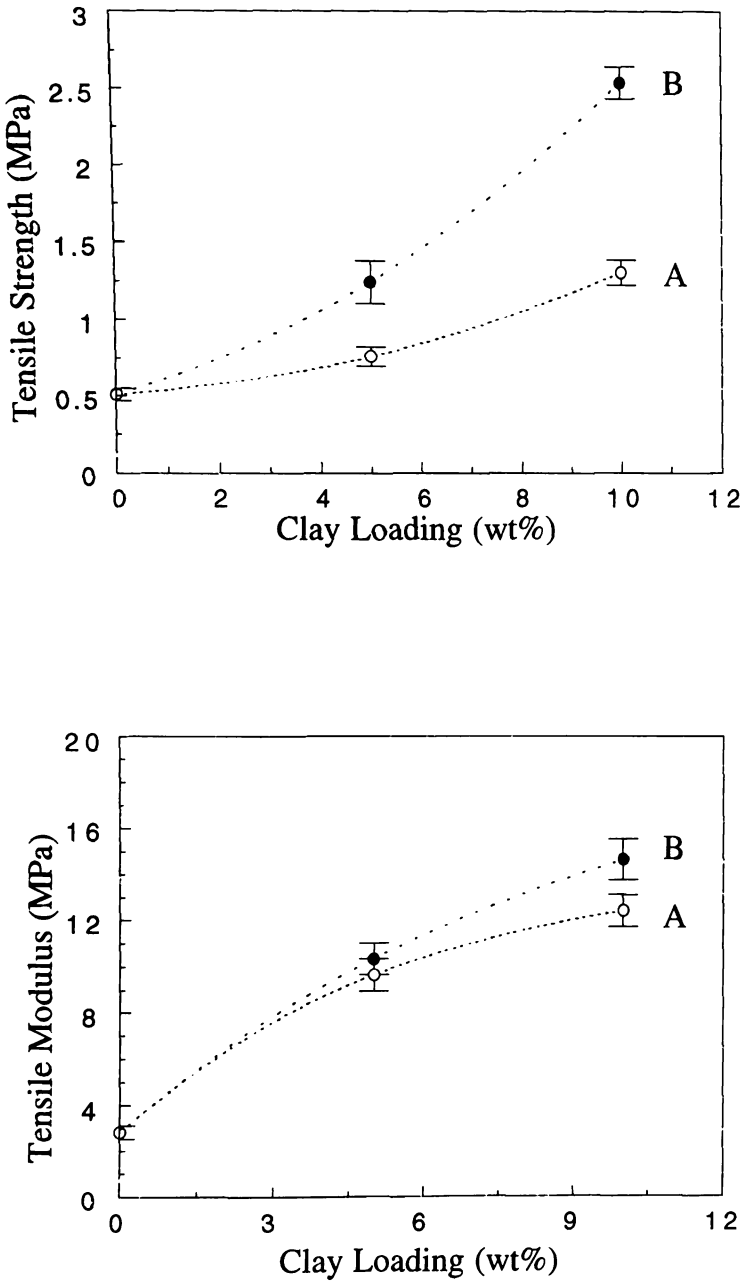



**Figure V 12.** Comparison of tensile strengths and moduli of intercalated nanocomposites with different clay layer separation distances. Curve A: $CH_3(CH_2)_{17}N(CH_3)_3^+$-fluorohectorite with $d_{001}$ = 38.8Å. Curve B: $CH_3(CH_2)_{17}NH_3^+$-fluorohectorite with $d_{001}$ = 110 Å.

## 3. Mechanism of Clay Reinforcement in Sub-Ambient $T_g$ Epoxy-Clay Nanocomposite

In our previous studies[19,20] of epoxide - *m*-phenylenediamine-clay nanocomposites, the tensile strength and modulus were marginally improved relative to the pristine polymer. In contrast, for the low $T_g$ epoxide-amine system of the present study, the reinforcement provided by the exfoliated clay is much more significant. Owing to the increased elasticity of the matrix above $T_g$, the improvement in reinforcement may be due in large part to shear deformation and stress transfer to the platelet particles. In addition, platelet alignment under strain may also contribute to the improved performance of clays exfoliated in a rubbery matrix as compared to a glassy matrix. The most significant difference between glassy and rubbery polymers is the elongation upon stress. The rubbery epoxy matrix used in this work exhibits 40 ~ 60 % elongation at break, whereas for the glassy epoxy matrix we reported previously it is only 5 ~ 8 %.[19,20] As illustrated in **Figure V 13**, the clay platelets in the cured polymer will be partially aligned in the direction of the matrix surface. When strain is applied in the direction parallel to the surface, the clay layers will be aligned further. This strain - induced alignment of the layers will enhance the ability of the particles to function as do the fibers in fiber-reinforced plastics. Propagation of fracture across the polymer matrix containing aligned silicate layers is energy consuming, and the tensile strength and modulus is reinforced. In a glassy matrix, clay particle alignment upon applied stress is minimal and blocking of the fracture by the exfoliated clay is less efficient. Future X-ray scattering studies may provide direct evidence for the proposed contribution of clay particle alignment to composite reinforcement.

The discovery of substantial reinforcement by exfoliated clay particles in a rubbery epoxy polymer above $T_g$ should advance the materials applications of these polymers. We are continuing to study the reinforcement mechanism by using smectite clays with complementary morphology and conducting modeling studies on the mechanical performance of the epoxy-clay exfoliated nanocomposites. The use of clay minerals as reinforcements in other rubbery materials, such as silicone rubber, and natural and synthetic rubbers also is being studied.

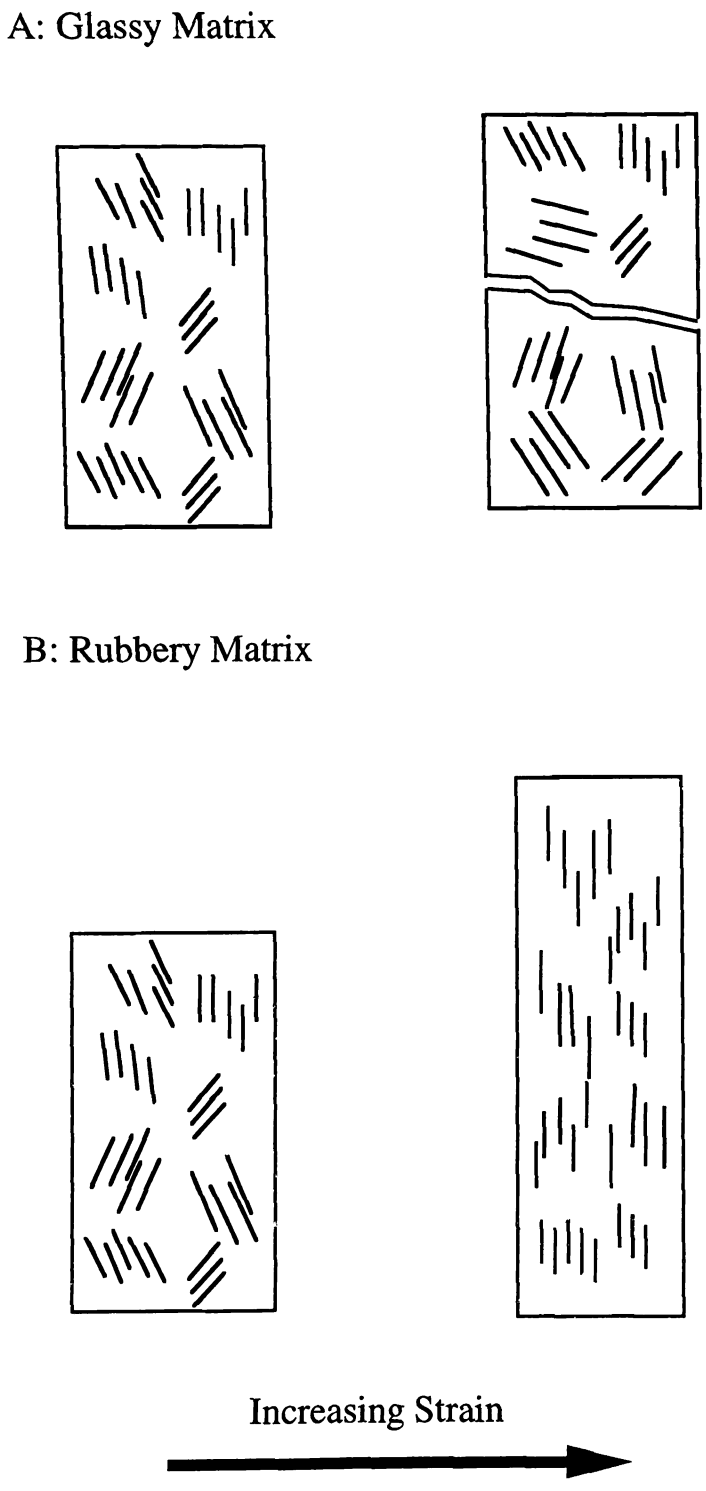



**Figure V 13.** Proposed model for the fracture of (A) a glassy and (B) a rubbery polymer-clay exfoliated nanocomposite with increasing strain.

## D. Conclusions

New epoxy-clay nanocomposites with sub-ambient glass transition temperatures have been prepared by the reaction of epoxy resin and a polyetheramine curing agent in the presence of alkylammonium ion exchanged forms of clays. Owing to the expansion of the clay galleries upon polymer network formation, the cured composites contain nanoscopic clay plates dispersed in a rubbery polymer matrix. Both the tensile strength and the modulus of the polymer-clay nanocomposite increased with increasing clay content. The reinforcement provided by the 10 Å-thick silicate layers at 15 wt% (~ 7.5 vol%) loading was manifested by a more than ten-fold improvement in tensile strength and modulus. Exfoliated nanocomposites exhibit better reinforcement on tensile properties than intercalated nanocomposites. The rubbery state of the polymer matrix above $T_g$ may allow alignment of the exfoliated silicate layers upon applying strain, thereby enhancing reinforcement.

**E. References**

1. E.P. Giannelis, *JOM* **44**, 28 (1992).

2. H. Gleiter, *Adv. Mater.* **4**, 474 (1992).

3. B.M. Novak, *Adv. Mater.* **5**, 422 (1993).

4. G. Philipp, H. Schimdt, *J. Non-Crystalline Solids.* **80**, 283 (1984).

5. G. Philipp, H. Schimdt, *J. Non-Crystalline Solids.* **82**, 31 (1986).

6. S. Wang, Z. Ahmad, J.E. Mark, *Proceedings of ACS, Div. of Polymeric Materials: Science and Engineering (PMSE)* **70**, 305 (1994).

7. M. Kakimoto, Y. Iyoku, A. Morikawa, H. Yamaguchi, Y. Imai, *Polymer Preprints,* **35-1**, 393 (1994).

8. M.W. Ellsworth, B.M. Novak, *Chem. Mater.* **5**, 839 (1993).

9. T.J. Pinnavaia, *Science* **220**, 365 (1983).

10. C. Kato, K. Kuroda, M. Misawa, *Clays and Clay Minerals*, **27**, 129 (1979).

11. Y. Sugahara, T. Sugiyama, T. Nagayama, K. Kuroda, C. Kato, *J. of the Ceramic Society of Japan* , **100**, 413 (1992).

12. R.A. Vaia, H. Ishii, E.P. Giannelis, *Chem. Mater.* **5**, 1694 (1993).

13. P.B. Messersmith, E.P. Giannelis, *Chem. Mater.*, **5**, 1064 (1993).

14. Y. Fukushima, S. Inagaki, *J. Inclusion Phenomena*, **5**, 473 (1987).

15. Y. Fukushima, A. Okada, M. Kawasumi, T. Kurauchi, O. Kamigaito, *Clay Miner.*, **23** , 27 (1988).

16. A.Usuki, M. Kawasumi, Y. Kojima, A. Okada, T. Kurauchi, O. Kamigaito, *J. Mater. Res.*, **8**, 1174 (1993).

17. A. Usuki, Y. Kojima, M. Kawasumi, A. Okada, Y. Fukushima, T. Kurauchi, O. Kamigaito, *J. Mater. Res.*, **8**, 1179 (1993).

18. Y. Kojima, A. Usuki, M. Kawasumi, A. Okada, Y. Fukushima, T. Kurauchi, O. Kamigaito, *J. Mater. Res.*,**8**, 1185 (1993).

19. T. Lan, P.D. Kaviratna, T.J. Pinnavaia, *Proceedings of ACS, Div. of Polymeric Materials: Science and Engineering (PMSE)* , 71, 528 (1994).

20. T. Lan, P.D. Kaviratna, T.J. Pinnavaia, manuscript in preparation.

21. C.-L. Lin, T. Lee, T.J. Pinnavaia, *ACS Symp. Ser.*, **499**, 145 (1992).

22. T. Lee, Ph. D. Thesis, Michigan State University, (1992).

23. Kamon, T.; Furakaw, H. in Epoxy Resins and Composites IV, Dusek, K. ed. *Advances in Polymer Science* vol. **80**. Springer-Verlag, Berlin, 177 (1986).

24. Barton, J. M. in Epoxy Resins and Composites I, Dusek, K. ed. *Advances in Polymer Science* vol. **72**. Springer-Verlag, Berlin, 120 (1985).

25. C.A. May, ed. *Epoxy Resins* 2nd ed., Marcel Dekker, New York, (1988).

# CHAPTER VI

## Synthesis and Characterization and Barrier Properties of Polyimide-Clay Nanocomposites

### A. Introduction

Barrier properties are very important for polymer materials used in the packaging industry. There are numerous of chemical, physical and chemical-physical methods that can be used to modify the polymer materials to improve their barrier properties. Typical chemical modification methods include increasing crosslinking degree, increasing crystallinity and grafting bulky groups to the polymer network. Normally, as barrier properties are increased, other properties of the polymer may be altered. Physical modification methods include blending other polymers with the parent polymer, mixing inorganic fillers and making multilayer polymers. Chemical-physical modification methods mean using chemically reactions such as intercalation reactions to introduce inorganic fillers which may physically mix with the parent polymer. If the filler particles are impenetrable to a diffusing gas, then the diffusing molecules must go around the filler particles or go through the film. This leads to a very tortuous path for molecules traveling through a filled polymer.[1]

Clay minerals such as talcs[2,4], micas[3,4] and smectite clays,[5,6] owing to their platy nature, have been used as fillers in some polymer materials to reduce their gas permeability. The method used to introduce clay minerals into polymer materials can be physical and chemical-physical. Physical methods such as melting-mixing have been applied to mix talc, mica and

kaolin into polyethylene,[2] EVOH,[3] nylon-6.[4] Under such processing conditions, the clay mineral particles retain their aggregate morphology. Therefore, the aspect ratios represent the platy nature of the clay minerals aggregate, which is only 10-30, and much lower than the aspect ratio of individual clay layer, which could be as high as 2,000. Due to the low aspect ratios of the clay aggregates (tactoids), some polymer systems filled with 40 wt% of mica only achieve 60 % decrease in permeability,[4] whereas, the properties of the parent polymer have been changed greatly. In order to apply clay minerals in the polymer materials to improve barrier properties, a new preparation approach must be developed.

Smectite clays are different from other clay minerals, because of their unique cation exchange property. This property provides a window to achieve the high aspect ratio of each individual clay layer. By exfoliating the clay layers, the high aspect ratios of each individual clay layer would be achieved. Indeed, a significant reduction in the permeability of helium, oxygen, and water has recently been reported for polyimide-clay composites containing embedded organocation exchanged forms of montmorillonite.[5,6] The rate of transport of a permeant molecule through a composite will be dependent upon the size, geometry and orientation of the embedded phase in the polymer matrix. It has been suggested that nearly complete dispersion (exfoliation) of the 10-Å-thick clay layers is needed to optimize the aspect ratio of the particles, which in the case of montmorillonite can reach a value of 2,000. However, relatively little is known concerning the extent of polyimide intercalation in organoclays.

Polyimide polymers have established the reputation based on their outstanding thermal stability, excellent mechanical properties and the ability

to be fabricate
applications,
temperature
application
implanting n
polymers, th
enhanced gr
network of
polyimide p

We exa
series of
conversion
polyimide i
length of th
18. Altho
long-chain
impressiv
measurem

to be fabricated into different articles. They have been used in electronic applications, polymer matrices for high temperature composites and high temperature adhesives. Due to high cost of their initial materials, the application of polyimide now is limited to only hi-tech. areas. By implanting naturally abundant minerals such as clays into the polyimide polymers, the cost will be reduced and also some properties will be enhanced greatly, such as the barrier property. Additionally, the silicate network of clay minerals will not sacrifice the thermal stability of the polyimide polymers.

We examined the intercalation of a polyamic acid in the galleries of a series of $CH_3(CH_2)_{n-1}NH_3^+$ montmorillonites and the subsequent conversion of the polyamic acid to polyimide. The results indicate that the polyimide intercalates in large part as a monolayer, regardless of the chain length of the initial clay exchange ion over the carbon number range n = 4 - 18. Although regular face-face layer aggregation is extensive even for a long-chain alkylammonium montmorillonite (n = 18), the composite exhibits impressive barrier film properties, as judged from $CO_2$ permeation measurements.

## B. Experim

### 1. Materials

Natura
Clay Miner
was purifie
followed b
solution an
unit cell o
with a catio

Organ
cation exc
alkylammo
~ 75 °C
ethanol:wa
M $AgNO_3$
-50 μm fra

### 2. Synth

Nanocom

Poly
4,4'-diam
acetamid
dianhydr
solution
dianhydr

**B. Experiment**

1. Materials

Natural montmorillonite from Wyoming, was obtained from the Source Clay Mineral Depository, University of Missouri, Columbia. The mineral was purified by sedimentation to exclude particles larger than 2 μm, followed by removing carbonates by using pH5 acetic acid/acetate buffer solution and eliminating iron oxide by employing sodium hydrosulfate. The unit cell of montmorillonite is $Na_{0.86}[Mg_{0.86}Al_{5.14}(Si_{8.00})O_{20}(OH)_4]$, with a cation exchange capacity of 88 meq./100g.[7]

Organoclays were synthesized by an ion exchange reaction.[8,9] The cation exchange reaction was carried out by using 500 ml of 0.05 M alkylammonium chloride ethanol:water (1:1) solution and 2.0 g of clay at 70 ~ 75 °C for 24 h.[26,27] The exchanged clays were washed with ethanol:water (1:1) for several times until no chloride was detected with 1.0 M $AgNO_3$ solution and air dried. Finally, the clays were ground and the 40 -50 μm fraction was collected.

2. Synthesis of Polyamic Acid-Clay Complexes and Polyimide-Clay Nanocomposites

Polyamic acid was synthesized by the condensation reaction between 4,4'-diaminodiphenylether and pyromellitic dianhydride in dimethyl-acetamide (DMAc).[10] The stoichiometric amount of pyromellitic dianhydride was slowly added to the 4,4'-diaminodiphenylether/DMAC solution with vigorous stirring at 15 - 20 °C. Upon adding of pyromellitic dianhydride, the color of the solution turns from colorless to light yellow.

The mixture

the adding of

a concentrati

n $H_2N$—

DMA

Polyar

of the desi

clay suspe

24 h, follo

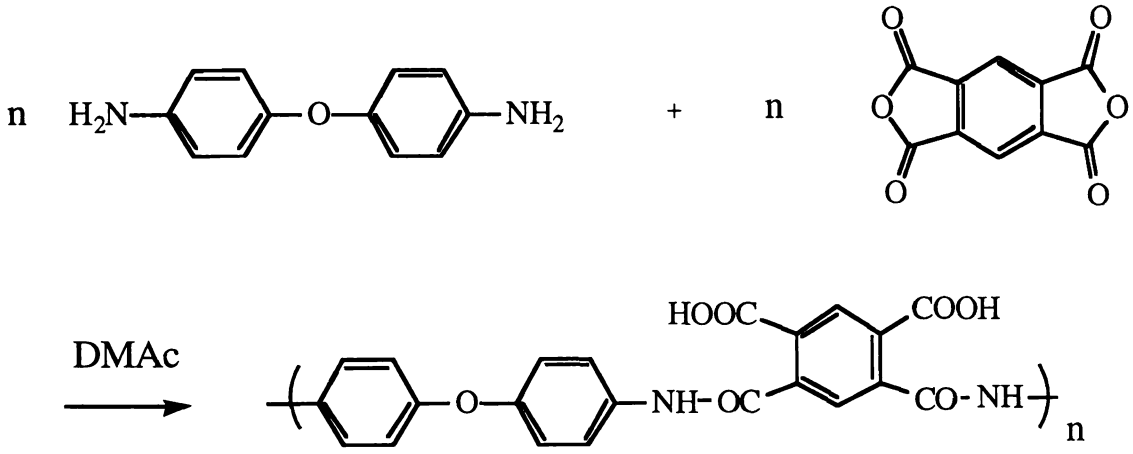
suspensior

air-dried p

kept at 3

composite

The mixture was kept stirring for 1 h at room temperature after completing the adding of pyromellitic dianhydride. The final polyamic acid solution has a concentration of 7 wt% without stirring difficulty.




Polyamic acid-clay intercalates then were prepared by reaction at 25 °C of the desired organoclay (2 - 15 wt%) with the polyamic acid solution. The clay suspension in polyamic acid/DMAC solution was vigorous stirred for 24 h, followed by 2 h settle down. Allowing the polyamic acid-organoclay suspensions to dry on a clean glass plate afforded self-supporting films. The air-dried polyamic acid-clay films were heated at 1 °C/min to 300 °C and kept at 300 °C for 3.0 h to form the cured polyimide - clay hybrid composites:



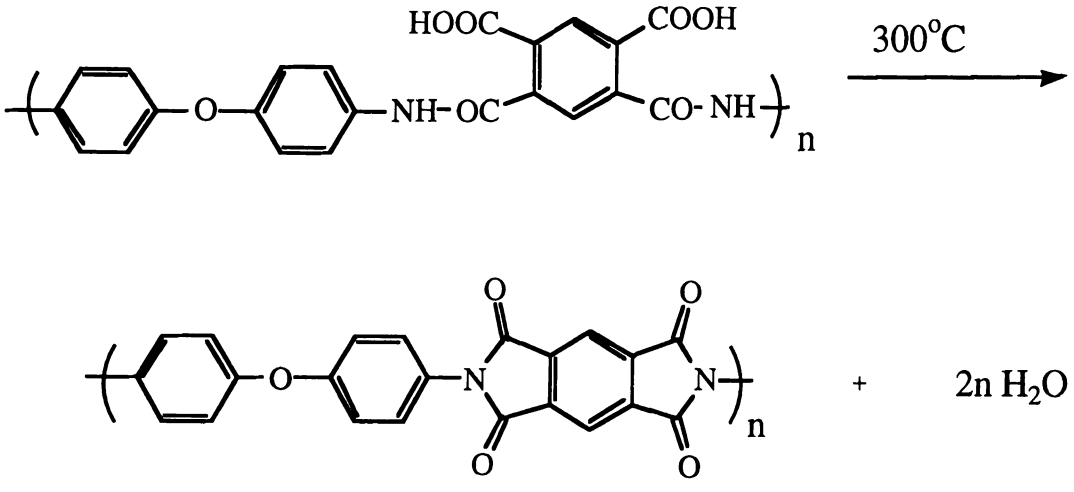


3. Physical M

X-ray d
anode X-ra
graphite mo
treated film

Therm
System 121
at a heating

Gas p
permeabili
2.5 cm ar
$N_2$ was us




3. Physical Measurements

X-ray diffraction patterns were obtained by using a Rigaku rotating anode X-ray diffractometer (Ru-200BH) with a Cu-k$\alpha$ target and curved graphite monochromater. The samples were either air dried films or heat treated films on microscopic glass slides.

Thermogravimetric analysis (TGA) was performed by using a Cahn TG System 121 thermogravimetric analyzer. All samples were heated to 700 $^{o}$C at a heating rate of 5 $^{o}$C/min; $N_2$ was used as a carrier gas.

Gas permeability measurements were performed by measuring the $CO_2$ permeability of polyimide-clay nanocomposites on films with a diameter of 2.5 cm and thickness of 25 $\mu$m at 1 atm on a Modern Controll Instrument; $N_2$ was used as the carrier gas.

## C. Results an

### 1. Structure o

The prec
to study the
understand th
patterns of t
**Figure VI 1**
wt% of dif
organoclay
thickness (9
$^{1}NH_3^+$ catio
the pristine
expected fo
ions.[11] Thu
the onium ca
the silicate l
acid and DI
cation.

There
DMAc, bec
observed i
$CH_3(CH_2)_{1}$
spacing inc
be vacuume
its original

## C. Results and Discussion

1. Structure of Polyamic Acid-Clay Complexes

The precursor to polyimide is polyamic acid. Therefore, it is essential to study the structural features of polyamic acid-organoclay intercalates to understand the structure of polyimide-clay composites. X-ray diffraction patterns of the air-dried polyamic-acid complexes reveal their structures. **Figure VI 1** shows the XRD patterns for polyamic acid films containing 10 wt% of different $CH_3(CH_2)_{n-1}NH_3^+$ montmorillonites. For each organoclay the basal spacing is approximately equal to the clay layer thickness (9.6 Å) plus the chain length of the intergallery $CH_3(CH_2)_{n-1}NH_3^+$ cation (**Chapter II**). Basal spacings of 13.5-17.6 Å are observed for the pristine organoclays in the absence of intercalated polyamic acid, as expected for horizontal monolayer or bilayer orientations of the onium ions.[11] Thus, when the polyamic acid and DMAc enter the clay galleries, the onium cations reorient from a horizontal to a vertical position relative to the silicate host layers. That is, the extent of gallery solvation by polyamic acid and DMAc is regulated by the chain length of the alkylammonium cation.

There is no doubt that polyamic acid is co-intercalated along with DMAc, because the basal spacings are significantly larger than the spacings observed in the presence of DMAc alone (**Figure VI 2**). For $CH_3(CH_2)_{17}NH_3^+$-montmorillonite intercalated by DMAc, the basal spacing increases slightly from 18 Å to 21.6 Å. The DMAc molecules can be vacuumed dry at 75 °C and the basal spacing of the clay returns almost to its original value.

Relative Intensity

**Figure VI**

$CH_3(CH_2)_n$

10 wt%.

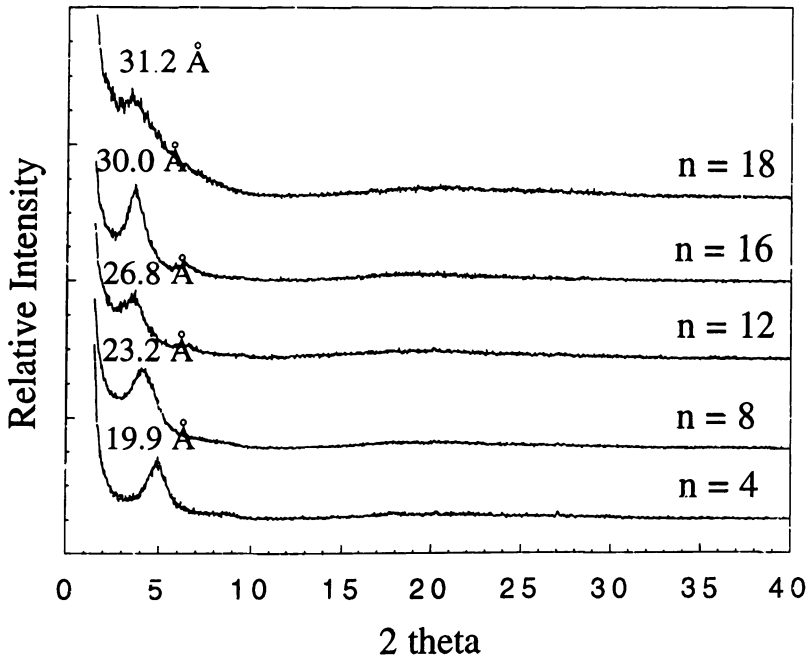



**Figure VI 1.** X-ray diffraction patterns of air dried polyamic acid-$CH_3(CH_2)_{n-1}NH_3^+$ - montmorillonite complexes with clay loading of 10 wt%.

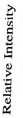



**Figure VI 2.**

llonites films sc

a. pristine organ

c. Vacuumed-dr

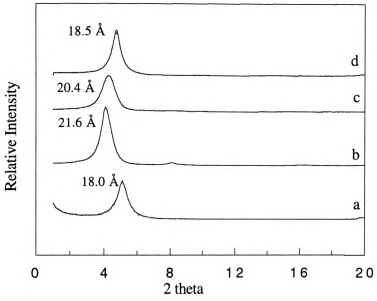



**Figure VI 2**. X-ray diffraction patterns of $CH_3(CH_2)_{17}NH_3^+$-montmorillonites films solvated by DMAc.

a. pristine organoclay b. air-dried after solvation by DMAc

c. Vacuumed-dried at room temperature d. Vacuumed-dried at 80 $^oC$.

2. Structu

Sinc
establish
further u
Indeed, t
polyimid
spacings
spacings
regardles

It is
acid-clay
the plots
VI 4. (cu
upon tra
polyimid

2. Structure of Polyimide-Clay Nanocomposites

Since the nuclearity of the intercalated polymer chain already is established at the polyamic acid stage, the clay galleries can not expand further upon thermal conversion of the polyamic acid to the polyimide. Indeed, the X-ray diffraction patterns (**Figure VI 3**) of the thermal cured polyimide-clay hybrid composites show that they have much lower basal spacings than their polyamic acid-clay complexes. Surprisingly, the basal spacings of the polyimide-clay hybrid composites are essentially the same, regardless of the initial gallery cations.

It is interesting to observe the basal spacing changes from the polyamic acid-clay complexes to the polyimide-clay hybrid composites. As shown by the plots of basal spacings *vs.* alkylammonium ion chain length in **Figure VI 4**. (curves A and C) a 6.7 -16.9 Å contraction in gallery height occurs upon transformation at 300 $^{o}$C of the polyamic acid to the more rigid polyimide.

Relative Intensity

**Figure VI**

the polyan

wt% clay

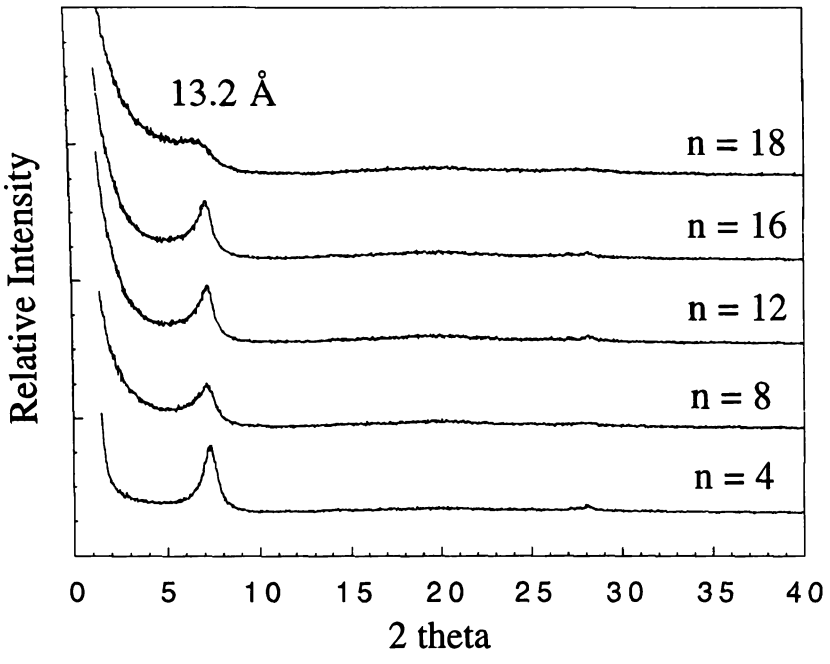



**Figure VI 3.** X-ray diffraction patterns of polyimide-clay films after heating the polyamic acid-$CH_3(CH_2)_{n-1}NH_3^+$-montmorillonite complexes with 10 wt% clay loading at 300 $^oC$.

$d_{001}$ (Å)

**Figure VI**

montmoril

polyamic a

cured poly

wt%.

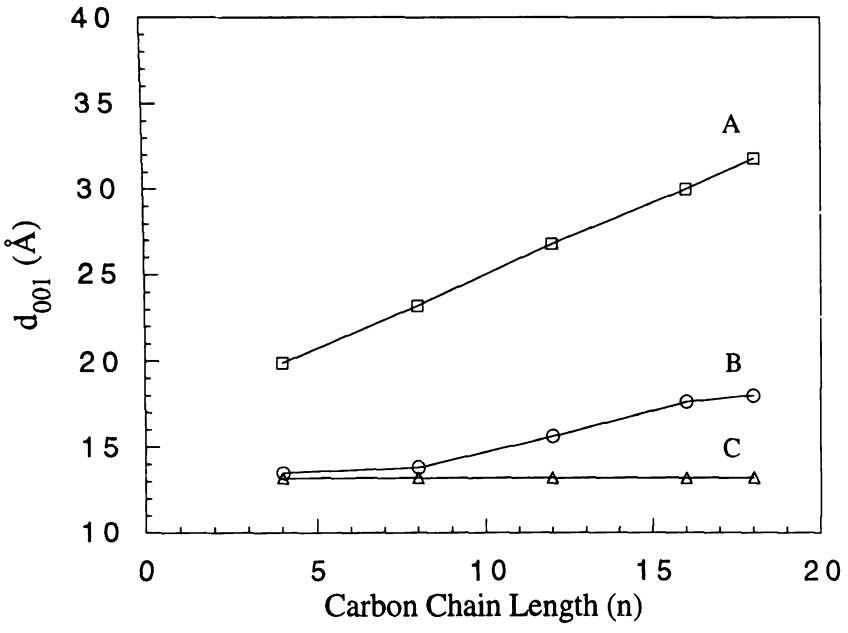



**Figure VI 4.** Dependence of the basal spacings of $CH_3(CH_2)_{n-1}NH_3^+$-montmorillonites on the carbon number, n : (A) clays dispersed in air-dried polyamic acid films, (B) air-dried pristine clays, and (C) clays dispersed in cured polyimide films. Curves A and C were obtained at clay loadings of 10 wt%.

In order
we studied
$CH_3(CH_2)_1$
ray diffracti
basal spacin
polyimide f
montmorill
the polyim
swelling fo
presence
temperatur
galleries, a

The t
montmoril
decompos
decompos
temperatu
polyamic
not deco

In order to confirm the intercalation of polyimide in the clay galleries, we studied the basal spacings of polyamic acid intercalated $CH_3(CH_2)_{17}NH_3^+$-montmorillonite at lower heating temperatures. The X-ray diffraction results (**Figure VI 5**) indicate that the same contractions in basal spacings occurs at 100 °C, a temperature well below that needed for polyimide formation. The polyamic acid intercalated $CH_3(CH_2)_{17}NH_3^+$-montmorillonite will retain its basal spacing at 13.2 Å up to 500 °C, when the polyimide thermal decomposition occurs. Thus, most of the gallery swelling for the air-dried polyamic acid - clay complex is attributable to the presence of intercalated DMAc. Eliminating the solvent at elevated temperature (~100 °C) leaves behind only a monolayer of polymer in the galleries, as judged from the basal spacing of 13.2 Å.

The thermal gravimetric analysis (TGA) result of $CH_3(CH_2)_{17}NH_3^+$-montmorillonites indicates that the onset temperature of organo clay thermal decomposition is 320 °C. The derivative curve shows that the thermal decomposition rate reaches a maximum at 380 °C. The clay decomposition temperature is higher than the thermal condensation reaction temperature of polyamic acid. Therefore, the alkylammonium cations in the clay gallery do not decompose in the polyamic acid condensation process.

**Figure VI**
$CH_3(CH_2)_1$
treatments.
polyamic a
heated at t
$^oC$.

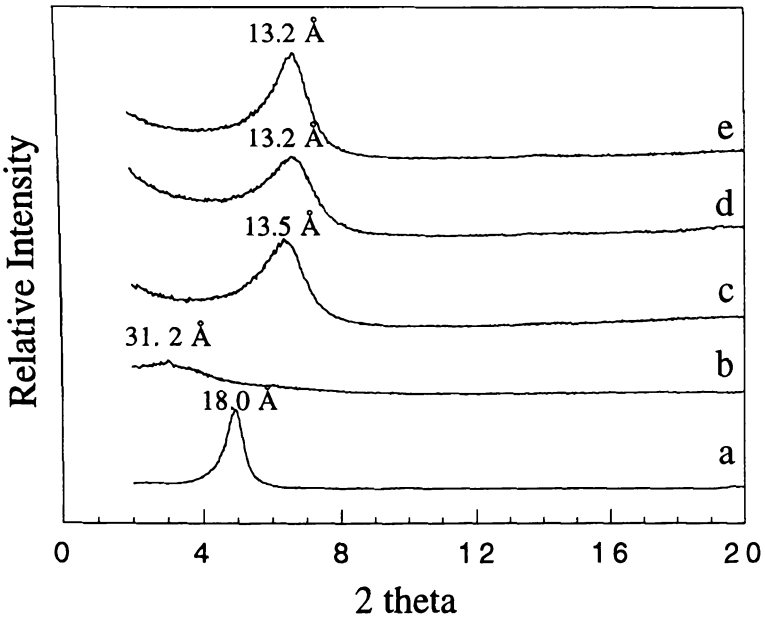



**Figure VI 5.** X-ray diffraction patterns of a polyamic acid-$CH_3(CH_2)_{17}NH_3^+$ -montmorillonite complex film after different heating treatments. The clay loading is 15 wt%. a. original clay, b. air-dried polyamic acid clay film; The air-dried polyamic acid clay films have been heated at the following temperatures for 3 h. c. 100 $^oC$, d. 200 $^oC$, e. 300 $^oC$.

Weight Loss (%)

1

**Figure V**

$^{0}$C/min; N

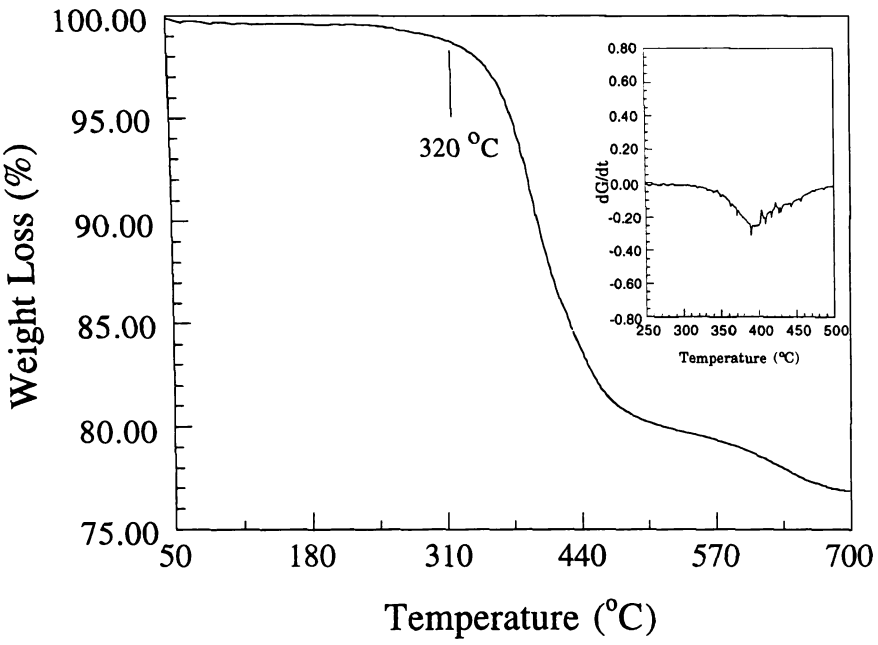



**Figure VI 6.** TGA profile of $CH_3(CH_2)_{17}NH_3^+$-montmorillonite at 5 °C/min; $N_2$ is the carrier gas. Insert is the derivative curve.

Relative Intensity

**Figure VI**

llonite after

c. 300 °C,

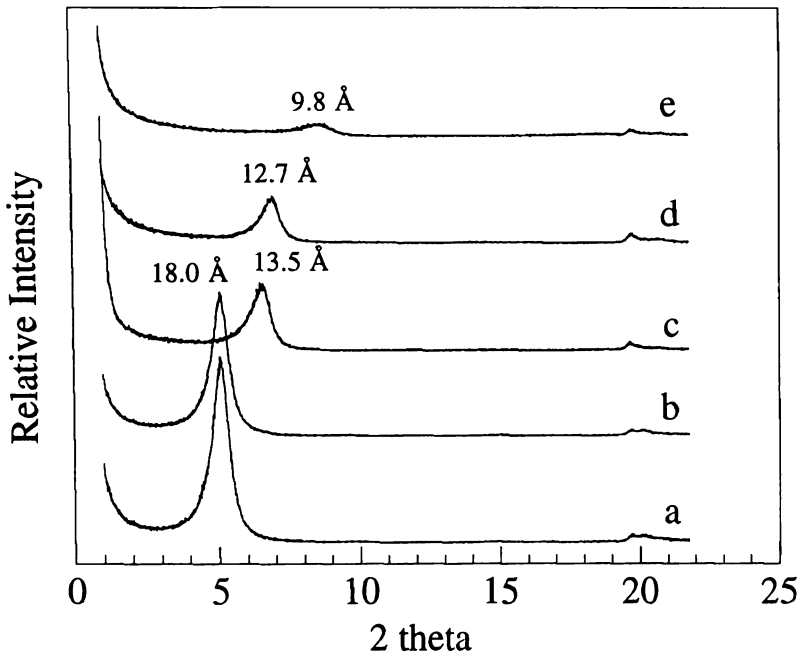



**Figure VI 7**. X-ray diffraction patterns of $CH_3(CH_2)_{17}NH_3^+$-montmorillonite after different heating treatment. a. original clay, b. 200 °C, 3 h; c. 300 °C, 3 h; d. 400 °C, 3 h; e. 600 °C, 3 h.

The bas
7) after diffe
upon therma
does not cha
at 200 °C
intercalated
5). This res
somehow
montmoril
alkylammo
of polyami

Signif
composite
independe
spacings f
in spacing
ions becau
intercalate
the polyi
whereas t
temperatu
intercalat
somewha
adopts a
of the ga

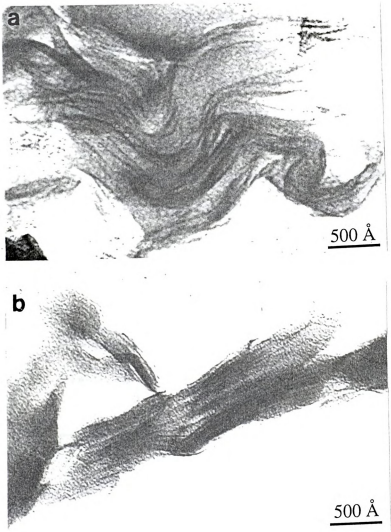
The basal spacings of $CH_3(CH_2)_{17}NH_3^+$-montmorillonite (**Figure VI 7**) after different heating treatments imply that the basal spacings decrease upon thermal decomposition of the organoclays. However, the basal spacing does not change when $CH_3(CH_2)_{17}NH_3^+$-montmorillonite has been heated at 200 °C in contrast to the basal spacing change of polyamic acid intercalated $CH_3(CH_2)_{17}NH_3^+$-montmorillonite complex film (**Figure VI 5**). This result indicates that the alkylammonium cations have been replaced somehow upon formation of the polyamic acid $CH_3(CH_2)_{17}NH_3^+$-montmorillonite complex film. Stated differently, there are no alkylammonium cations present inside the clay galleries upon the formation of polyamic acid-clay complexes.

Significantly, the basal spacing of the thermally cured polyimide-clay composite ~13.2 Å, which corresponds to a gallery height of ~ 3.6 Å, is independent of the initial onium ion chain length and smaller than the spacings for the starting alkylammonium montmorillonites. This contraction in spacings cannot be due to the thermal decomposition of the gallery onium ions because essentially identical values are observed for the polyamic acid intercalates dried at 100 °C, where intercalated onium ions are stable. Also, the polyimide composites retain their 13.2 Å spacing even at 450 °C, whereas the pristine onium ion clays give collapsed (10 Å) spacings at this temperature. Hence, a polyamic acid monolayer and not onium ions is intercalated in the clay galleries upon thermal elimination of DMAc. The somewhat constrained gallery height of 3.6 Å suggests that the polymer adopts a flattened conformation and/or is keyed into the hexagonal cavities of the gallery surfaces.

The al
retained in
In contras
exfoliation
using esse
The exfoli
film prope
texture of
obtained
$CH_3(CH_2$

The above X-ray diffraction results demonstrate that much of the clay is retained in an ordered intercalated state upon hybrid composite formation. In contrast, previous studies[5,6] have reported the essentially complete exfoliation of $CH_3(CH_2)_{11}NH_3^+$ montmorillonites in a polyimide matrix using essentially the same chemistry and methodologies as the present work. The exfoliated state of the clay was considered to be important to the barrier film properties of the composite. To more fully characterize the particle texture of the materials prepared in the present work, TEM images were obtained on thin sections of the polyimide-clay hybrids formed from $CH_3(CH_2)_{17}NH_3^+$-montmorillonite (**Figure VI 8**).

**Figure VI 8.** TEM images of polyimide-$CH_3(CH_2)_{17}NH_3^+$-montmorillonite composite films with clay content of 10 wt%. (A) the exfoliated structure and (B) the ordered intercalated structure.


a
500 Å
b
500 Å

In the

clay silicat

separations

separated b

accord with

We conclu

in the poly

exfoliated

the struct

alkylamm

shown in

In the TEM images, the dark lines are the intersection of 10 Å-thick clay silicate layers. Both delaminated layers with more or less random separations of 30 - 100 Å (A) and ordered aggregates with the layers separated by about 15 Å were observed (B). The ordered domains are in accord with the X-ray diffraction results for a regularly intercalated phase. We conclude, therefore, that a major fraction of the clay indeed is embedded in the polymer matrix as an ordered intercalate rather than as a completely exfoliated array of single layers. The polyimide-clay nanocomposites have the structure of intercalated nanocomposites. Replacement of the alkylammonium ions is due to ion-pair formation and proton exchange, as shown in **Figure VI 9**.

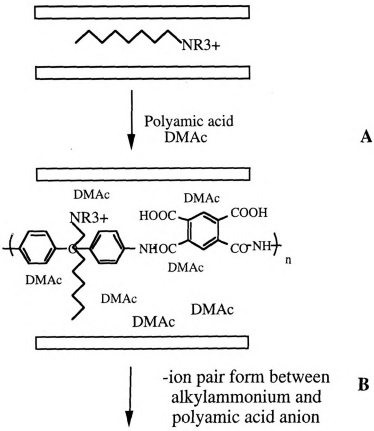


**Figure**
intercala
A. Solva
B. Dein
pairs be
C. Elim
D. Ther

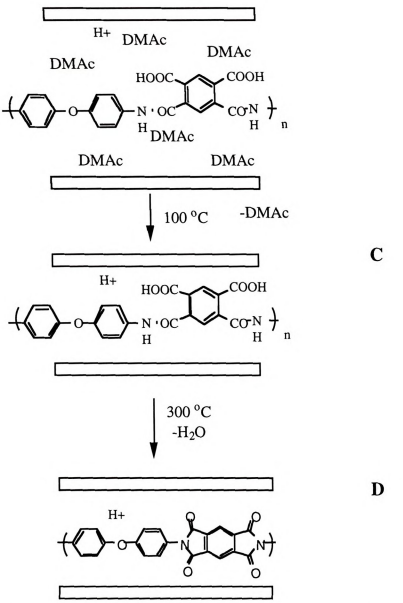



**Figure VI 9.** Proposed four steps of the formation of polyimide-clay intercalated nanocomposite

A. Solvation of DMAc and polyamic acid to the organo clays.

B. Deintercalation of alkylammonium cations through the formation of ion pairs between polyamic acid and onium ions.

C. Elimination of DMAc solvent molecules.

D. Thermal condensation of polyamic acid to polyimide.

3. $CO_2$ Perm

$CO_2$ p

$CH_3(CH_2)1$

evaluate the

of a substa

materials o

low clay loa

The da

$CO_2$ perm

0 - 7.4 vol

montmoril

diffusion

dependen

where P

unfilled

of polyr

filler.

dramati

parallel

3. $CO_2$ Permeability of Polyimide-Clay Nanocomposites

$CO_2$ permeability measurements were carried out for polyimide-$CH_3(CH_2)_{17}NH_3^+$-montmorillonite films with different clay loading to evaluate the barrier properties of such composite films. Despite the presence of a substantial fraction of highly ordered clay aggregates, the hybrid materials of the present work exhibit impressive barrier film properties at low clay loadings.

The data points in **Figure VI 10** illustrate the nonlinear dependence of $CO_2$ permeability on clay loading for a series of composite films containing 0 - 7.4 vol % (0 - 5 wt%) (density of clay ~ 2.6 g/cm$^3$) $CH_3(CH_2)_{17}NH_3^+$-montmorillonite. Since non-permeable platy particles act as a barrier to gas diffusion by increasing the tortousity of the diffusion pathway,[1] the dependence of permeability on loading can be estimated from the equation:

$$\frac{P_c}{P_p} = \frac{\phi_p}{1 + (W/2T)\phi_f}$$

where $P_c$ and $P_p$ is the permeability of the composite film and that of the unfilled (pristine) polymer, respectively, $\phi_p$ and $\phi_f$ are the volume fractions of polymer and filler, and W/T is the width-to-thickness aspect ratio of the filler. As indicated by the above equation, a large aspect ratio will dramatically decrease permeability, provided the particles can be oriented parallel to the surface of the film.

**Figure**
curing
The me
thickne
permea
calcula

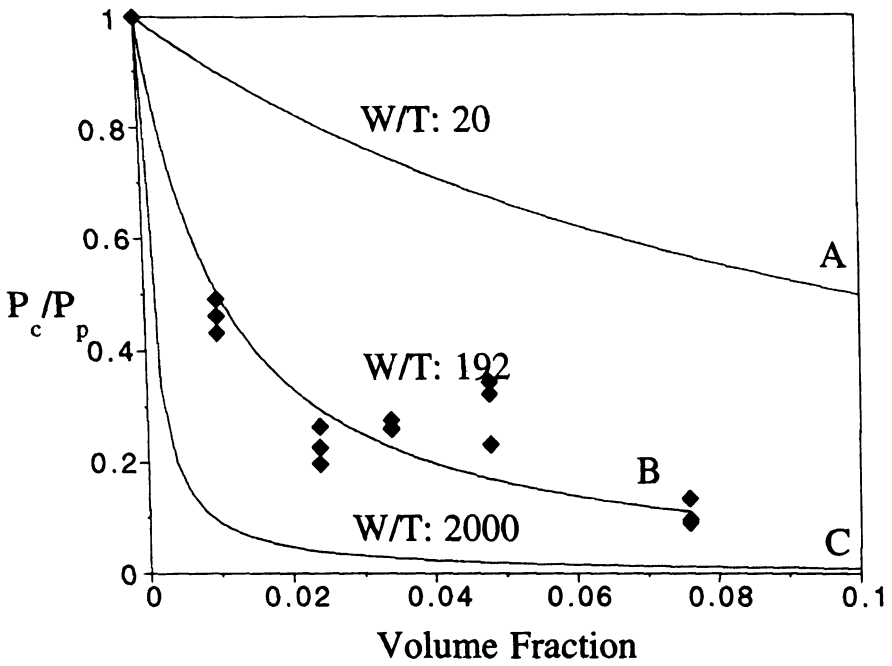



**Figure VI 10**. $CO_2$ permeability of polyimide-clay composites prepared by curing polyamic acid-$CH_3(CH_2)_{17}NH_3^+$montmorillonite films at 300 °C. The measurements were performed on films of 2.5 cm diameter and 25 μm thickness. Curve B was generated by least-squares fitting of the permeability equation to the experimental data. Curves A and C are calculated for fillers with W/T aspect ratios of 20 and 2,000, respectively.

Curve
permeabil
comparis
ratios of
particles,
loading w
to the res
ratio of 2
exfoliate
clay ret
monolay
crystallo
mechan
polyam

4. Clay

Pc
have b
in acc
depen

$D_{hkl}$
and e
1.542

Curve B in **Figure VI 10** which represents the best fit of the permeability equation to the data, yields a particle aspect ratio of 192. For comparison, curves A and C were generated by assuming particle aspect ratios of 20 and 2000 for non-intercalated and completely exfoliated particles, respectively. The relationship between permeability and clay loading which we observe for our hybrid composites is quantitatively similar to the results of Toyota investigators[5,6], who also report an apparent aspect ratio of 200. These latter workers have concluded that the clay is completely exfoliated into 10-Å-thick layers. However, our results clearly show that the clay retains a crystallographically regular layer stacking order with a monolayer of polymer intercalated between the clay layers. The retention of crystallographic order is in part a consequence of the unique intercalation mechanism wherein the onium ions are displaced from the galleries and the polyamic acid becomes encapsulated upon removal of the DMAc solvent.

4. Clay Stacking Coherence in Polyimide-Clay Nanocomposites

Powder X-ray diffraction patterns of the polyimide-clay composites have been used to obtain the clay stacking coherence in the composite films in accordance with the Scherrer equation. This method is based on the dependence of the spectrum line width on the scattering domain size.

$$D_{hkl} = \frac{k \lambda_{Cu}}{2 I_{hkl} \cos\theta}$$

$D_{hkl}$ is the crystallinity or coherent scattering domain (Å); k is a constant and equal to 1 in our experiments. $\lambda_{Cu}$, the X-ray wavelength is equal to 1.542 nm; $I_{hkl}$ is the half-height width of the sample (hkl) diffraction peak.

In our exper
domain, or t

The s
montmorill
peaks of c
weak to ob

In our experiments, where h = k = 0, we obtain the "c" direction scattering domain, or the stacking coherence of the clay in the polyimide matrix.

The scattering domain size of the polyimide-$CH_3(CH_2)_{17}NH_3^+$-montmorillonite composite films are listed in **Table VI 1**. X-ray diffraction peaks of composite films with weight percentage less than 7 wt% are too weak to obtain accurate half-height widths.

**Table VI 1.**

llonite in po

wt%

Tog

matrix,

compos

clay lat

than 2

purifie

single

This a

simila

5. M

Nanc

can

slip

**Table VI 1.** Coherent Scattering Domain of $CH_3(CH_2)_{17}NH_3^+$-montmorillonite in polyimide-clay films.

| wt% of clay | domain size (Å) | particle size (μm) |
|---|---|---|
| 7.0 | 276 | 5.5 |
| 10.0 | 401 | 8.0 |
| 15.0 | 441 | 8.7 |

Together with the basal spacing data of the clay in the polyimide matrix, 13.2 Å, the clay lateral particle sizes have been calculated for the composite films with different clay loadings (**Table VI 1**). Surprisingly, the clay lateral particle sizes for all the polyimide-clay composites are larger than 2 μm, which is the largest possible dimension of montmorillonite purified by the sedimentation method. The lateral size of montmorillonite single layers is typically much smaller, usually in the range 0.1 -2.0 μm. This apparent contradiction in particle size may be explained by a self-similar clay aggregation mechanism.

5. Mechanism of Barrier Property Enhancement of Polyimide-Clay Nanocomposites, Fractal Structure

Van Damme et al.[12] have proposed that clays dispersed in liquid media can adopt fractal structures in which the face-face associated layers are slipped in staircase like fashion (**Figure VI 11**)

These se
rise to 001 X
work. A str
and is show

In **Figu**
linkage; th
diffraction
TEM, are
polyimide
plate to b
explain th
structures

These self-similar structures can exhibit enhanced aspect ratios and give rise to 001 X-ray scattering in accord with the observations of the present work. A structural model has been proposed to explain the fractal structure and is shown in **Figure VI 12**.

In **Figure VI 12**, the different original clay aggregates form a staircase linkage; therefore, the ordered phases which contribute to the X-ray diffraction and the exfoliated amorphous region, which is observed in the TEM, are all present here. The clay fractal structures merge in the polyimide matrix as an island, and each of them functions as a single filler plate to block the pathway of diffusing molecules. A model is proposed to explain the barrier property enhancement upon the formation of clay fractal structures (**Figure VI 13**).

Normal Sta

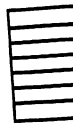


**Figure V**

stacking.





**Figu**

mat

sam




**Figure VI 11**. Structural difference of clay normal stacking and staircase stacking.

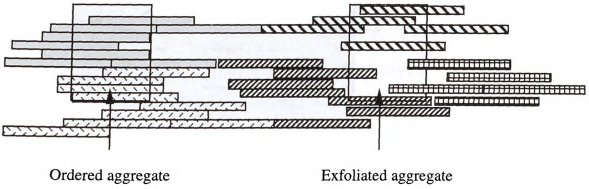



**Figure VI 12.** Proposed model for the clay fractal structure in the polyimide matrix. Same fill-in patterns indicate that the clay plates come from the same original clay aggregates.

A. Interca



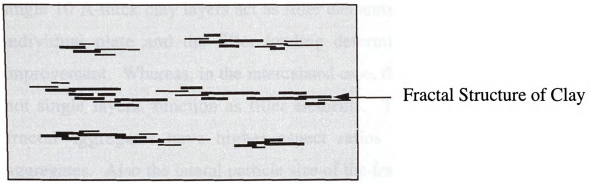
B. Exfo



Figu

nano

A. Intercalated Polyimide - Clay Nanocomposite




B. Exfoliated Polyimide - Clay Nanocomposite

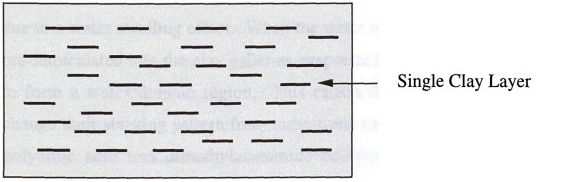



**Figure VI 13**. Comparison between exfoliated polyimide-clay nanocomposite and intercalated polyimide-clay nanocomposite.

**Figu**

intercalat

single 10

individu

improve

not sing

fractal

aggrega

larger th

Th

due to

pre-int

to for

chang

polya

DMA

of the

polya

struc

poly

DM

low

to t

is a

**Figure VI 13** illustrates the structural difference between exfoliated and intercalated polyimide-clay nanocomposites. In the exfoliated structure, the single 10 Å-thick clay layers act as filler elements. The aspect ratio of the individual plate and the filler loading determine the barrier property improvement. Whereas, in the intercalated case, the clay fractal aggregates, not single layers, function as filler elements. The clay layer associated fractal aggregates have higher aspect ratios than the ordinary clay aggregates. Also the lateral particle size of the fractal aggregates should be larger than the original clay particle size.

The formation of the fractal clay structure for natural clay minerals is due to a water swelling effect. When the water molecules which have been pre-intercalated into the clay galleries evaporate from the system, they tend to form a water domain region. This causes the clay layers to slip and change their stacking pattern from turbostratic to staircase fashion. For the polyamic acid and dimethylacetamide co-intercalated organoclays, the DMAc upon heating (*e. g.*, 100 $^{o}$C) will leave the system. A rearrangement of the clay stacking then occurs to form the fractal structure of the clay in the polyamic acid matrix. After further heating at 300 $^{o}$C, the clay fractal structure will remain simply because of the low mobility of the pre-formed polymer chains.

As stated earlier, there is no driving force for the polyamic acid and DMAc co-intercalated organoclay to undergo exfoliation. However, at very low clay loading the "diluted" fractal fragments may display some similarity to the exfoliated structure. But, the nature of the polyimide-clay composite is an intercalated nanocomposite.

D. Concl

Poly
intercala
$_1NH_3^+$
convers
transmi
exfoliat
The ex
increas
of the
interca
regula
exhibi
range
the p
impr
nano

## D. Conclusion

Polyimide - clay hybrid composites have been prepared by the intercalation of polyamic acid / dimethylacetamide (DMAc) in $CH_3(CH_2)_{n-1}NH_3^+$ montmorillonites (n = 4, 8, 12, 16, and 18) and subsequent thermal conversion of the polyamic acid to polyimide. X-ray diffraction and transmission electron microscopy studies indicate the presence of both exfoliated and regularly intercalated clay aggregates in the polymer matrix. The extent of clay gallery swelling by polyamic acid / DMAc increases with increasing onium ion chain length. Owing to the concomitant displacement of the onium ions from the galleries upon removal of DMAc, the polyimide intercalates in all cases as a monolayer (gallery height ~ 3.6 Å). Although regular face-face clay layer aggregation is extensive, the hybrid composite exhibits greatly improved $CO_2$ barrier film properties at clay loadings in the range 1.0 - 8.0 vol %. The fractal structural model proposed for the clay in the polyimide matrix may provide an incisive understanding of the improvement on the barrier properties of an intercalated polymer-clay nanocomposite.

## E. Refere


1. L.E. N

2. M. Ar
**19**, 30 (1

3. T.C.

4. N.S.
*Science*

5. K. Y
*Prepri*

6. K.
*Polyr*

7. J.
Wac

8. C

9. T

10.
Ol

11

## E. References

1. L.E. Nielsen, *J. Macromol. Sci. (CHEM.), A1* **5**, 929 (1967).

2. M. Arina, A. Honkanen, V. Tammela, *Polymer Engineering and Science*, **19**, 30 (1979).

3. T.C. Bissot, *ACS Symp. Ser.*, **423**, 225 (1989).

4. N.S. Murthy, A.M. Kotliar, J.P. Sibilia, W. Sacks, *J. of Applied Polymer Science*, **31,** 2569 (1986).

5. K. Yano, A. Usuki, A. Okada, T. Kuraychi, O. Kamigaito, *Polymer Preprints*, **32**, 65 (1991).

6. K. Yano, A. Usuki, A.Okada, T. Kuraychi, O. Kamigaito, *J. Polym Sci: Polym. Chem.*, **31**, 2493 (1993).

7. J. Butrulle, T.J. Pinnavaia, "Characterization of Catalytical Materials" I.E. Wachs, Ed. Butterworth-Heinemann, Boston, 149 (1992).

8. C.L. Lin, T. Lee, T.J. Pinnavaia, *ACS Symp. Ser.*, **499**, 145 (1992).

9. T. Lee, Ph. D. Thesis, Michigan State University, (1992).

10. C.E. Sroog, A.L. Enerey, S.V. Abramo, C.E. Beer, W.M. Edwards, K.L. Oliver, *J. Polym. Sci. Part A: Polym. Chem.*, **3**, 1373 (1965).

11. G. Lagaly, *Solid State Ionics*, **22**, 43 (1986).

12. H

Berga

Eds.;

12. H. Van Damme, P. Levitz, J.J. Fripiat, J.F. Alcover, L. Gatineau, F. Bergaya, In Physics of Finely Divided Matter; Boccara, N.; Daoud, M., Eds.; Springer-Verlag: New York, 2/8 - 8/8, (1985).

MICHIGAN STATE UNIV. LIBRARIES
31293010201675